Since January 2020 Elsevier has created a COVID-19 resource centre with free information in English and Mandarin on the novel coronavirus COVID-19. The COVID-19 resource centre is hosted on Elsevier Connect, the company's public news and information website.

Science of the Total Environment 751 (2021) 141727

Contents lists available at ScienceDirect

Science of the Total Environment

journal homepage: www.elsevier.com/locate/scitotenv

Review

On the linkage between urban heat island and urban pollution island: Three-decade literature review towards a conceptual framework

Giulia Ulpiani *

School of Civil Engineering, The University of Sydney, Sydney, New South Wales, Australia

HIGHLIGHTS

- 30 years of knowledge on the link between urban heat and pollution islands are revised.
- Results from 16 countries and 11 climatic zones are collected and analyzed.
- Geographical dependencies, methodological and experimental trends are compared.
- Five prominent aspects related to chemistry, meteorology and urbanism are covered.
- Major findings, areas of debate and outstanding research questions are identified.

GRAPHICAL ABSTRACT

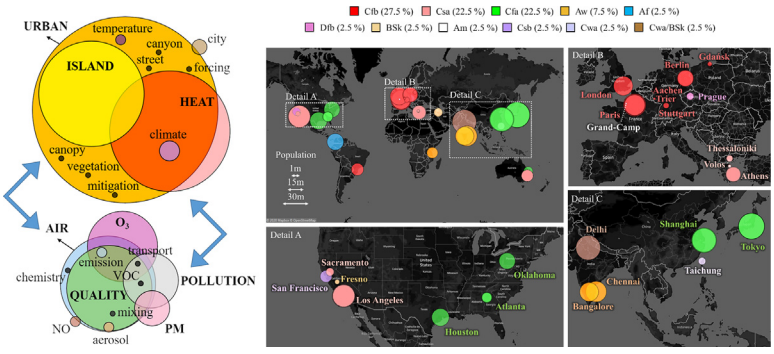

ARTICLE INFO

Article history:
Received 22 June 2020
Received in revised form 3 August 2020
Accepted 14 August 2020
Available online 18 August 2020

Editor: Pavlos Kassomenos

ABSTRACT

With the doubling of urban population within the next two decades and the disproportionate growth of megacities, it is critical to explore the synergism between urban heat and pollution. In this paper, a systematic review is conducted on the existing knowledge, collected since 1990, on the link between urban heat island (UHI) and urban pollution island (UPI). Results from 16 countries and 11 Köppen-Geiger climatic zones are perused and compared to delineate methodological and experimental trends, geographical dependencies and research gaps. Detailed content analysis is conducted according to five prominent topics: i) the role of UHI on temperature-dependent chemistry, ii) the daytime/nighttime variability in the UHI-UPI interaction, iii) the role of urban

Abbreviations: A2, Medium-high emission scenario for the 2050; AERONET, Aerosol robotic network; AOD, Aerosol optical depth [nm]; AOT, Aerosol optical thickness [nm]; ArcGIS, Aeronautical reconnaissance coverage geographic information system; ASTER, Advanced spaceborne thermal emission and reflection radiometer; AUHI, Atmospheric urban heat island; AUPI, Atmospheric urban pollution island; BAU, Business as usual; BEM, Building energy model; BEP, Building effect parameterization; BVOC, Biogenic volatile organic compound; CAMx, Comprehensive air quality model with extensions; CAQI, Common air quality index; CART, Classification and regression tree; CGCM2, Canadian global climate model, version 2; Chem, Atmospheric chemistry model; CMAQ, Community multiscale air quality model; CSIRO Mk2, Commonwealth scientific and industrial research organisation GCM mark 2; DI, Discomfort index; DJA, Winter; ECHAM4, European centre Hamburg model, version 4; ECMWF, European centre for medium-range weather forecasts; EPA, Environmental protection agency; ERA-40, Reanalysis of global atmosphere and surface condition over 45 years; GCM, General circulation model; GIS, Geographic information system; HIC, Heat island circulation; H_g, Ground heat flux [W/m^2]; Hl, Latent heat flux [W/m^2]; HRV, High resolution visible; Hs, Sensible heat flux [W/m^2]; I↓, Downward surface insolation [W/m^2]; ILW,↓, Downward longwave radiation [W/m^2]; JJA, Summer; Kv, Vertical eddy diffusion coefficient; LBNL, Lawrence Berkeley national laboratory; LLJ, Low level jet; LST, Land surface temperature; LULC, Land use land cover; MM5, Mesoscale meteorological model, version 5; MODIS, Moderate resolution imaging spectroradiometer; NAAQS, National ambient air quality standards; NASA, National aeronautics and space administration; NCEP, National centers for environmental prediction; NDVI, Normalized difference vegetation index [dimensionless]; NHC, National hurricane center; NSUPI, Near-surface urban pollution island; P80, 80th percentile; P90, 90th percentile; PM, Particulate matter; POA, Primary organic aerosol; PSU, Penn state University; RegCM, Regional climate model; ROG, Reactive organic gas; SOA, Secondary organic aerosol; SoCAB, South coast air basin; SPOT, Satellite pour l'observation de la terre; SUHI, Surface urban heat island; TAPM, The air pollution model; TEB, Town energy balance; Ts, Surface temperature [°C]; UCM, Urban canopy model; UHI, Urban heat island; UHII, Urban heat island intensity [°C]; uMM5, urban MM5; UPI, Urban pollution island; UV, Ultraviolet; VOC, Volatile organic compound; WRF, Weather research and forecasting model; α, Surface albedo [dimensionless]; ε, Surface emissivity [dimensionless]; σ, Stefan Boltzmann constant [W/m^{2}K^4].

* School of Civil Engineering, Building J05, The University of Sydney, NSW 2006, Australia.
E-mail address: giulia.ulpiani@sydney.edu.au.

https://doi.org/10.1016/j.scitotenv.2020.141727

Keywords:
Urban heat island
Urban pollution
Air quality
Heat mitigation
Tropospheric ozone
Climate change

geomorphic types, forms and growth schemes, iv) future trends and v) primary and secondary effects of UHI mitigation on urban air quality. Different approaches and observations are eventually harmonized to outline opportunities and challenges towards the disentanglement and/or the two-way mitigation of both phenomena. This will help governments and urban planners to deliver coping strategies and precautions towards a more salutogenic urban design.

Contents

1. Introduction

Urban heat island (UHI) and urban pollution island (UPI) are both manifestations of the intensive changes in the patterns of human settlement, energy use, transportation, industry and of the pressure on natural resources caused by rapid urbanization, population growth and ongoing encroachment into the unbuilt realm (Imhoff et al., 2010; Izrael et al., 1990). UHI is the alteration of the thermal balance in urban spaces compared to the near rural areas due to modifications of the heat and momentum transfer between the land surface and the atmosphere in terms of heat storage, partitioning between sensible and latent heat fluxes (Bowen ratio), frictional drag and ratio between natural and anthropogenic emissions (Vailshery et al., 2013; Dousset and Gourmelon, 2003). The UHI intensity (UHII, calculated as temperature difference between a representative urban area and the rural background) can reach 11/12 °C (Santamouris, 2015; Santamouris and Kolokotsa, 2016) with an average cooling penalty in urban versus rural buildings of 13.1%, a peak electricity penalty per degree of temperature rise of 0.45% up to 4.6% and an electricity penalty per degree of temperature rise and per person of 21 (±10.4) W/°C/person (Santamouris et al., 2015). If we consider that the average cooling energy needs of residential and commercial buildings will increase by 750% and 275% in about 30 years, a measure of the expected impacts can be estimated (Santamouris, 2016). Further, urbanization is currently encouraged in many cities in the world to accommodate the increasing population and to boost economic development. The growth mostly affects the periurban fringe, (areas non adjacent to traditional downtown city centers) thus exacerbating the sprawl level. To put things in perspective, only in the United States, the encroachment of forested or agricultural hinterlands resulted in a loss of >2000 green hectares each day in the 21st century, on average (Kostmayer, 1989).

The term urban pollution island (UPI) has been introduced only recently (Crutzen, 2004; Li et al., 2018) to identify the onset of spatial and temporal variations in pollutants concentration ascribable to the presence of typical urban features and activities. The difference between urban areas and suburban/rural areas is what defines the UPI intensity, in analogy with the UHII. UHI and air pollution are far from being independent phenomena, to the point that where urban heat islands exist, most likely urban pollution islands coexist (Crutzen, 2004). High temperatures accelerate certain atmospheric chemistry cycles, most of which leading to enhanced ground-level (tropospheric) ozone production, higher emission of biogenic hydrocarbons (BVOCs) and higher evaporation of synthetic VOCs from vehicle engines (Elsayed, 2012; Bretz et al., 1998). Further, UHIs and UPIs are both strictly related to combustion processes from transport, industry and other anthropogenic processes (e.g. air-conditioning and cooking) as these are at the same time pollutants and heat sources. To name one mechanism, under intense heat islands, air conditioning units are activated for longer during the day and during the year. This directly increases the emission of CO_2 and ozone-precursors from regional power plants (Rosenfeld et al., 1998) and, contingently, pours exhaust heat in the urban air thus feeding UHI amplification in ever-increasing spirals. Further, UHI-assisted peak power absorptions (e.g. under heat wave) call for additional generation capacity which is typically supplied by less sustainable power plants. This means that UHI is not just conducive to the development of a dust dome over the urbanscape, but also to its self-sustainment by consolidating a recirculating pattern that prolongs and aggravates pollution episodes. On the other hand, warmer air stimulates turbulent mixing that promotes primary pollutants dispersion to higher atmospheric layers (Sarrat et al., 2006).

Even though UHI and UPI are the most documented phenomena of urban climatology and are evidently correlated, their interaction is comparatively underexplored (Czarnecka and Nidzgorska-Lencewicz, 2014). Pioneering works in the late '60s found that the wind patterns associated with the onset of urban heat islands sharpened the pollution gradient between urban and rural areas (Chandler, 1968; Santamouris et al., 2012). Yet, even if a substantial coincidence between UHIs and UPIs is expected (Jun Li et al., 2007), UHI and pollution co-exist in an intricate and intimate pattern of feedbacks at regional and local scale, as well as at vertical and horizontal level (Oke, 1982).

The UHI depends upon the following land surface energy budget (Dickinson, 1986):

$$(1-\alpha)I_{\downarrow} + I_{LW,\downarrow} - \varepsilon\sigma T_s^4 - H_s - H_l - H_g = 0 \quad (1)$$

where α, ε and T_s are the surface albedo, emissivity and temperature, $I_{\downarrow}$ is the downward surface insolation, $I_{LW,\downarrow}$ is the downward longwave radiation, σ is the Stefan Boltzmann constant, H_s ad H_l are the sensible and

latent heat fluxes and H_g is the ground heat flux. According to Eq. (1), higher albedo curbs the amount of solar radiation retained at surface-level and increases the quota reflected back to the atmosphere. On the other side, higher emissivity increases the amount of radiation re-irradiated to the atmosphere which can be sent back to the surface by moisture, aerosols and other pollutants, whose load is intensified by urbanization. Aerosols interact differently with shortwave and longwave radiation with opposing results on the near-surface energy balance (He, 2018). A cooling effect is linked to the blockage of incoming shortwave radiation (lower $I_\downarrow$) conversely, their absorbance and emittance in the longwave atmospheric window emphasizes the $I_{LW,\downarrow}$ term (Jacobson, 1998). The net effect determines the UHI offset (Haywood and Boucher, 2000; Jin and Shepherd, 2008). For instance, Estournel et al. (1983) found that the city of Toulouse received 30 W/m^2 less solar radiation and up to 25 W/m^2 more longwave radiation than the rural areas during cloudless polluted days. Similar results are reported by Jauregui and Luyando for Mexico City (Jauregui and Luyando, 1999), by Robaa for the Greater Cairo region (Robaa, 2009) and by Wang et al. for Beijing (Wang et al., 2015). Furthermore, as aerosols warm up the atmosphere (Ramanathan et al., 2007) they tend to stabilize the boundary air layer right above the city thus deteriorating the efficiency of energy dissipation from the surface to the atmosphere. The amount of absorption and reflection depends on the urban form too, e.g. on the multiple bounces that may occur inside canyons. In turn, the availability of radiation at surface level determines ozone's concentration. Ozone is produced by the photooxidation of VOCs in the presence of nitrogen oxides (NO_x) (Leighton, 2012). It coexists with its precursors in a complex photostationary equilibrium between photolysis and titration driven by light and OH radicals. The net effect is governed by the amount of available precursors, which is typically larger over dense urban areas (Cardelino and Chameides, 1990).

The scenario is further complicated by the other terms in Eq. (1). Drier soils and less greenery impact on the Bowen ratio (H_s/H_l) since more energy is spent to heat up the surface rather than being redistributed into latent heat flux (Jin et al., 2011). The presence of greenery, in turn, may have countervailing effects on the formation of UPIs. While being beneficial against temperature-enhanced chemistry, plants are BVOC-emitters. BVOCs are secondary metabolic products that protect plants from high-temperature stress (Sharkey and Yeh, 2001), whose contribution may be especially high in marine and tropical environments. Indeed, the volatile emission of dimethyl sulfide from coastal areas is been reported to be sufficiently high to affect global budgets (Rinnan et al., 2014). The availability of aerenchymatous plants affects the net emission: these species have developed aerenchyma in their roots and shoots through which they can conduct air into their rhizosphere where gases like methane and other VOCs are produced. This system represents a fast transport for produced gases into the atmosphere (Joabsson et al., 1999). The sensible-latent heat balance is also affected by the variety of meteorological phenomena that occurs in the urban airshed including the heat island circulation (HIC), land and sea breezes, mountain and valley flows. Typically, under intense urban heat islands, local near-surface centripetal winds advect the encountered pollution during the travel from surrounding areas and maintain it in suspension (Padmanabhamurty and Hirt, 1974; Yoshikado and Tsuchida, 1996).

All these phenomena make urban areas not just receptors but also drivers of climate change impacts (Wilby, 2008). The result is that, with the ongoing expansion of large conurbations and megacities, major disruptions in the biogeochemistry of the local atmosphere, in the regional precipitation patterns and in the radiative forcing will be recorded (Folberth et al., 2012; Givati and Rosenfeld, 2004). The impacts will be especially severe in tropical, developing countries, where nearly 90% of the next-coming urbanization processes is expected to occur and where industrialization and vehicular availability are predicted to rise exponentially with no countermeasures currently in place (Emmanuel, 2005; Parrish and Zhu, 2009; Escobedo et al., 2011). The superposition of overheated and polluted conditions will exacerbate people vulnerability to each single threat (Lai and Cheng, 2010; Meng et al., 2012; Burkart et al., 2013), which makes disentanglement and/or two-way mitigation of both phenomena a high priority.

Against this backdrop, many questions are currently subject of international research. To help disclose the multiple phenomena behind the strong linkage between UHI and UPI and move towards cohesive and effective coping strategies, this review offers itself as a compendium of the most representative studies on the topic in the latest 30 years.

The structure of the paper is schematized in Fig. 1: the inclusion criteria are first presented and justified (Section 2), then a synthesis of the evidence is presented to determine geographical, climatological and methodological patterns (Section 3). Detailed content analysis is conducted according to five prominent topics (Section 4): i) the role of UHI on temperature-dependent chemistry, ii) the daytime/nighttime variability in the UHI-UPI interaction, iii) the role of urban geomorphic types, forms and growth schemes, iv) future challenges and potential exacerbation of both heat islands and pollution levels and v) primary and secondary effects of UHI mitigation on urban air quality. By amalgamating results and observations, opportunities and challenges towards a two-pronged action against both UHI and UPI are delineated. This will help governments and urban planners to deliver coping strategies and precautions.

2. Review methods

The method by Pickering and Byrne (2014) was used to screen the existing knowledge on the link between UHI and UPI in search of patterns, methodological trends and climate dependencies, drawing on five main databases (ScienceDirect, Scopus, Google Scholar, PubMed and Web of Science). The search was systematically conducted by looking for keywords obtained by coupling the urban-related and air quality-related taxonomy reported on the left and right side of Fig. 2, respectively. The analysis was then conducted on the manuscripts that respected the following inclusion criteria:

- written in English, to focus on literature of international impact;
- pertaining to the last 30 years (1990– March 2020), namely since when the term UHI started to be widely used, to keep track of both pioneering works and most recent developments;
- specifically addressing the link between UHI and UPI. Urban temperature and urban forcing were considered proxies for UHI when the heat island was not explicitly quantified. Health-focused manuscripts, only mentioning the heat island effect, were excluded;
- contemplating experimental observations in real urban scenarios. Wind tunnel or lab investigations were excluded;
- in case of multiple publications by the same authors or research groups, only one/two studies conducted from substantially different perspectives were retained;
- for multi-city studies, the largest one was used for reference whenever easily identifiable.

According to the above criteria, a total of 40 manuscripts was selected for in-depth analysis (reported in Appendix), while >200 were mentioned or outlined to corroborate the main findings and show the volume of back-up literature. The size of the circles in Fig. 2 is proportional to the number of instances including each different lemma in their title, keywords or abstract, among the 40 manuscripts.

3. Synthesis of evidence

The considered papers were published in 29 journals. In detail, 12.5% were published in Atmospheric Environment, 10% in Science of the Total Environment and 7.5% in Journal of Geophysical Research. The dominant disciplines are boundary-layer meteorology, biometeorology, atmospheric chemistry and applied geography. While the conceptual

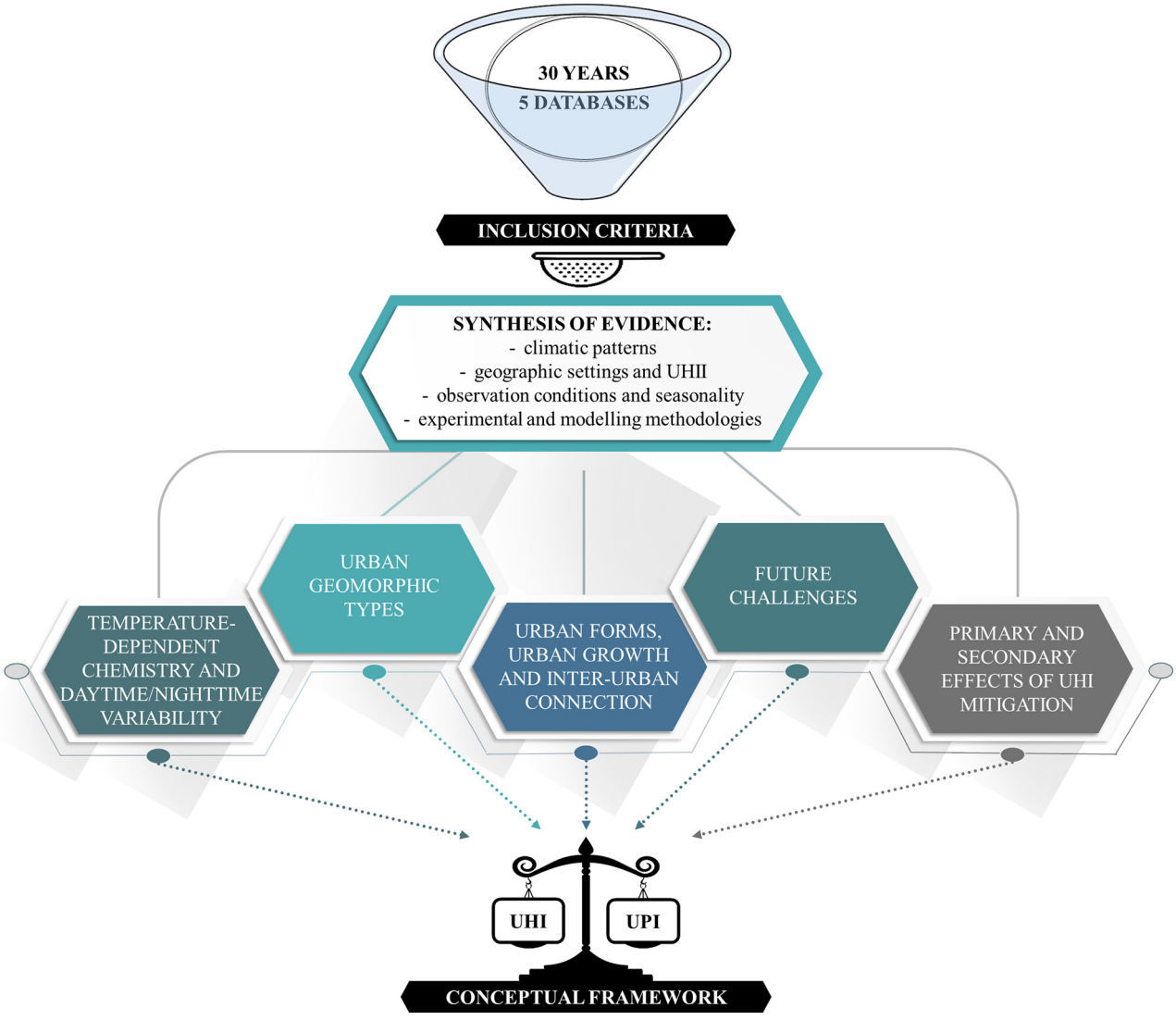

Fig. 1. Schematics of the structure and contents of the present review.

basis was laid in the 1990s, the interest in the topic has been increasing almost linearly over the last decades (13 papers in the 2000–2010 decade and 24 papers in the 2010–2020 decade), owing to both technological advancement (in terms of sensing instruments and computational power) and increased social concern (escalation of heat waves, weather extremes and mortality rates). The reported average UHII varies between slightly negative values and 6 °C, with an average of 1–2 °C, while the peak UHII touches 12 °C in (Stathopoulou et al.,

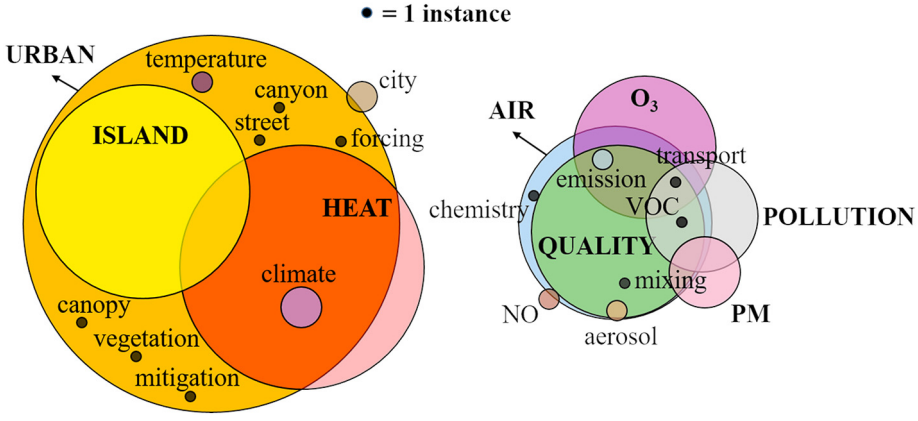

Fig. 2. Lemmas used to scan the databases and relative occurrence. UHI taxonomy (left side) was combined with air quality taxonomy (right side).

2008) fluctuating on mean values of about 3–5 °C. Nine papers refer to surface urban heat island (SUHI), while all the others deal with atmospheric urban heat island (AUHI). This is highlighted in Table A1. Most papers detailed accurately the panorama of land use and land cover (LULC) in the considered geographic settings. Some of them discretized the domain in >15 LULC types (Li et al., 2018; Jin et al., 2011; Merbitz et al., 2012). Most papers focused on summer conditions (47.5%) and among them >40% limited the analysis to clear sky conditions. Another 40% developed year-round assessments, while few instances covered other seasons, such as winter (2), autumn (2), spring (1) and wet/dry season (1). The reader is referred to Table A1 in Appendix for further details, including the list of observational data reported in each of the analyzed manuscripts. Table A2 focuses on simulation-based studies and specifies software, spatial and temporal domain, input data and parameterizations. Non-hydrostatic, mesoscale models are the most used, with the Weather Research and Forecasting model WRF at the forefront, usually coupled with the atmospheric chemistry model Chem or the Community Multiscale Air Quality Model CMAQ, the Land Surface Model Noah and the building effect parameterization + multilayer building energy model (BEP + BEM). The spatial domains typically comprise 3 or more nested telescopic domains of <30 km horizontal resolution and tenths of vertical layers reaching up to 100 hPa (Khiem et al., 2010). Other than sensitivity analyses on the inputs, several parametric analyses are conducted, mostly on scenarios of i) emission control and urbanization (Yoshikado and Tsuchida, 1996; Martilli et al., 2003; Rendón et al., 2014; Taha, 2015), ii) heat flux change (usually obtained by replacing urban land with cropland or by integrating anthropogenic sources or by changing the soil moisture level) (Sarrat et al., 2006; Khan and Simpson, 2001; Chen et al., 2011; Zhu et al., 2015; Huszar et al., 2020), iii) different circulation, vertical diffusion (Wilby, 2008; Huszar et al., 2020) or wind intensity (Krüger et al., 2011; Swamy et al., 2017) and iv) future UHI/UPI exacerbation and/or mitigation (Taha, 2015; Fallmann et al., 2016; Epstein et al., 2017; Taha, 1996).

In terms of geographical coverage, investigations from 16 different countries around the globe are reported in this review. The vast majority focuses on heat and pollution islands in the United States (20.5%), with three studies dedicated to the city of Los Angeles, two to the city of Atlanta and other single instances to the cities of Sacramento, San Francisco, Fresno, Houston and Oklahoma. One manuscript covers 45 cities in the USA territory (Stone, 2008) by statistical means. The second, most targeted countries are Greece and Germany (both accounting for 12.8%) with special emphasis on the cities of Athens (3 studies), Thessaloniki and Volos (2 studies) as for Greece and the cities of Berlin, Stuttgart, Trier and Aachen as for Germany. Another 10.3% of the observations took place in China (notably in the Yangtze River Delta and the Pearl River Delta Greater Bay Area) and in France, with the cities of Shanghai and Paris holding particular interest (3 studies each). Significant contributions to the investigation of heat and pollution triggers in urban settings are also reported in India (7.7%), Japan and Australia (5.1%) as well as in Brazil, Colombia, Czech Republic, Iran, Poland, Taiwan, Tanzania and the United Kingdom, yet to a lesser extent (2.5/2.6%). From a climatological perspective and considering the updated Köppen-Geiger classification by Peel et al. (2007), the interlacement between urban heat and pollution appears to find fertile ground in temperate oceanic climates (Cfb) across Europe, most likely due to the extensive urbanization, the frequency of heat waves and the complex interaction between land and sea breeze. On the other hand, humid climates with subtropical and Mediterranean nuances (Cfa and Csa classes) stimulated almost half of the revised investigations. These climates are typically characterized by extremely hot summers, anticyclonic conditions, low inversion and low wind speeds conducive to both heat and pollutants entrapment. Another 12.5% of the observations is related to type A climates (Aw, Af and Am) in the low-latitude belt around the Earth where high solar irradiation is recorded throughout the year and significant day/nighttime and seasonal temperature fluctuations are ascribed to trade winds, intertropical convergence and monsoons. The large availability of solar power co-triggers photochemical chemistry (hence higher ozone levels) and heat absorption by conventional urban materials. Few studies focus on warm-summer humid continental and Mediterranean climates (Dfb and Csb), cold semi-arid climates (BSk) and dry-winter humid subtropical climates (Cwa). The geographic and climatological distribution is displayed in Fig. 3, along with the percent occurrence of each Köppen-Geiger class. To further strike connections between urbanization and magnitude of the UHI-UPI link, the size of the circles is proportional to the population of each investigated city at the time of the observation. Three studies involving extensive clusters of >25 cities in China and the United States were not included in the figure for the sake of clarity (Stone, 2008; Wang et al., 2018; Cao et al., 2016).

4. Contents overview

In this section, each of the 40 publications selected for detailed analysis is accurately discussed according to the dominant topic ranging from daytime/nighttime variability, urban form and growth patterns, future drivers and countervailing effect of heat mitigation techniques.

4.1. Temperature-dependent chemistry and daytime/nighttime variability

In 1990, Cardelino and Chameides posed the basis and the method for the analysis of temperature-induced direct and indirect effects over ozone pollution, focusing on: i) enhancement of ozone photochemistry owing to temperature-enhanced thermal decomposition of peroxyalkyl nitrates (Carter et al., 1979); ii) enhancement of BVOCs emissions from trees in their growing season (highly reactive olefinic hydrocarbons) (Tingey, 1981); iii) enhancement of evaporative anthropogenic hydrocarbon emissions from motor vehicles (Halberstadt, 1989) and nitrogen oxide emissions from air conditioning (Cardelino and Chameides, 1990). Empirical evidence from 9 years of observation for the city of Atlanta confirmed a positive linear association between temperature and ozone. The temperature during ozone-event days (ozone exceeding the 120 ppvb NAAQS limit) was higher than on non-event days by 3.1 °C, on average. By numerical modelling, the authors simulated 5 scenarios of emission control and urbanization effects. The base case was a 50% VOCs reduction. When a 20% natural emissions reduction was additionally considered (scenario 2) the ozone production was strongly mitigated and always stayed below the limit. The counteracting effect of the average summertime UHI (2 °C) was investigated by progressively adding the 3 afore-mentioned temperature-induced mechanisms (scenario 3 to 5). Scenario 5 totally compensated the benefit achieved in scenario 1. This entails that a 2 °C UHI can cancel out the ozone benefit of a −50% VOC policy. The simulations were later repeated by considering a different base case (NO_x reduction in place of VOC reduction). Significantly lower ozone maxima were identified, suggesting that NO_x abatement could be a more effective strategy. As remote sensing started being extensively used in climatology, further evidence was collected and other players in the UHI-UPI interaction were identified (e.g. water vapor). For instance, in (Jin et al., 2011), the authors examined the interlink between heat and pollution islands in Shanghai by combining land skin temperature, albedo AOT, water vapor, cloud fraction and land cover satellite data (MODIS). In addition, ground instantaneous, continuous AOT (AERONET) observations were used to pinpoint the diurnal, seasonal, and inter-annual variations. Finally, monthly ERA-40 reanalysis from the European Centre for Medium-Range Weather Forecasts (ECMWF) were considered to track the regional wind circulation. Over an eight-year horizon (2000–2008), the AOT for Shanghai exceeded that of the rural regions on both monthly and instantaneous scale. Abrupt changes occurred, mostly after rainfall events and after high traffic hours. The monthly AOT gradually increased from January to June and then sharply dropped due to the onset of the rainfall season. Strong differences in terms of cloud fraction and water vapor emerged between Shanghai and rural

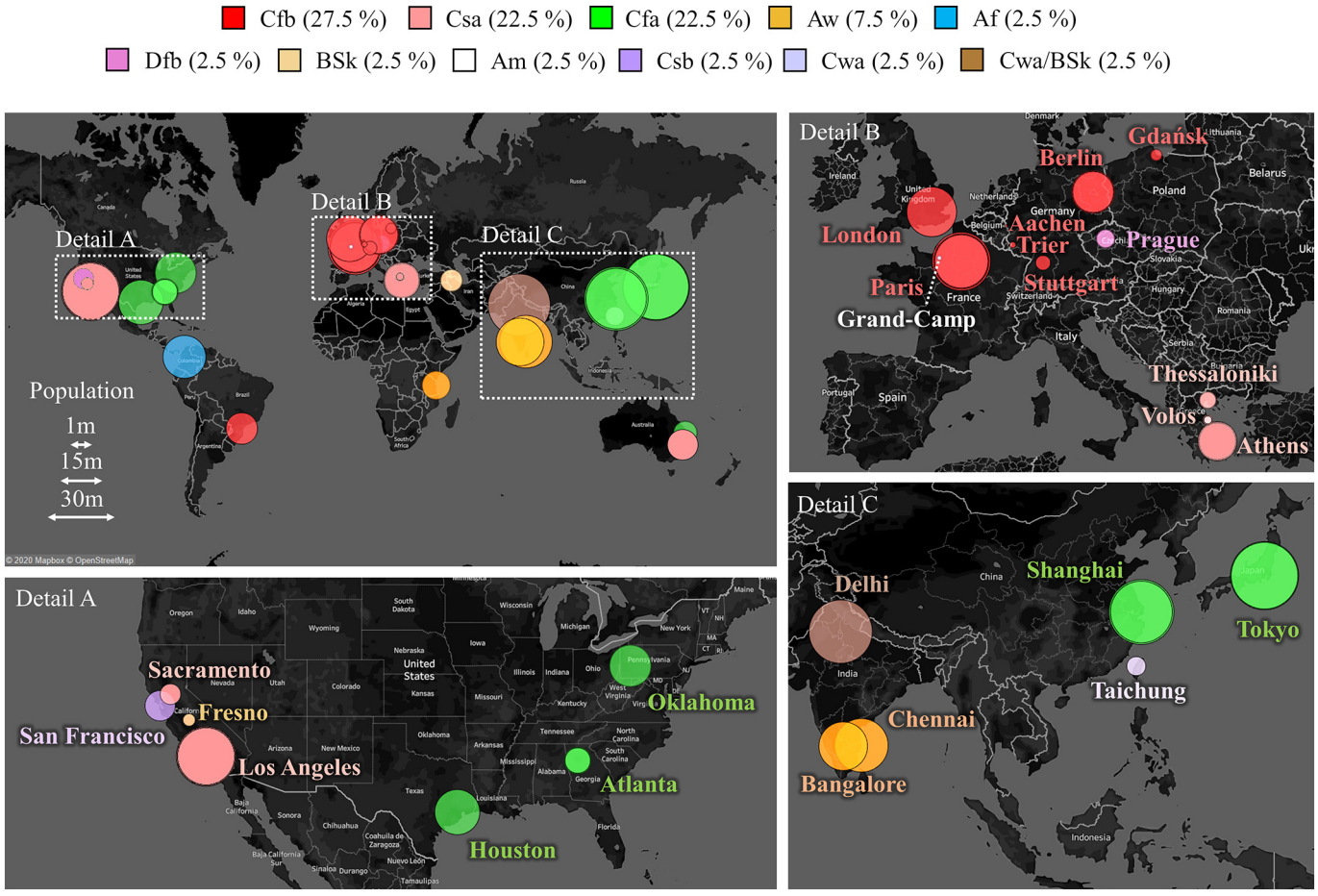

Fig. 3. Geographic distribution, climatic classification and population data for each analyzed city: Details A, B, C are close-ups on United States, Europe and East Asia, respectively.

regions as a result of higher aerosol concentration (more condensation nuclei) and land skin temperature. Similarly, in Delhi (Pandey et al., 2012), daytime cool islands (maximum intensity of 4–6 °C) over the central urban area emerged in contrast with an equally intense nighttime heat island (maximum of 4–7 °C), strongly related to massive emissions of waste heat due to vehicular, industrial activities, and poor soil moisture. In their study, the authors retrieved satellite thermal maps of the area, surface wind data from the local airport meteorological station and PM2.5 concentration from the Central Pollution Control Board, and field monitored the solar spectral irradiance at 4 sites. Observed daytime cool islands peaked under low wind conditions and clear sky conditions. It was inferred that the attenuation of incoming solar radiation by the aerosol layer outweighed the absorption of the outgoing long-wave radiation during daylight hours. These findings perfectly match those by Singh et al. (2005), Jin et al. (2010) and Ramanathan et al. (2005) who associated the surface cooling to the solar dimming induced by the "Asian Brown Cloud" (namely a dense layer of black carbon, organic carbon and dust as well as sulfates, nitrates, and fly ash) over the Indian subcontinent. The authors also observed that, immediately after an intense rainfall episode over Delhi, the difference in the surface temperature as well as incoming solar radiation was much attenuated, possibly due to the cleansing effect of raindrops. Same equalizing effect was found on windy days. Significant negative/positive correlations were identified between aerosol optical depth and day/night time surface temperature, respectively. In the same vein, a recent paper published in Nature Communications (Cao et al., 2016), brings up evidence in favor of the long-held hypothesys that the biogeochemical effect of city haze pollution contributes to the UHI. The authors utilized satellite observations (MODIS) from 2003 to 2013 combined with climate model calculations to quantify such a contribution in 39 cities across China at night. The UHII was magnified by 0.70 ± 0.26 °C in semi-arid urban sites. Humid and semi-humid climates were less sensitive to the longwave radiative forcing of coarse aerosol, in agreement with (Jonsson et al., 2004). High mean nighttime surface UHI and weak daytime surface UHI were identified, regardless of the annual mean precipitation (Zhou et al., 2014). The spatial nocturnal variations were significantly correlated to the AOD difference between urban and surrounding rural areas, implying that thicker haze was precursor to stronger UHI. Such correlation vanished in the daytime. The authors concluded by associating the accelerated warming in China (nighttime temperature increase per decade twice the global mean) to haze pollution. Following a similar approach, Li et al. used multiyear satellite observations of LST and AOT and in-situ measurements of PM10, air temperature, incoming radiation, clouds and wind speed at twelve stations (details in Appendix) to establish potential UHI-UPI interactions for the city of Berlin, Germany (Li et al., 2018). Notably, LST and air temperature were used as proxies for surface and atmospheric UHI (SUHI and AUHI, respectively) whereas PM10 and AOT were proxies for near-surface and atmospheric pollution (NSUPI and AUPI, respectively). The urban-rural difference was investigated in terms of incoming solar radiation and atmospheric longwave radiation. Prominent findings can be summarized as follows: i) AUHI and NSUPI were negatively correlated as higher temperatures strengthened the turbulent dispersion and enhanced the boundary layer height in agreement with (Fallmann et al., 2016; Wagner and Schäfer, 2017), ii) the response of urban surface materials to the AOD-induced change in net solar radiation was strong in the nighttime and weak in the daytime due to lower energy redistribution factor and longwave component

dominance in the balance (as in (Cao et al., 2016)), iii) the UPI-induced different net solar budget reflected in up to +12% higher SUHI, iv) SUHI was higher in the daytime and lower in the nighttime, contrary to AUHI. The study considered only clear days and low wind speeds (<3 m/s). Hence, more stable wintry conditions with weaker turbulent mixing were not considered and advection of heat and pollution was disregarded.

The source of pollution is also a key player in such dynamics. Jonsson et al. (2004) delved into the typical patterns of different sources of pollution as a function of four climatic parameters: UHI intensity, air temperature, relative humidity and wind speed. The monitoring campaign took place in the city of Dar es Salaam, along the Tanzanian coastline. The authors stressed the fundamental difference in anthropogenic air pollution compared to industrialized countries that lies in the dominance of bushfire and fuelwood emissions rather than transport/industry. Biomass, industry, sea spray, soil and traffic were the broad source categories considered in the study, respectively linked to the presence of potassium, zinc, chlorine, titanium and lead in fine and coarse particulate matter, measured by means of a dichotomous impactor and energy dispersive X-ray fluorescence technique. The field campaign captured both rainy and dry season nuances. The authors found that, at the rural site, industry particulate was dominant during the day, while, at the urban site, anthropogenic pollutants (biomass + industry + traffic) were dominant during the night. Pollution was intensified within the urban fringe especially in the dry season. Statistically speaking and due to increased atmospheric stability, the nocturnal UHI intensity was positively correlated with particulate levels, in contrast to wind speed which was strongly negatively correlated. Local large emission sources might further complicate the investigation. In (Plocoste et al., 2014) the specific case of urban sites close to landfill was examined. Landfills are major sources of organochlorine, aldehydes and aromatic VOCs formed by aerobic fermentation. UHI intensity up to over 4 °C was measured in inhabited areas attached to a wide landfill in Guadeloupe, from 8 measurement sites, representative of the 4 main LULCs (urban, mangrove, landfill and suburban). The UHI intensity was negatively correlated with nebulosity and Tradewinds speed. More in detail, daytime UHI was strongly mitigated by the unstable atmospheric conditions produced by 6 to 10 m/s Tradewinds, while reached its maxima under low wind speeds (<2 m/s) and clear skies (nebulosity<4 octa). Conversely, at night, the UHI engendered a surface convergent flow responsible for higher nocturnal pollution. Landfill-specific VOCs were measured overnight at 15 sites and tracked. Concentrations greatly increased when 1 m/s heat island breezes formed in response to 3.5–4 °C UHI intensity.

As a rule of thumb, the UHI-UPI interaction shows pronounced differences in the daytime and nighttime (Oke et al., 2017). Nocturnal ozone can be depleted by NO_x titration ($NO+O_3 \rightarrow NO_2 + O_2$) and dry deposition in the nocturnal boundary layer but not in the nocturnal residual layer, which emphasizes the importance of vertical mixing on surface-residual layer coupling (Zhang and Rao, 1999; Klein et al., 2014). Conversely, in the daytime, the reaction tends to be balanced by NO_2 solar photolysis (Pulikesi et al., 2006), except in the immediate vicinity of very large emissions of NO (e.g. power plants). Indeed, one of the pivotal factors driving photochemical reactions is high energetic shortwave radiation (Seinfeld and Pandis, 2016). Dry and wet deposition phenomena are critical too, as they represent the main sinking processes through which the atmosphere cleans itself. The former occurs at the ground surface (e.g. soil or vegetation), and the latter at the contact with water droplets (e.g. rain or fog) (Zannetti, 1990). To elucidate these time-specific mechanisms, in (Sarrat et al., 2006), Sarrat et al. coupled a mesoscale meteorological and chemical model (Meso-NHC) with the Town Energy Balance (TEB) to verify how nocturnal and diurnal UHI and other urban effects impinged on primary and secondary regional pollutants. A 2-day anticyclonic episode with abundant solar radiation and low-speed wind of about 2 m/s was considered, ideal scenario to analyze the atmospheric pollution dynamics over a large urban area. Two heat flux scenarios were considered: URBAN (with TEB, urban surface), NO-URB (without TEB, natural surface). In the nighttime, UHI and pollution events were primarily of thermal origin, associated with a convergence area south-west of Paris. The effect of the synoptic wind was to displace the UHI-induced plume of warm air above the surrounding suburban areas. In the daytime, the urban processes were dominated by thermal and dynamical effects. The NO_x spatial distribution was sensitively impacted by the modification of the atmospheric boundary layer induced by the UHI and the roughness of the urban fabric. Much milder was the effect on ozone concentration. In the urban areas, the dominant nocturnal budget term for NO was the kinetic energy (destructive term) that prevented its near-ground accumulation, whereas for O_3 the dominant mechanisms was deposition (destructive term) followed by chemical processes on par with turbulent mechanism (destructive and constructive terms, respectively). In agreement with several studies (Neu et al., 1994a; Jacobson, 2001; Lai and Cheng, 2009), the authors reported how the day-after spatial distribution of the ozone fields was strongly influenced by the nocturnal pockets contained in the residual boundary layer. Finally, they calculated the VOC/NO_x ratio concluding that, in Paris, the regime of ozone production is NO_x-limited in the urban plume and in the suburban areas and becomes VOCs-limited in the rural areas, thus paving the way towards targeted pollution abatement strategies. Overall, the study highlights the positive effect of urban turbulence on pollutants dispersal under low-speed winds and clear days. (Klein et al., 2014). This was already pinpointed in 1994 by Neu et al. who showed that half of daytime pollution events in the Swiss plateau were associated with the downward mixing of ozone from the residual layer (Neu et al., 1994a) proving that vertical mixing processes could outweigh chemical production and advection. Similarly, in (Swamy et al., 2017) an attempt was made to delineate the influence of UHII and mixing height on local air quality by studying the diurnal variation of secondary pollution levels in the Indian city of Chennai, affected by heavy traffic emissions, poor dispersion, and regional transport of pollutants. Three locations were simulated with ENVI-met, accounting for different sky view factors (0.357, 0.546, 0.711) and land use (background, commercial and residential). Under four velocity profiles (from 0.2 to 5 m/s), the UHII (calculated between commercial and background sites) reached 0.54 °C, 0.77 °C, 0.79 °C, and 0.64 °C in terms of daytime average and 0.35 °C, 0.57 °C, 0.59 °C, and 0.53 °C in terms of daily average. The UHII increased for wind speeds up to 2 m/s with the highest temperatures corresponding to flat mixing layers, usually occurring after sunset. Indeed, if sunlight prevails in the ozone photochemical formation during the day and especially at midday, nocturnal ozone is strongly associated with local temperature and thus with UHII. Further, WRF-Chem modelling and measurements by Klein et al. (2014) proved that near-surface ozone concentration were enhanced by mixing processes occurring when the nocturnal atmospheric boundary layer was unstable, because of i) increased dispersion of nitrogen oxide responsible for ozone titration and ii) downward motion of ozone from the residual layer to the ground. The authors focused on a peculiar airflow pattern that is typical of U.S. Southern Great Plains: the formation of nocturnal low-level jets (LLJs). LLJs are fast-moving fluid ribbons that form in the atmosphere caused by the cooling of high-elevation air relative to air at the same geopotential height further away and deflected by the Coriolis force. LLJs are thus associated with sloping terrains and are especially efficient at advecting heat and promoting vertical mix. They are also responsible for the initiation of long-lived mesoscale complexes bringing heavy rainfall overnight. In terms of pollution, it was observed that the expected decreased ozone levels overnight were frequently interrupted by secondary peaks whenever the stability of the boundary layer was jeopardized by strong vertical wind shear. The highest values were associated with LLJs owing to both strong long-range transport and accentuated coupling with the residual layer, since the emission rates were identical for each simulation. Correlations were established between nocturnal wind speed and ozone concentration during nights

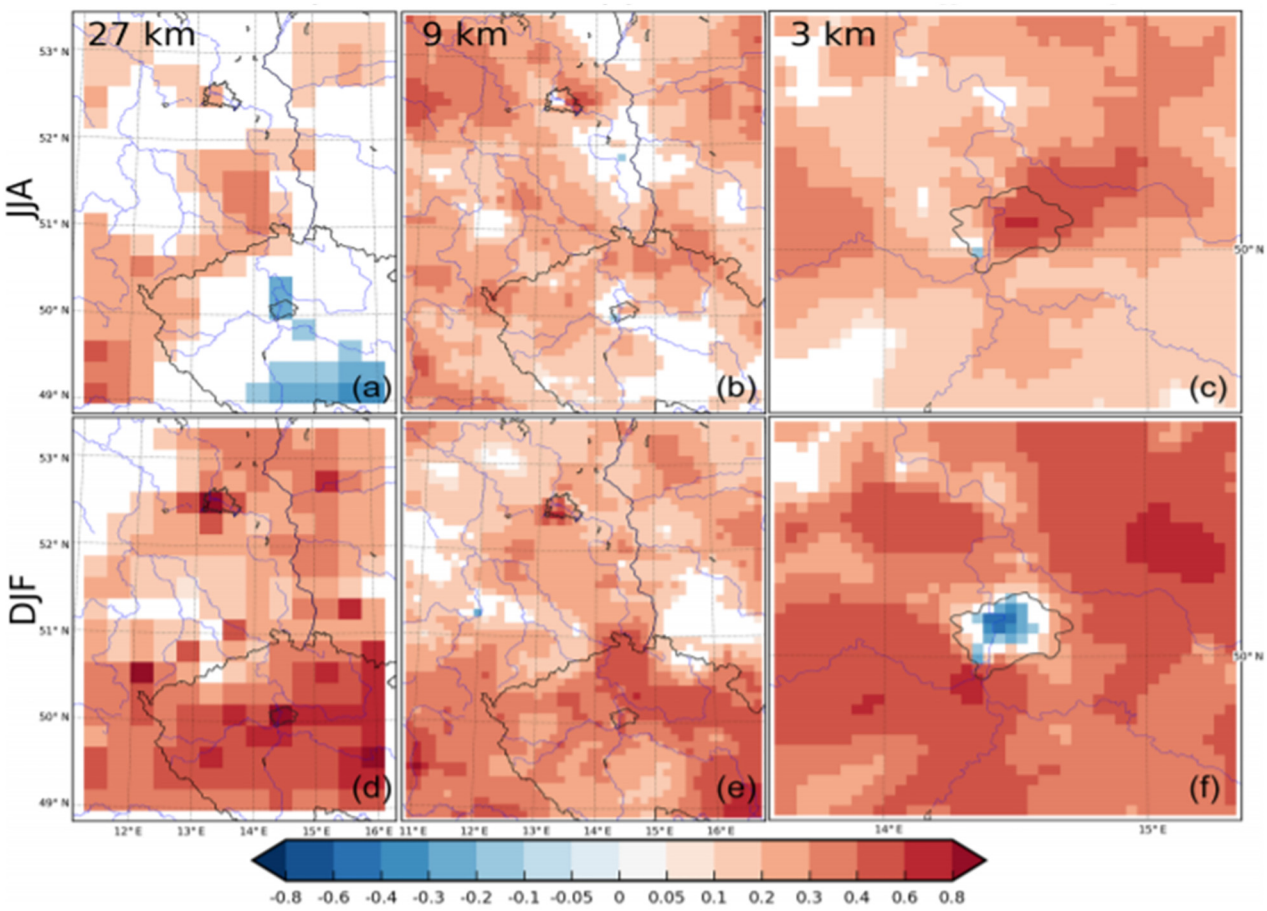

(a) Spatial changes in O_3 in Jan (ppb)

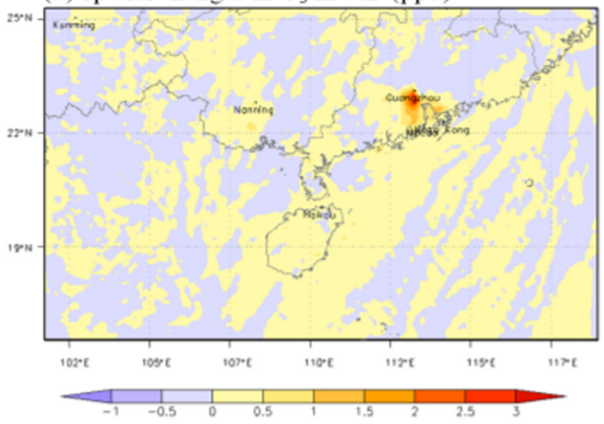

(b) Spatial changes in O_3 in Jul (ppb)

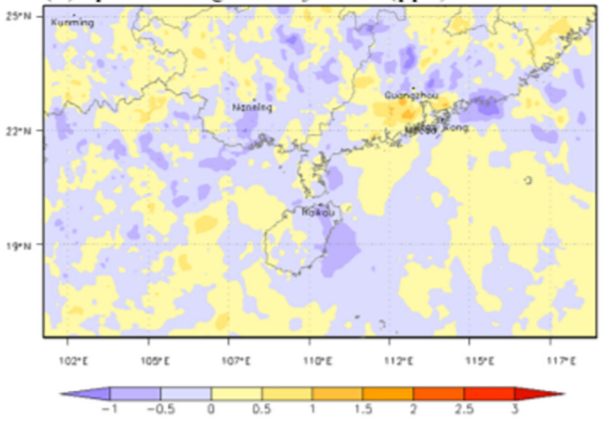

(c) Vertical changes in O_3 in Jan (ppb)

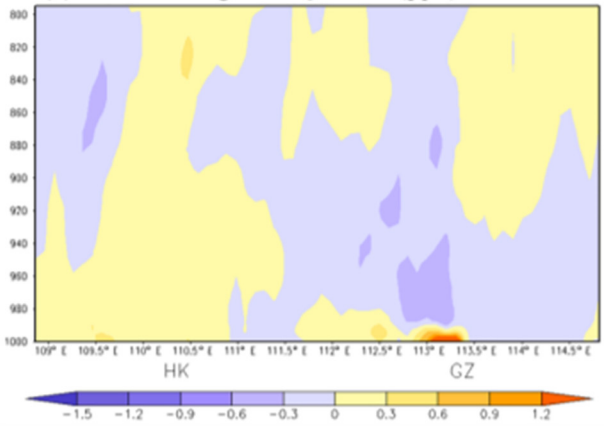

(d) Vertical changes in O_3 in Jul (ppb)

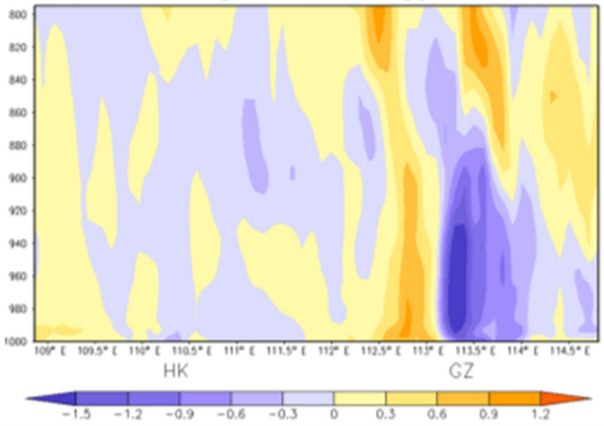

with higher and sustained winds. A co-effect of LLJs is to reduce the contrast between urban and rural temperatures (Hu et al., 2013a): the mean UHI intensity at 9 m height was reported at 2.48 °C on low-LLJ nights and dropped down to 0.88 °C on high-LLJ nights. Strong jets impact on rural nocturnal boundary layer making it deeper and less stable, thus cancelling or mitigating the onset of UHI. Hence the stronger UHI signature that typically emerges overnight was attenuated in concomitance with LLJ's peaks. This specific meteorological context is thus conducive to counter effects in terms of UHI and UPI. Similar LLJ impacts are reported by Reitebuch et al. in an urban park in Essen, Germany, based on ground-level meteorological and air quality measurements (Reitebuch et al., 2000). However, the impact of synoptic weather patterns on daytime/nighttime UHI/UPI evolution is rarely addressed. Another notable instance is the short communication by Lai and Cheng (2009). The authors combined ground-level meterological and air quality data (PM10, PM2.5, CO_2, CO, SO_2), wind field profiles from tethersonde monitoring (at 6 vertical levels between 0 and 1000 m) and air pollution simulations (TAPM model) to pinpoint which synoptic weather conditions worsened UHI and air quality in the Taiwanese city of Taichung. Through statistical analyses, the authors related UHI intensity to concomitant and day-after pollutants concentration. Out of the 13 weather patterns, those typified by anticyclonic conditions, low inversion layer and clear convergence phenomena occurring overnight were conducive to accumulation of ozone precursors and other pollutants (NO_2, CO_2, CO) as well as to severe UHI events. These patterns impacted on the lee cyclogenesis at micro scale thus resulting in high ozone concentrations (Lee et al., 2000). Furthermore, leeward low-pressure systems formed favoring high cloudlessness and thus UHI magnification. UHI intensity and air pollutions were not clearly associated in the daytime. In colder areas, more residual ozone existed as less NO was available. Conversely, intense UHI, occurring at night, tended to reduce ozone, exhausted by NO, while increasing its precursors due to convergent phenomena. As a result, high O_3 levels were recorded on the following day, when despite low daytime UHI, abundant sunlight and NO_2 stimulated the production. This confirms the 1996 results by Yoshikado and Tsuchida (1996). The study was then expanded to link air quality, UHI and respiratory hospitalizations in 29 districts (Lai and Cheng, 2010). GIS was used to determine the spatial links. The heat stress and worsened air quality mostly affected youngsters' health. GIS had already been used by Dousset and Gourmelon to analyze the physical processes that determined the near-surface heat fluxes and their impact on ozone concentration in Paris by combining statistics of thermal infrared images, near-infrared and visible SPOT-HRV images and in-situ data (Dousset and Gourmelon, 2003). The results show the contrast between intense nocturnal UHI and many distinct microclimates during the day associated with local surface properties. Upward LST trends were paralleled by ozone concentration variations.

The role of mixing height and turbulence induced by the urban heat island on the up/downtrends of urban pollution is extensively covered by the studies of Huszár et al. (2018); Huszar et al. (2020). In a recent comprehensive publication, the authors designed a suite of simulations all over Europe (focus on the cities of Prague and Berlin) and all over the seasons by coupling the Regional Climate Model (RegCM4) and the Comprehensive Air Quality Model with Extensions (CAMx). The aim was to investigate the vertical turbulent effect of the urban canopy meteorological forcing on ozone and PM2.5 dispersion by considering: i) cascading domains (of 27, 9, and 3 km horizontal resolutions), ii) urban VS rural land cover and iii) six different calculation methods for the vertical eddy diffusion coefficient (Kv). Again, the presence of the urban canopies is simulated using the "annihilation method", namely by replacing urban surface with rural surface most typical for the surroundings (Baklanov et al., 2016). The presence of urbanized land resulted in a pronounced temperature increase (up to 2 °C), wind slowdown (by up to 2 m/s), and Kv enhancement under all considered calculation methods (from nearly 1 up to 30 m^2/s at the surface and 100 m^2/s at higher elevations). This trend propagated to pollutants' dispersion, with ozone increasing by 0.4 up to 4 ppbv (maximum 10% difference between summer and winter) and PM2.5 decreasing by up to 1–2 $\mu g/m^3$ in summer and winter, respectively. By isolating each forcing contribution and then merging them together (see Fig. 4), the authors could verify how enhanced vertical eddy diffusion easily upends the thermal, hygrometric and fluid dynamic effects composing the urban forcing signature, although temperature's influence increased overnight. Similar results on the impacts of different urban canopy forcing on regional climate and air quality are further reported by Liao et al. for the Yangtze River Delta, by means of WRF/Chem simulations (Liao et al., 2014), by Kim et al. for the Greater Paris area, by means of Polair3D/Polyphem simulations (Kim et al., 2015) and by Li et al. for Southern California, by means of WRF/Chem+UCM (Li et al., 2019a). Analogous results are also reported for the Pearl River Delta Greater Bay Area in China as a result of the mutual interconnectedness among cities (Li et al., 2016; Zhu et al., 2017). Notably, in (Zhu et al., 2017), the authors investigated and quantified the multifarious effects of urbanization in the area via WRF/Chem by comparing post and pre-urbanization conditions in wintertime (January) and summertime (July). The results can be summarized as follows: i) sensible heat flux +40 W/m^2 and +80 W/m^2, ii) latent heat flux −50 W/m^2 and −120 W/m^2, iii) 2-m air temperature +1–2 °C, iv) planetary boundary layer height +150 m and +300 m, v) 10-m wind speed −1.2 m/s and −0.3 m/s, vi) 2-m specific humidity −0.8 g/kg and −1.5 g/kg with precipitation +120 mm in summertime, vii) surface concentrations of PM10–40 mg/m3 and −80 mg/m3, viii) O_3 surface concentrations +6 ppb and +12 ppb. Very similar results were obtained by Xie et al. (2016) in the same region, same historical period and same modelling platform (WRF/Chem), yet with special focus on the role played by anthropogenic heat and emissions (estimated at 0.87 W/m^2 in rural areas and up to 60 W/m^2 in urban areas). The results are showed in Fig. 4. Urban-enhanced vertical eddies are also found to drive SO_2 dispersal (Chen et al., 2014), whereas primary and secondary organic aerosols (POAs and SOAs) exhibit dissimilar patterns (Janssen et al., 2017): POAs get diluted under intense urban forcing, while SOAs accumulate owing to downward transport from the residual layer. This holds true as long as the emission rates are assumed constant during higher/lower UHI episodes. Otherwise, a competition is established between urban-induced near-surface dilution and urban-induced increased emission. This is highlighted by Zhong et al. in their evaluation of the UHI-UPI interaction in the megacity cluster of the Yangtze River Delta (Zhong et al., 2018; Zhong et al., 2017). They performed a suite of simulations of the air quality impacts of urbanization and anthropogenic emissions via WRF-Chem model coupled with an urban canopy model. The land-cover change stimulated a sizeable reduction of near-surface aerosol concentrations, counterbalanced by more polluted air masses at higher altitudes over the surrounding rural areas. Nonetheless, when the increase in aerosol emissions was taken into account, the net result was reversed, with increases in surface particle concentrations of up to 50 $\mu g/m^3$. Despite these studies don't quantify the urban heat island effect, they thoroughly represent the link between pollution and the change of land-use from natural to artificial surface induced by urban expansion, which is also cause to UHI onset. Similar results are further reported by Liao et al. (2014).

Fig. 4. Urban forcing and ozone pollution. Top picture: the total impact of urban meteorological changes (i.e., temperature, humidity, wind and vertical eddy diffusivity) on near-surface ozone concentrations (in ppbv) for 27, 9 and 3 km resolutions (left to right) during 2007–2011 summers and winters (indicated with JJA and DJA, respectively). Reproduced with permission from (Huszar et al., 2020) © Author(s) 2020. Bottom picture: impacts of anthropogenic fluxes on near-surface ozone concentrations (in ppb): (a,b) and (c,d) show the spatial and vertical distribution of monthly-averaged ozone differences with and without anthropogenic fluxes, respectively, in January (a,c), and July (b,d). Reproduced with permission from (Xie et al., 2016) © Author(s) 2016.

4.2. Urban geomorphic types

In this subparagraph the link between UHI and UPI is discussed in relationship with the local landscape (continental, coastal, valley-like, mountainous).

Several studies aimed at investigating how geolocalization impinge on UHI/UPI. In 1996, Yoshikado and Tsuchida (1996) presented strong evidence of exacerbated pollution episodes when wintertime small-scale sea breeze coupled with urban heat island circulation into a persisting convergence zone over Tokyo Bay. The authors examined air temperature, wind and pollution (PMs, NO_2, O_3) data from a number of urban, suburban and rural sites. Heavily urbanized areas tended to be systematically more polluted, while the temperature difference between less urbanized sites tended to level out. A positive correlation was established between vertical stability and urban pollution. Warm southwesterly winds were associated with both higher UHI and poorer air quality, while northern winds (winter monsoon) exerted a cleansing effect near the surface. On highly polluted days the UHI intensity could exceed 5 °C. Ozone increased in response to vertical air exchange and divergence between seaward breeze and westward inland wind, while very similar patterns were identified between PMs and NO_2 with maxima generally recorded in the morning and in the evening. PMs and NO_2 peaked in response to traffic density and the establishment of a stable layer in evening hours. The afternoon decrease was jeopardized on sea breeze days. Two types of severe air pollution events were discerned and associated to the presence of sea breeze: a synchronous type that occurred in the frontal area over the urban center and a delayed type that occurred on the second or a later day due to the accumulation of pollutants in the air mass floating over the bay before the onset of the sea breeze. This is in agreement with (Lai and Cheng, 2009). The authors concluded that "the winter sea breeze possesses a characteristic of the heat island circulation" thus creating a convergence zone that persists for several hours.

The role of sea breeze is also the focus of a 2011 study by Chen et al. (2011). The authors adopted a single-layer UCM coupled to Noah in WRF to investigate the impacts of UHI, land-sea circulations, sea surface temperature (SST) and soil moisture on the formation of stagnant air masses within the urban fringe. A pollution episode associated with weak synoptic forcing and persisting heat wave in Houston, USA was selected for the investigation. A detailed calibration of the model allowed accurate prediction not just of the wind rotation around the city core, but also of the typically destructive interference between large-scale background flows and sea breeze which results in the buildup of high ozone concentrations. The authors reported on the additional challenge of capturing the wind patterns when the sea breeze manifests in two or more components (e.g. land-bay and larger-scale land-gulf). The model, calibrated on data from 29 stations and six wind profiles, was used to conduct three numerical experiments by replacing i) daily with hourly SST data, ii) urban lands with croplands and iii) soil moisture realistic values with two capacity extremes (completely dry and completely wet). It was demonstrated that: i) SST strongly influenced the meteorological conditions along the coastline; ii) urban roughness smoothed the vigor and the penetration of the sea breeze thus proving that the effect of higher surface friction outshone that of higher water-land temperature gradient, iii) dry soils promoted higher daytime temperatures due to lower evaporative cooling, yet lowered the nighttime temperatures owing to the reduced thermal conductivity. Overall, the city was found to favor stagnant and thus polluted conditions by destructive interference between background winds and sea breeze and by higher roughness-induced wind breaking, especially when the root zone soil moisture approached the wilting point.

Another investigation of sea breeze role over UHI/UPI is reported by Stathopoulou et al. for the greater Athens area (Stathopoulou et al., 2008). They used data from 23 meteorological stations (out of which 3 were also used to get ozone, NO and NO_2 concentrations) to establish statistical correlations between air temperature and pollution in urban and photochemically polluted areas. In detail, seven stations were placed in the central urban area, fifteen radially covering the bordering suburbs and one served as reference rural station. Compared to greener suburban areas, the city center appeared less polluted. The authors posited that the ozone generated over the sea and advected towards the city could better penetrate the shoreline and the further inland areas, bypassing the city center due to the interaction with the UHI circulation. A neural-network approach based on both ambient temperature and ozone precursors returned accurate predictions of the ozone level ($R^2 = 0.89–0.94$), with slight reductions (11–30%) when temperature was the only input. A key role on diurnal ozone levels was thus ascribed to thermal contrasts, assuming temperature as a proxy for solar radiation. Concerning Greece again, Poupkou et al. studied the interlink among Discomfort Index (DI), Common Air Quality Index (CAQI) and UHI in the Greater Thessaloniki Area, where NO_x emissions from road/maritime transport and industrial activities variously combine with transboundary transport of gaseous pollutants and aerosols from Central and Eastern Europe and dust advection from Sahara (Poupkou et al., 2011). Three main pollutants (ozone, NO_2 and PM10) were measured together with temperature, relative humidity, wind speed and direction at four sites representative of trafficked urban, urban industrial, rural industrial and suburban conditions. The temperature difference between the trafficked urban and the rural locations was used to calculate the UHI. Collected data covered a 9-year period from 2001 to 2009. At the urban stations, poor air quality was the most frequent condition (45%) while medium quality levels dominated outside the urban fringe (50.2%–54.7%). PM10 was the major contributor. O_3 played a significant role only in summer and in spring. Furthermore, very polluted days (CAQI ≥76) were associated with stagnant conditions under light sea breeze (0.5–3.6 m/s). Discomfort was strongly related to high pollution: 67% of the occurrences were recorded under high and very high CAQI values. Additionally, as the air temperature went above the seasonal mean, the probability of high DI values soared, with a minor role played by relative humidity.

A similar perspective on coastal cities is given in (Khiem et al., 2010) for the central Kanto area of Japan. Using both measurements and numerical simulations (MM5/CMAQ model), the authors determined heat/pollution correlations via multiple linear regression analysis. Extensive datasets were used to analyze the long-term variation in summer-averaged daily maximum ozone (21 years, 34 monitoring sites) as a function of summer-averaged daily maximum temperature and wind speed (21 years, 1 monitoring site). The short-term variations were analyzed as well, by considering additional measurements (daily averaged values) over one single summer month. Up to 84 and 70% of the long-term and short-term summer variation in peak ozone concentrations could be described by changes in meteorological conditions. The interaction between HIC and sea breeze was identified as the major driver for daily variations in ozone distribution (see Fig. 5). Tokyo's HIC strongly prevented the penetration of the sea breeze inland and favored severe ozone accumulation. Furthermore, when the sea breeze was stronger, as during the morning, the high-ozone air masses formed over the urban area moved inland, sweeping the northwestern regions. This study complements the wintertime results by Yoshikado and Tsuchida, previously mentioned (Yoshikado and Tsuchida, 1996).

In (Khan and Simpson, 2001) the authors analyzed the complex UHI-UPI nexus in southern hemisphere subtropical climates (Brisbane, Australia). Local natural and man-made features promoted sea-breeze circulations, mountain valley airflows and the heat island effects, all contributing to transport, entrapment and dispersion of pollutants. A mesoscale hydrostatic model, (described in detail in (Pielke and Mahrer, 1978)) was used to track the air flows generated by differential surface heating and terrain irregularities and was modified to incorporate anthropogenic heat fluxes and heterogeneous surface characteristics. Anthropogenic heat release was dominated by motor vehicles. Three numerical experiments were conducted on a typical summer day potentially conducive to high pollution (sunny, light winds):

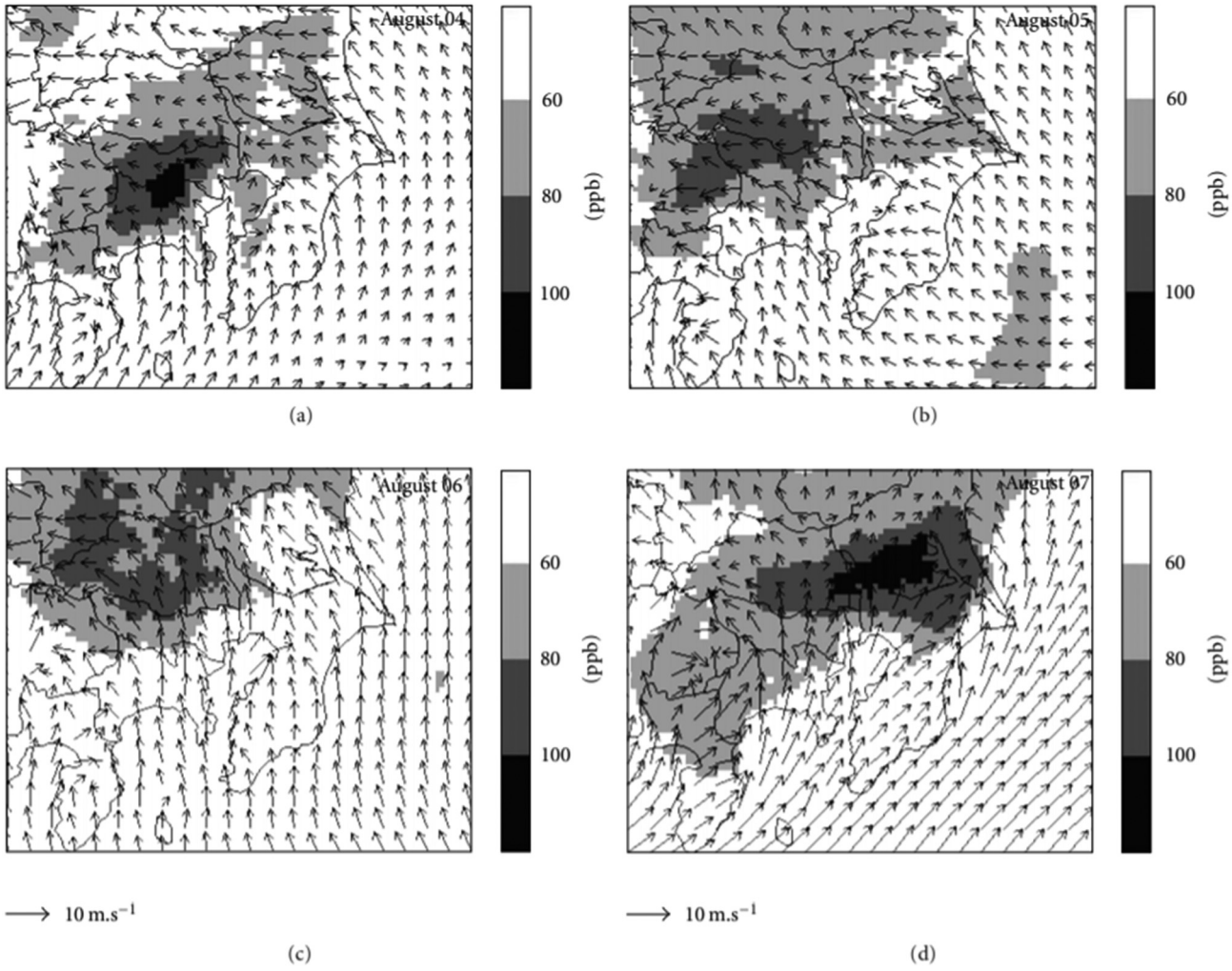

Fig. 5. The impact of wind patterns on near-surface pollution: ozone spatial distribution (in ppb) under various local circulations at 2 pm during August 2005 over the Kanto area. Reproduced with permission from (Khiem et al., 2010) © 2010 Mai Khiem et al.

1) disregarding UHI and anthropogenic heat, 2) reintroducing UHI, 3) contemplating both UHI and anthropogenic heat. Only in experiment 3) good agreement was achieved with the measurements at two sites (urban/industrial and suburban). In this scenario, during hours of intense anthropogenic heat release, i) a strong convergence zone formed over the urban core, ii) the sea breeze moved inland faster towards the city and iii) winds over the city were sustained during the night. Cumulatively, the UHI increased by 5 °C. Apparently, a vicious loop was established between UHI, convergence and pollutants emission. The authors concluded that urban areas characterized by anthropogenic heat fluxes in the order of 60–70 W/m^2 would exhibit a variety of sizeable effects on local weather phenomena.

From a numerical perspective, Martilli et al. highlighted the need for a detailed urban surface exchange parameterization to capture the structure of the turbulent layer above a city and the impacts of land/sea breeze, opining on the limits of standard mesoscale models built on constant flux-layer and surface energy budget assumptions (Martilli et al., 2003; Martilli, 2002). The author's urban parameterization (detailed in (Martilli et al., 2002)) was integrated with a non-hydrostatic, Boussinesq and anelastic mesoscale model to account for i) the vertical structure of the turbulent field in the urban roughness sublayer, ii) the modification of the length scale that limits the turbulent kinetic energy in the canopy layer and iii) the shadowing and radiation trapping in street canyons. The coastal city of Athens was considered due to the high level of pollution and nocturnal UHII (8–10 °C), further aggravated by low synoptic forcing. The urban detailing allowed to depict all major transport and dispersal mechanisms. The most sensitive parameters were nighttime temperature (differences up to 3 °C compared to undetailed urban parameterization) and ozone concentration (difference up to 30 ppb) in response to deviations in wind speed, turbulence intensity, heat flux, nocturnal land breeze intensity, timing, duration and extension of sea breeze. During the night, ozone precursors were trapped in a shallow layer close to the city surface, transported by the land breeze. Given the high NO availability, urban ozone was mostly destroyed by titration. The highest ozone concentrations were recorded in response to the sea breeze arrival, with peaks measured close to the front. This was associated with the photochemical transformation of the pollutants emitted the previous night and stored over the sea. Urban details were also responsible for modifications in type and spatial extension of the ozone chemical regimes: NO_x-saturated areas tended to be more extended and more intense with a mix of NO_x-limited and NO_x-saturated areas over the sea, not apparent in the rural-type simulation. The model neglected latent fluxes and biogenic emissions.

Different, yet as much complex is the UHI-UPI interaction in mountain, hill and undulated sceneries. In 2003, a study on the urban climate and air quality in Trier, Germany focused on the blend of limited ventilation, UHI capping effect and altered thermal stratification in a valley (Junk et al., 2003). The study was motivated by the frequent complains issued by the local citizens about uncomfortable microclimatic

conditions and insufficient air circulation, especially during calm autochthonous weather. An extensive monitoring network was deployed: meteorological data were retrieved from 8 weather stations, while air quality data (including NO_2, SO_2, CO, O_3 and PM10) were retrieved from 3 stations. On top of that, mobile meteorological and air quality data were collected by an instrumented van. The UHI was quantified at 1.2 °C on average and peaked at 2.6 °C. High NO_2 emission rates were detected in the morning at rush hours when the mixing layer was stable and low. As the layer labilized before noon reaching the valley rim, NO_2 abruptly inverted its increasing trend due to enhanced vertical turbulence. Concomitantly, ozone production outweighed its depletion, especially under clear-sky, photo-oxidative conditions. The vertical mix quieted later in the afternoon. Nightly second peaks in NO_2 and O_3 were associated with evening rush-hours, nighttime stabilization and with the inflow of ozone-enriched catabatic cold air. The authors concluded that "the complex interaction between orography, city building structure, land use, anthropogenic emissions and boundary layer controls the air quality in Trier".

Indeed, valleys are especially interesting contexts since peculiar and tangled is the interplay between UHI, orographic barriers and temperature inversion (Haeger-Eugensson and Holmer, 1999; Savijärvi and Liya, 2001; Romero et al., 1999). Such intricate scenario was thoroughly investigated by Rendón et al. (2014). The authors simulated a reference urban valley inspired by the Colombian Aburrá metropolitan area to investigate the impact of increasing urban land cover from 0% (rural) to 100% (urbanscape from valley to mountain top) by means of a non-hydrostatic model in terrain-following coordinates that uses a reference passive tracer representative of urban pollutant emissions in Eulerian-Lagrangian approach. The urban fraction and related SUHI were found to dictate i) the formation, lifetime and breakup pattern of the temperature inversion, ii) the evolution of the cross-valley wind system form a confined to an open system, iii) the reversal of the slope winds and iv) the formation of smog traps. The temperature inversion, in turn, was strongly related to the accumulation/dispersion of pollutants in the valley, together with upslope flows and emissions (Malek et al., 2006). Below 20% urban cover, the inversion layer was intact. Increasing urban areas engendered: i) higher surface temperatures that speeded up the destruction of the inversion layer in agreement with (Bader and McKee, 1985; Anquetin et al., 1999; Colette et al., 2003), but up to a saturating percentage (around 80% of urban surface); ii) stronger vertical mixing due to the UHI-induced buoyant thermals; iii) the onset of downslope winds (for medium urbanization percentages) opposed to the convective flow over the core and of upslope winds when the urban land covered the sidewalls and provoked subsidence warming over the valley center; iv) higher morning pollutant concentrations along the slopes, countervailed by lower afternoon levels, after the inversion breakup. The 40% urban cover was the most penalized in terms of air quality due to the combined effect of high urban emissions and temperature inversion persistence. A following manuscript by the same authors reinforced how valley ventilation deteriorates if the inversion layer remains unbroken with pollutants trapped within a closed slope-flow circulation (Rendón et al., 2015). It was thus proved that urbanization is key factor to the microclimate and air quality of mountain valleys. UHI-induced circulation dominates the flow field above the valley floor through a mix of convergence, rising motions and compensating downslope winds, all leading to poor air quality. This is in agreement with analysis for the city of Santiago, in Chile (Romero et al., 1999).

4.3. Urban forms, urban growth and inter-urban connection

Beyond the geographical context, urban design and urban growth are key players in the mutual intensification of UHIs and UPIs. Indeed, as the number and distribution of urban patches changes along with urbanization, so does the temperature distribution within the city and intercity (Wang et al., 2018). To name one mechanism, sprawling cities characterized by high-rise, packed buildings favor stagnation and thus aggravation of both UHI and pollution (Khiem et al., 2010). This was investigated in 2008, by Stone, who examined the link between the sprawling characteristics of 45 large USA metropolitan regions and the UHI/UPI patterns over 13 years (1990–2002) (Stone, 2008). Four measures of urban sprawl (centeredness, connectivity, density and land use mix) were individually tested and then lumped into a composite index (proposed by Ewing et al. (2002)) to gauge the overall influence of urban form on NAAQS annual ozone exceedances, ozone precursors emission and heat island promotion. Density emerged as the most impactful urban form predictor: for each standard deviation increase, a 19% reduction in the mean tonnage of ozone precursors and a reduction of ozone exceedances of about 16 days was observed per year, on average. Decentralized development demonstrated to be conducive to ozone formation and to a greater number of ozone exceedances compared to compact urban textures. The most sprawling cases could experience up to 62% more high-ozone days. As well stressed in the abstract, "this relationship was found to hold when controlling for population size, average ozone season temperatures, and regional emissions of nitrogen oxides and volatile organic compounds, suggesting that urban spatial structure may have effects on ozone formation that are independent of its effects on precursor emissions from transportation, industry, and power generation facilities". This significant result may support the hypothesis that the urban spatial texture impacts on air quality also through non-emissions-related mechanisms (Romero et al., 1999). In the same vein, in (Lo and Quattrochi, 2003), the authors analyzed the ramifications on UHI, pollution and health of the intensive LULC change the city of Atlanta underwent between 1973 and 1998 to accommodate almost twice the original population. The 119% increase in the periurban low-density urban use produced a distinct increase in surface temperature and UHI while reducing the Normalized Difference Vegetation Index (NDVI). These impacts were strongly correlated to VOCs and NO_x emissions and, in turn, to enhanced ground-level ozone production. VOCs and NO_x closely tracked the spatial patterns of surface temperature and NDVI, increasing significantly with the former and decreasing with the latter, whereas ozone accumulated when a UHI-induced convergence zone formed over the urban areas. UHI was also found to initiate and/or enhance urban precipitation (with urban pollutants acting as condensation nuclei) owing to roughness-induced surface convergence and instability caused by urban heating (Braham et al., 1981; Bornstein and Lin, 2000). This is in line with (Diem and Mote, 2005), where the fast-paced development and growing heat island in suburban Atlanta was associated with a 40% increase in heavy rainfall events in 50 years.

At local-scale, anthropogenic activities and their urban distribution also play a role. This is described in (Feizizadeh and Blaschke, 2013). The authors integrated Spectral Mixture Analysis and Endmember Remote Sensing Indices to investigate the relationships between land use/land cover, land surface temperature UHI and air pollution, using ASTER thermal remote sensing satellite images and eight ground-based PMs measurement stations. The Iranian city of Tabriz was discretized in 8 LULCs. The two most intense UHI zones were identified at the Tabriz' petrochemical industrial site and at the bazar market area in the central part of the city. The same areas, although inverted in order, were associated with the highest PM levels. Hence, a high correlation between highly air-polluted areas and UHI zones was established, denoting how high population density, fervent commercial activities and heavy traffic were major drivers of severe pollution concentration. Moreover, in (Krüger et al., 2011), the authors presented an experimental and numerical approach to determine how urban morphology, changes in microclimate and air quality relate within a city center. Measurements took place in the first pedestrian street built in downtown Curitiba, Brazil over 14 sunny days throughout year 2009, to cover a wide range of air temperatures, wind patterns, solar angles and heights. Daytime UHI was maximum 2.2 °C. Simulation were additionally performed in ENVI-met to investigate the impact of prevailing winds and street orientation on the dispersion of traffic-generated NO_x. Four

simulation scenarios were considered accounting for minimal (0.3 m/s) and average wind speeds (1.4 m/s) in perpendicular and longitudinal direction to the main street axis. The greatest pollutant accumulation corresponded to perpendicular low-speed winds, under minimal easterly wind. In general, wind speed was more impactful than wind direction on pollutants dispersal.

On another note, in densely inhabited cities, ozone regime is usually (VOC)-limited (or NOx-saturated) owing to strong volatile organic carbon conditions. Conversely, in the downwind region, the regime gradually shifts to NO_x-limited (or VOC-saturated) thus boosting ozone production rates (Kley, 1997). Smaller cities downwind of large conurbations may thus result even more polluted due to the urban land forcing, precursors emissions and heat island circulation. This is addressed in a recent (2018) study by Wang et al. (2018). The authors focused on the transport patterns of intercity heat energy and air pollution by looking at the triangle-shaped megalopolis of Yangtze River Delta, one of the fastest-growing, densest inhabited and most extensively built regions in China that encompasses Shanghai, the Jiangsu Province and the Zhejiang Province. Multi-source remote sensing data, (land cover, LST, NDVI and elevation) were combined with extensive measurements, including hourly ground-level O_3 and NO_2 at a total of 139 monitoring stations. The results can be summarized as follows: i) the average hourly O_3 concentration was 61.83 μg/m^3, hitting higher values at coastal stations rather than those inland, ii) the average daytime UHII was 1.24 °C, positively correlated with ozone concentration, especially in the cities at the core of the cluster; iii) surface landscape, topography and population favored the concerted action of UHI and UPI.

The extremely sensitive topic of inter-urban land surface forcing is further detailed by Zhu et al. considering the influence of Shanghai over the downstream city of Kunshan (Zhu et al., 2015). The authors expanded the study by Kang et al. (2014) by combining WRF model, CMAQ air quality model, Noah land surface scheme and the aforementioned multi-layer Building Effect Parameterization (BEP) developed by Martilli et al. (2002). Physical and chemical processes included chemistry, total advection, vertical diffusion and dry deposition. Simulations were replicated with and without Shanghai's urban forcing (urban land replaced with cropland). During the high-pressure episode considered in the simulation, the strong horizontal advection of warm air from Shanghai onto Kunshan caused an increase in Kunshan's surface air temperature by 0.5–3 °C. A pronounced difference in terms of air circulation was also observed: the presence of the city mitigated the wind speed by 3–4 m/s and favored the onset of a convergence zone. The maximum differences in terms of wind speed and boundary layer (nearly 300 m) occurred in the afternoon and evening. Owing to the strong heat island circulation, the horizontal transport of ozone and its precursors was, at the same time, suppressed in the lower boundary layer (by 2ppbv on average) and emphasized in the upper boundary layer (by up to 40ppbv) where the ozone photochemical regime was NOx-limited. These findings are aligned with those by Zhang et al. who reported on how upstream urbanization exacerbated UHI and could cascade well downwind during heat wave episodes in the Baltimore metropolitan region (Zhang et al., 2009; Zhang et al., 2011). In this perspective, decentralization and sprawl may also expand the influence area of UHI-associated pollutant downwind transport.

4.4. Future challenges

All future climatological scenarios point towards remarkably higher temperatures, increased downward solar radiation, lower likelihood of precipitation and higher likelihood of air stagnation, which converge into stronger UHI-UPI interactions (Leung and Gustafson, 2005; Langner et al., 2005; Livada et al., 2019). Besides, higher temperatures and irradiance result in increased emission of biogenic VOCs and enhanced photochemical processes that prelude to ozone formation (Sillman and Samson, 1995). Another well-acknowledged future trend is the increase in magnitude and frequency of heat waves. The annual number of days falling into this category is escalating (Hayhoe et al., 2004; Meehl and Tebaldi, 2004; Habeeb et al., 2015) and even conservative outlooks suggest an increase of associated mortality and morbidity (Abadie et al., 2019). This tandems with the forecasted increment of pollutant emission levels, especially ozone (Huszar et al., 2011; Pyrgou et al., 2018). Furthermore, heat waves impact not just on higher energy consumption and consequently higher emissions of greenhouse gases, but also on forest fires, wilted crops, reduced photosynthesis flux, droughts, boundary layer anomalies and thereby, on air quality (Garcia-Herrera et al., 2010; Ciais et al., 2005). Extremely hot, persisting events reinforce temperature inversions that trap pollutants near the surface, as well documented for the European summer heat waves of 2003 (Stedman, 2004; Mangold et al., 2011; Mues et al., 2012; Solberg et al., 2008) and 2006 (Struzewska and Kaminski, 2008).

In this perspective, Wilby investigated the future urban heat island and peak ozone concentration in the city of London for a medium-high (A2) emission scenario for the 2050s (Wilby, 2008). He used the technique of statistical downscaling, a hybrid of regression-based and stochastic weather generator from four different general circulation models, GCMs (NCEP, CGCM2, CSIRO Mk2, ECHAM4). Predictor-predictand statistical correlations were calibrated on almost 40 years of data (1961–1990). In August, nocturnal UHI was positively associated with the 850 hPa geopotential height and negatively associated with the near surface vorticity, relative humidity and airflow. On the other side, the maximum 15-minute ozone concentration was strongly positively associated with the mean regional temperature at 2 m and strongly negatively associated with the near-surface relative humidity. Hence both predictands were reduced under humid conditions. The main results for 2050 can be summarized as follows: i) all GCMs projected intensification of the nocturnal UHI between May and October but disagreed on the trend during the rest of the year, ii) all GCMs identified pollution-favoring weather patterns in stagnant anticyclonic conditions, iii) statistical downscaling tended to truthfully reproduce means and peak timing while underestimating the peak values and the compounding effects of long lasting heat waves. The author stressed the importance of serial correlation, especially for summer ozone concentration given the dependency from previous day's concentration as documented also elsewhere (Sarrat et al., 2006; Neu et al., 1994a; Jacobson, 2001; Lai and Cheng, 2009). The mean maximum ozone increase was 12 ppb comparable to that found by Knowlton et al. for New York City (Knowlton et al., 2004). This combines with the results of a previous study, according to which by 2080, a disproportionate increment in high-UHI nights (UHI > 4 °C) would occur (+40% relative to 1961–1990), with an increase in nocturnal UHI of 1 °C even assuming unchanged anthropogenic heat sources, population and infrastructure (Wilby, 2003). Similar results are also reported by Rosenzweig et al. in New Jersey (Rosenzweig et al., 2005).

In (Papanastasiou et al., 2015), Papanastasiou et al. studied the synergy between urban pollution and extreme hot weather. They monitored air quality at three sites in Athens (city center, near the city center, suburb), two in Thessaloniki (city center, suburb) and one in Volos (city center), selected for the heterogeneity in population and spatial coverage. The authors focused on the difference between heat wave and non-heat wave days during the 2001–2010 summers. The analysis was based on O_3, NO_2 and PM10 at up to six urban and suburban sites. Temperature and relative humidity were monitored in the three city centers. Air quality degraded during heat wave days. PM10 showed the highest sensitivity, increasing by 25%–38%, followed by NO_2 (14%–29%). In contrast, ozone's increment didn't surpass 12%. The minima were recorded at the suburban stations. These findings complemented the results of a previous study in the city of Volos (Papanastasiou et al., 2010). Again, the authors found that the major pollutions events in 2007 summer coincided with heat wave events, when also UHI reached a high. A causal link was established between the presence of low-speed sea breeze and higher aerosol concentration (by up to 31%) due to i) the development of an internal boundary layer in the marine

air mass that hampered any efficient vertical diffusion of pollutants and ii) the increased production of secondary aerosol from gas-to-particle conversion processes (Boy, 2002), strongly enhanced by sea breeze-like mesoscale circulations. These findings are in line with those by Colbeck et al. (2002). A study by Theoharatos et al. (2010) confirmed the negative effects of the synergy between extreme high temperatures and excessive pollution levels during the same heat wave also for the city of Athens.

Another intense heat wave swept across Europe in July 2010. An investigation by Czarnecka and Nidzgorska-Lencewicz (2014) in Gdańsk (Poland's principal seaport and core of the country's fourth-largest metropolitan area) pointed out the strengthening between UHI and UPI. The authors statistically assessed the interrelation between UHI (measured between the urban centre and three different suburban stations) and urban pollution based on hourly measurements of air temperature, relative humidity, wind speed and pollutants composing the Common Air Quality Index (CAQI), namely NO_2, O_3, CO, PM10, PM2.5 and SO_2. The UHII peaked at over 4 °C, mostly shaped by local circulation and sea breeze. Correlation analysis and linear regression revealed the significant interlink between UHII and each analyzed pollutant, although, generally, the highest significance was manifested with a 1–5 h delay, with characteristics depending on time of the day and specific pollutant.

The superposition of UHIs and UPIs is thus very likely to characterize the future scenarios worldwide, with major repercussions on people vulnerability (Lai and Cheng, 2010; Meng et al., 2012; Burkart et al., 2013). These concerns are raised by Merbitz et al. (2012) who aimed at identifying hot spots with high health risks for distinct groups of urban population, based on temperature and PM concentration measurements coupled with geo-statistics. They examined several locations in the City of Aachen, Germany, different in density, greenery, topography and traffic to identify predictors for the onset of potentially critical conditions. ArcGIS and Matlab were adopted: circular buffers of 200-to-800 m size were applied to investigate the influence of different neighborhoods and distances from emission sources. For both temperature and PM contents, the strongest impacts of influencing factors were found within several hundred meters (200–400 m for temperature, 400–800 m for PMs), in accordance with previous research (Johnson et al., 2010; Hoek et al., 2008). Out of 19 influencing factors, five showed the most significant correlations and were used as spatial predictors. Land use, canopy height, building area and degree of surface sealing were best predictors for both hot and polluted spots, whereas population and traffic kernel density were significant to temperature and PMs respectively. Areas exceeding the 80th and 90th percentile (P80, P90) of each predictor were considered at high risk of air pollution and heat stress and mostly overlapped the major traffic lines. Healthier areas corresponded to extended greenery. For risk-enhanced zones, estimation of vulnerable people exposure was carried out: 15/13% of the population exposed to over P80/P90 levels was over-65. Toxicological analyses revealed that accumulation of health-threatening species (e.g. metals and polycyclic aromatic hydrocarbons) was likely associated with temperature stress.

Bushfires are among the calamitous events that are envisioned to escalate in the future due to global and local climate change. The drawbacks in terms of UHI and UPI were recently investigated by Ulpiani et al. (2020). The authors carried out an environmental and air quality monitoring campaign in the inner west of the city of Sydney, during the massive bushfires that afflicted Australia between December and January 2020. Under a combination of extreme pollution, heat waves and drought, a suite of dependencies could be established: i) near-surface particulate matter tended to accumulate within specific thermohygrometric ranges adverse to deliquescence as found in (Monn et al., 1995; Csavina et al., 2014) and under the transport of sea breeze; ii) high PM concentration were likely recorded in the nighttime/early morning, especially after daytime heat waves; iii) PM-rich atmosphere attenuated UV radiation maintaining the UV index under health-threatening levels in line with (Kalashnikova et al., 2007; Chubarova et al., 2012; Urmy et al., 2016); iii) heavy rain splashing generated the most intense concentration of dust due to the ejection of submicrometre organic matters from the soil surface into the air (Wang et al., 2016; Cotrufo et al., 2015); iv) a steady and accentuated UHII emerged, in contrast with the historical trends due to the change in radiative forcing and the disappearance of any cool island events. It was thus demonstrated that during days of high pollution, rich in particulate matter, the UHI was exacerbated, providing fertile ground for increased mortality and morbidity rates. Some of the above results are displayed in Fig. 6.

4.5. Primary and secondary effects of UHI mitigation

In light of the above considerations, the quality of life and the health conditions of urban populations, especially high-sprawl ones, would plummet in a BAU scenario (Wilby, 2008). Mitigating the UHI effect curtails the demand for cooling energy in commercial and residential buildings with reduction in emissions of CO_2 and smog (Santamouris et al., 2018). Since ozone is formed when its precursors (NO_x and VOCs) photochemically react with heat and solar radiation, actions taken to mitigate urban overheating are in principle strongly beneficial in terms of air quality too (Gorsevski et al., 1998). Nonetheless, well-established mitigation technologies and techniques (e.g. highly reflective surfaces, greenery, water features) usually do not limit their action to sensible cooling, but may variously alter the local thermal and chemical balance. By way of example, Table 1 demonstrates the intricate and countervailing effects of tree planting on UHI and or UPI and vice versa: changes in albedo, evapotranspiration, roughness and canopy alter air temperature, relative humidity, solar budgets, wind speed and chemistry at the local scale. The product of the interaction between vapor pressure deficit, air temperature, stomatal conductance, tree hydraulic status, soil water availability and wind speed must be carefully evaluated (Block et al., 2012). This applies to most mitigation strategies.

Several papers tackle the controversial question of whether urban heat island mitigation impacts positively or negatively on local pollution. EPA has teamed up with NASA and LBNL since 1998 to untangle the knot (Gorsevski et al., 1998). Negative impacts are intimately related to the reduced vertical mixing that comes with air cooling. As air layering is more stable, primary pollutants (SO, NO) tend to remain close to the ground sources from where they are emitted. Nonetheless, the net effects are strongly connected to the specific mitigation strategy.

Trees are generally found to deflate both primary and secondary pollutants in cities. Already in 1996, Taha investigated the impact of increased urban vegetation on ozone concentration throughout the South Coast Air Basin (SoCAB) in California (Taha, 1996). He numerically explored the temperature and air quality impacts of a 1% and 2% increase in urban vegetation considering low, medium and high BVOCs-emitting species. Low-emitting species release <2 and 1 $\mu g g^{-1} h^{-1}$ (micrograms per gram of dry-leaf mass per hour) of isoprene and monoterpenes, whereas high-emitters' release is of about 20 and 5 $\mu g g^{-1} h^{-1}$, respectively. The concentration of different species was modelled according to turbulent dispersion, chemical reactions, man-made and natural as well as mobile and stationary emissions, and deposition on the vegetative canopy. The temperature drop amounted to 1.5 °C on average with peaks of 3.5 °C. A net ozone reduction was achieved with low-emitters only. Planting medium and high-emitting trees negatively impacted the air quality. At peak smog hour (3 pm) a 1% increase of low-emitting species reduced the population-weighted ozone exceedance exposure by 11% (NAAQS threshold considered), while an equal increase of medium-emitting species upturned the benefit into a +9% penalty. This has implications for the future selection of species used for biofuels or urban tree planting (Stewart et al., 2003). In the same vein, in (Vailshery et al., 2013), the authors explored the impact of street trees on mitigating daytime temperatures and on improving the air quality in Bangalore. Second fastest growing city in India with technologically intensive industries, highest national

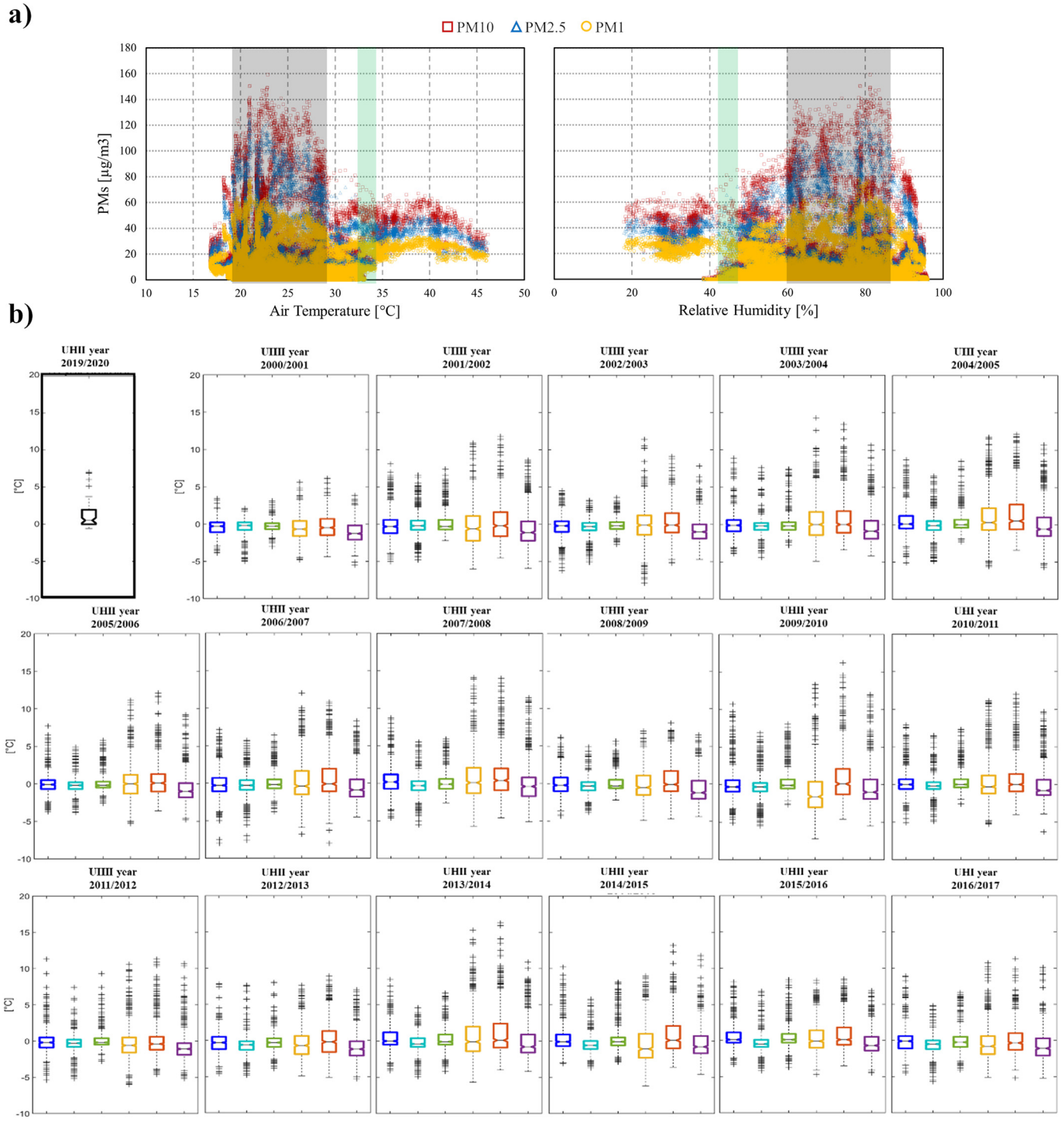

Fig. 6. Effect of intense combined weather extremes (bushfires, heat waves and drought) on near-surface pollution, reported for the city of Sydney during the 2019/2020 bushfire season: a) thermohygrometric conditions conducive to high PMs and b) anomalies in UHII trend by comparing the top-left single boxplot (UHII statistical distribution during the bushfires at the monitoring site) against the historical trends (UHII statistical distribution at six near locations between 2000 and 2017). Reproduced from (Ulpiani et al., 2020) © IOP Publishing Ltd. CC BY 4.0.

vehicle-to-person ratio and tropical climate, Bangalore is facing escalating UHI and UPI. The monitoring campaign focused on ten major roads in different parts of the city, having tree cover for about 150 m along one segment and no tree cover along the adjacent. Variation in ambient air temperature, road surface temperature, relative humidity, air pollution (PMs and SO_2) and traffic intensities were synchronously recorded for paired segments on summer sunny working days. Street trees lowered i) air temperatures by up to 5.6 °C, ii) road surface temperatures by up to 27.5 °C and iii) SO_2 levels by up to 65%. Furthermore suspended PMs stayed within prescribed limits for 80% of the vegetated roads, while surpassed twice the limit in 50% of the non-vegetated roads. Greenery was linked to urban climate and pollution also by Makhelouf (2009). His study was based on a four-year monitoring campaign on temperature, humidity, precipitation and pollution in green and built-up areas of the city of Paris, France. The influence of different types of gardens and extensions of parkland was highlighted. A maximum temperature difference of 3 °C was observed between green and inhabited zones, which was enough to engender a local breeze that pushed away local pollutants (especially SO_2). The extent of this washing action was largely a function of the park size and was negligible in less-than-1-

Table 1
Tree-planting effects on UHI-UPI interaction (Taha, 1996; Solecki et al., 2004; Nowak, 2002; Smith, 1984; García de Jalón et al., 2019). Specific references are provided where appropriate.

Cause	Effect
Photosynthesis	Direct CO_2 reduction (photosynthesis sequesters carbon)
Dry-deposition and stomatal uptake	Direct SO_2, NO_x, CO, O_3 and particulate matter reduction. Dry deposition depends on cuticular, stomatal and mesophyll resistances of leaves, stems, and other organs which in turn are temperature and water dependent.
Evapotranspiration	Direct air cooling which causes i) indirect CO_2 reduction (by reducing the demand for cooling energy), ii) indirect SO_2, NO_x, CO, O_3 and particulate matter reduction (by reducing combustion of fossil fuels and emissions from power plants), iii) inhibition of all temperature-dependent ozone-forming chemicals, iv) enhancement of wet deposition. On the other side, evapotranspiration rates increase with temperature, hence trees may exchange ~30% more water on paved urban areas than in vegetated areas (Kjelgren and Montague, 1998). However, excessive ambient overheating caused trees to close their stomata and suppress water loss even in well-watered conditions (Whitlow et al., 1992).
Strategic planting of deciduous trees	Significant reduction of summer solar exposures of structures, parking lots and streets. This limits re-emitted long-wave radiation that triggers ozone photochemistry and reduce evaporative emissions from vehicles (VOCs and NO_x). On the other side, evergreen species are most effective at dry deposition.
Growth	The benefits of urban trees increase with time (e.g. larger crowns, denser foliage, carbon storage) especially when periodically replacements with new mature trees are scheduled (storage capacity increased by up to 33%). On the other side, maintenance activities may require large inputs of energy from fossil fuels, thus affecting the overall budget.
Albedo change	Replacement of manmade materials (concrete, asphalt) with trees increases the reflectivity and reduces the heat absorption capacity.
Surface roughness	The physical barrier breaks the wind force and depreciates mixing, stimulating accumulation of pollutants.
BVOCs emission	Tree emit biogenic VOCs (especially isoprene) that contribute to ozone and CO formation. The emission rate depends on the species (beefwood and eucalyptus on the front line, elm, crape myrtle, cedar and Judas trees on the bottom line). Anyway, some high-emitting species exert also the higher cooling effect (Feyisa et al., 2014).

hectare gardens. On the above grounds, the author suggested to avoid built-up areas longitudinally to extensive green areas and to place large avenues facing the parklands at the crossing with neighboring inhabited spaces to take maximum advantage of the local pollutant-dispersing and fresh breeze. Substantiated protocols for precinct ventilation design and characterization are, indeed, increasingly needed (He et al., 2019).

Another widely applied UHI countermeasure relies on the use of high-reflective materials. Cool roofs and pavements reduce temperature-dependent emissions of ozone precursors and PMs and curtail greenhouse emissions by cutting buildings' cooling needs (Akbari and Levinson, 2008; Levinson and Akbari, 2010). By lowering the ambient temperature, they also reduce the rate of VOC evaporation and ozone formation (Millstein and Menon, 2011). A variety of studies by Taha et al. linked higher reflectance roofs to ozone concentration on episodic scale. For instance, in 2015, Taha examined the impacts of increased surface albedo on regional/urban meteorology and air quality during Californian summers (Taha, 2015). The author relied on CART (Classification And Regression Tree) to select episodes of high, medium and low ozone concentration between 1999 and 2005. An updated version of the mesoscale meteorological model (PSU/NCAR MM5) dedicated to heat-island applications, named uMM5 (Taha, 2008a, 2008b) was adopted to simulate horizontal and vertical transport, advection, diffusion, emissions, chemical transformations and pollution sinks (e.g. deposition). The change in albedo was applied only where no glare or multiple inter-reflections between buildings could be potentially detrimental, thus mostly on wide highways for a city-averaged increase of 0.02–0.05. The implications can be summarized as follows: i) cooling of up to 2 °C or more, ii) reduction in degree-hours per day between 90 and 155, iii) city-wide significant reduction of cumulative and 8-h ozone peak, iv) small ozone increases in case of reduced mixing and modified transport of precursors. The positive impacts were always more pronounced i) in Southern rather than Central California, because of the larger modifiable surface and the strong interconnectedness between urban areas, and ii) under non-extreme heat conditions. In a future scenario that included emission caps, these impacts were limited to 40–100%, possibly due to UHI magnification prevaricating over the effects of the abatement strategies (in line with the 1990's result by Cardelino and Chameides (1990)). Finally, the photochemical model CAMx was adopted to verify the effects of a 20% stepwise emission reduction in NO_x, then in reactive organic gases (ROG) and then in both. A suite of isopleth diagrams was derived, showing the response in the 1-h peak ozone. It was found that, in order to achieve a 1 ppb reduction, ROG emission had to be reduced by up to 9.3% and 8.5% in Central and Southern California, respectively.

In most of the studies concerning high-albedo materials, UHI and UPI it is assumed that cool surfaces would not alter the UV reflectance. Yet, UV reflectance can significantly modify the rate of ozone production. Enhanced pollution is reported, for instance, in the Uintah basin as a consequence of the snow cover (Edwards et al., 2014). A first comprehensive study is reported by Fallmann et al. (2016), who investigated the impact of greenery (fractional increase from 0.12 to 0.8), highly reflective materials (albedo increase of roof and facades from 0.2 to 0.7) and building density (main road width increased by 16–20%) on air quality inside the urban canopy. They coupled the mesoscale chemical transport model WRF-Chem with the multi-layer Building Effect Parameterization (BEP) developed by Martilli et al. (2002) to account for the three-dimensional local heterogeneity of the urbanscape and capture its perturbation in terms of heat, moisture and momentum. The city of Stuttgart, in Germany, served as test bed and the 2003 European heat wave as climatological context. The core novelty lies in the analysis of both primary (CO, NO) and secondary pollutants (O_3) to i) depict the full gas phase urban chemistry and ii) further entangle the dynamics of formation and transport of different pollutants. The near surface concentration of primary pollutants was negatively correlated to the turbulent kinetic energy. Conversely, the turbulent term was always positively correlated with ozone concentration during the morning and the evening, when ozone was higher in the residual layer than at ground level (less titration, less deposition). Around noon the boundary layer was well mixed and the vertical ozone gradient was attenuated, while during the night ground-level ozone was strongly depleted by NO titration. The decrease in near surface temperature, due to mitigating strategies, resulted in an increase of primary pollutants (NO, CO). Extra vegetation led to 5% increment of both compounds, while the increase of albedo led to +25% NO and +9% CO (mean concentrations). Ozone was decreased by 8% and 6%, respectively. While urban density had negligible impacts, greenery was steadily effective in curbing ozone at any time of the day due to the stronger cooling over vegetative surfaces than over impervious surfaces. When assuming an increase in the urban albedo, peak ozone concentration showed a tendency to increase (+12%) between 2 pm and 4 pm. This was ascribed to accelerated photochemistry (higher photolysis rates) owing to enhanced

intensity of reflected shortwave radiation from highly reflective surfaces (up to 170% increase in reflected shortwave radiation). However, on average, the O_3 mean concentration could be reduced by 5–8% (Fallmann et al., 2016) in response to a 1.1/1.7 °C UHII mitigation with greenery and increased albedo, respectively. Despite no direct correlation could be established between primary pollutants and air temperature, a linear regression could be observed when relating ozone and temperature. The authors concluded that daily average ozone concentration could be more efficiently decreased by low-emitting urban vegetation than highly reflective surfaces, as advocated also in (Donovan et al., 2005). These results contrast with the results by Taha (2008a) who reported a decrease in peak ozone concentration between 2 pm and 4 pm in the urban area of Los Angeles (−4.7%) and Sacramento (−18%) when the surface albedo was increased from 0.2 to 0.5. The maximum temperature reduction was much stronger in both locations (−4.5 and −3 °C) compared to those observed by Fallmann et al. (2016).

The influence of increased albedo is further examined in 2017 by Epstein et al. who warned on the need to keep the adverse air quality side-effects of wide-spread cool installations to a minimum (Epstein et al., 2017). They quantified the UV enhancement and demonstrated the complex and non-linear impacts on both ozone and PM2.5 concentration if cool-roofs were to be applied as prescribed by California's Title 24 building energy efficiency standards to face the extreme pollution in the South Coast Air Basin (SoCAB). The authors built up a high-resolution classified database of building rooftop areas and combined WRF v3.6 with Community Multiscale Air Quality model (CMAQ v5.0.2) to project pollution concentrations under four different scenarios to determine the individual effects of changes in meteorology, emissions, enhanced visible/infrared reflectance, and a range of hypothetical changes in UV reflectance. Basecase values were extracted from monthly MODIS and aircraft-based solar reflectance measurements of rooftops in Los Angeles and Long Beach. The prominent results can be summarized as follows: i) the annual averaged daily temperatures and the daily maximum planetary boundary layer height decreased throughout the domain (up to 0.35 °C and 40–65 m in high-albedo-change and most polluted areas); ii) the lower surface temperatures on land hindered the penetration of daytime sea breeze; iii) the average PM2.5 concentrations increased due to limited mixing and partitioning of semivolatile species by maximum 0.3 $\mu g \cdot m^{-3}$ with minimal impact from increased UV reflectance; iv) the population-weighted 8-h ozone concentrations increased when changes in UV reflectance were at an upper bound. The authors concluded that "although the other benefits of cool roofs could outweigh small air-quality penalties, UV reflectance standards for cool roofing materials could mitigate these negative consequences. Results of this study motivate the careful consideration of future rooftop and pavement solar reflectance modification policies".

Overall, the impacts of high-albedo urbanscapes on global scale and climate-dependencies remain unsettled in literature (Jacobson and Ten Hoeve, 2012), especially if aging and long-term performance loss are taken into account in contrast with the time-growing benefit of greenery (Table 1). On the other side, there is no doubt that the cost of inaction would be much higher (Lee, 1993).

5. Discussion

Already in 2004, Crutzen (2004) advocated the importance of exploring the consequences of combined urban heat and pollution island effects, since, despite the strong entanglement, UHI and UPI are generally investigated separately (Li et al., 2018). Recently, holistic approaches are gaining ground to enable the conceptualization of double-acting countermeasures (Crutzen, 2004; Baklanov et al., 2016), as demonstrated by the European Project MEGAPOLI (Baklanov et al., 2010) and dedicated conferences (Sokhi et al., 2017).

Assessing the interlink between UHI and UPI is no trivial matter. The setup and maintenance of a dense sensor network is indispensable to investigate near-surface parameters, but expensive. Alternatively, unmonitored areas can be assessed by geo-statistics based on relatively few direct observations (Merbitz et al., 2012) or by applying complex algorithms on remotely acquired images (Nichol et al., 2006). Multiyear assessments should also be encouraged when looking at trends and not occurrences, to make sure anomalous years are smoothed in their contribution. Nevertheless, meaningful information are collected also from shorter experiences, especially if weather extremes such as heat waves, droughts or fires are under scrutiny. Numerical modelling encounters several challenges as well due to the uncertainty on chemistry mechanisms, weather forecasts and emission inventories, especially for long-lived species (Huszar et al., 2020). The exclusion of anthropogenic heat is what depreciates the validity of most proposed models, since, reportedly, this term can increase the near-surface temperature by nearly 1–3 °C (Ichinose et al., 1999; Ohashi et al., 2007; Ryu et al., 2013) with the highest impact overnight (Fan and Sailor, 2005; Chen et al., 2009). Resultantly, even high-detail architectures coupling WRF with Noah and multilayer urban representations fail at depicting the nighttime surface air temperature, with underestimation in the order of 2–4 °C due to the lack of consideration for anthropogenic sources (Zhu et al., 2015). Furthermore, despite relative humidity plays a relevant role in transforming the reactive pollutants and increasing the secondary pollutants concentrations, its inclusion and its role is sparsely covered (Swamy et al., 2017). Additionally, as expressed by Huszar et al. (Huszar et al., 2020), special care should be devoted to balance the uncertainties on the vertical eddy diffusion. This term strongly influences pollution dispersal, with extremely complex dynamics when it comes to secondary pollutants or pollutants having secondary components. In this vein, detailed large scale eddy simulations (LES) recently proved to have an edge over mesoscale models in representing urban-induced turbulence (Li et al., 2019b).

Despite the investigatory difficulties, the most important determinants of both UHI and UPI have been progressively identified over recent years. In a nutshell, the probability of UHI and UPI formation increases with proximity to the city center and/or heat/emission sources, air stagnation, clear anticyclonic conditions, warm/hot seasons, nocturnal conditions, city size and/or population. The impacts affect climatological aspects like sunshine, precipitation, temperature and air quality. Under specific contingencies, the positive correlation between UHI and UPI can reverse owing to the stimulation of vertical transport, mixing and inversion breaking. Further, since the budget terms in UHI and UPI formation and magnification relate to the mechanisms of advection, chemical production/loss tendency, turbulence, dry/wet deposition and anthropogenic emissions, the net tendency might differ between nighttime and daytime (Sarrat et al., 2006). As a rule of thumb, nocturnal chemistry substantially depends on altitude and local orography. Air from different elevations interact and mix, each with its own chemical history. Nocturnal ozone maxima are reported in a variety of studies owing to the vertical mixing from higher levels ("leaky" residual layer, as dubbed by Hu et al. (Hu et al., 2013b)) or horizontal transportation through local and mesoscale wind systems like low-level jets (Eliasson et al., 2003). Major gaps exist in the understanding of the underlying causes, as reported by Tong et al. in their review on urban ozone and its evolution upon change of boundary layer characteristics (Tong et al., 2011). The mechanisms through which the availability of pollutants for a given day affects the next day's is also a grey area and a major uncertainty in atmospheric pollution models (Sarrat et al., 2006). It is however acknowledged that while the ozone contained in the atmospheric boundary layer tends to be titrated near the surface at night, it remains available at the higher residual layer. As turbulent kinetic processes develop during the day, especially in presence of rough urban fabrics, the convective boundary layer starts eroding the residual layer and makes its ozone pockets available for mixing near the ground (Fochesatto et al., 2001). Further, due to thermal and chemical processes occurring in the city, the urban residual layer is higher, deeper and richer in ozone compared to the rural surroundings (Sarrat et al., 2006).

The urban canopy meteorological forcing (by and large represented by higher Bowen ratio), is repeatedly found to significantly impact the spatial and vertical distribution of air pollutants. The enhanced updraft can reduce the surface concentrations of particulate matter and NO_x, which, in turn, lessens titration and triggers the production of near-surface ozone, with important variations at different altitudes (Rendón et al., 2014; Huszar et al., 2020). Another key-player is the HIC, namely the mesoscale urban breeze generated by the UHI and characterized by a surface convergent flow onto the city center (Oke, 2006). This phenomenon is enhanced by urban sprawling. Urban sprawl has been vastly documented to elevate the economic and environmental cost of services and daily routines by incrementing the average travelling distance and traffic congestion from/to expanded urban fringes/city center (Burchell et al., 2002; Wang et al., 2014) with a broad spectrum of health-related implications (Frumkin et al., 2004). The revised literature additionally points out a positive association between sprawl and ozone exceedances, possibly due to the hypothesis that lower density, but spatially extended patterns of urbanization generate more surface that heats up compared to compact textures. Hence, sprawling cities may experience severer air quality deterioration due to a mightier and more extended HIC. From observed results and considering the present trend towards congested city centers with less parking lots and expanded traffic lanes, the issue of establishing thresholds for minimum airflow within the pedestrian street should be sought (Krüger et al., 2011). Additionally, advecting plumes of ozone precursors could travel further downwind thus exposing the periurban areas and neighboring smaller cities to poorer air quality. As suggested by Stone, strategies like "urban growth boundaries" and "form-based codes" should replace traditional zoning ordinances to limit peripheral growth and to promote higher density.

Generally speaking, the patterns of UHI and UPI and, even more, their linkage gets more complex in case of coastal cities, because of a variegated interrelation between land and sea breezes with the heat island circulation and convergent fronts (Yun et al., 2020). Typical characteristics of the sea breeze observed in dense coastal metropolitan areas include formation of suburban stagnant regions, frontal intensification, and delay of inland advance (Ado, 1992). Sea breeze and synoptic forcing typically interfere destructively thus producing weaker winds over urban areas conducive to stagnation. The ability of sea breeze to counteract background winds is especially vivid during heat waves when the synoptic circulation is lowest (Martilli et al., 2003). As a result, ozone precursors emitted from a coastal city and advected to the sea by the land breeze transform into ozone directly over the water body. From there O_3-rich air masses are advected back to the city by the sea breeze, where they merge and combine with the HIC creating stationary systems of stalling polluted air. In most cases, the HIC interfering effect outweighs the UHII driving effect over sea breeze propagation due to larger thermal gradients (Yoshikado and Tsuchida, 1996; Khiem et al., 2010; Chen et al., 2011), yet multi-directional sea breezes (e.g. land-bay and land-gulf circulations) further complicate the interaction (Chen et al., 2011). Equally complex is the HIC role in valleys, where the temperature inversion tends to decouple the wind fields above and below thus restricting the vertical motion, the growth of the canopy boundary layer and the subsidence from the atmosphere aloft. As a result, the ozone trapped within the shallow decoupled surface layer is depleted by titration. This persists in rural and lightly urbanized contexts. The inversion breaking induced by intense urbanization couples back the two fields thus freeing the transport of pollutants out of the valley (Rendón et al., 2014).

In the future, heat waves, droughts, bushfires and other weather extremes are expected to progressively loosen their sporadicity and expose the fragility of urban infrastructures and resources. The built form tends to amplify and distort the natural hazard by multiplying the UHIs and UPIs and by strengthening their interaction (Wilby, 2008). There is little controversy worldwide on the potential occurrence of more hot anticyclonic summer episodes conducive to capping temperature inversions and hence to pollutants trapping near the surface. According to Lee, a unitary increase in ambient temperature would be associated to enough catalyzing sunshine to increase the surface ozone concentration by 14% in London (Lee, 1993). Higher temperatures would likely increase VOC emissions too by triggering VOC production, by increasing the volatility of gaseous compounds and by altering the local flora and fauna (Rinnan et al., 2014). On the other side, adaptation strategies may come into play: for instance, some tree species drop their leaves under drought conditions, which results in less emissions, less wind breaking but also less evapotranspiration (Keller et al., 2013). Predicting these impacts is especially difficult, as our understanding of VOC emissions in extreme environments is still very limited (Rinnan et al., 2014). On top of that, catastrophic bushfires are occurring more and more frequently with intense pollution emission and substantial erosion of the green lungs worldwide (Ulpiani et al., 2020). Bushfires were also found to alter UHI patterns towards more intense and stable episodes (Ulpiani et al., 2020). In this scenario, PM levels are of special concern since the related mortality rate escalates during hot days, due to the physiological stress and evermore altered response to toxic agents (Roberts, 2004).

Since UHI and UPI share most of the driving forces, UHI mitigation strategies appear to be a valuable measure against urban pollution too. The effects of albedo modifications manifest themselves in multiple ways: on temperature, cloudiness, wind, moisture, mixing, all potentially related to intensity and characteristics of both UHI and UPI (Taha, 2015). Competing effects on photolysis rates, titration rates due to enhanced shortwave radiation and reduced temperature have been vastly reported (Fallmann et al., 2016; Epstein et al., 2017). The ozone increase due to highly reflective surfaces is generally limited to peak values (Fallmann et al., 2016) and is however strongly dependent on the UHI mitigation intensity.

Greenery appears to be especially promising, provided that low-BVOC-emitting species are selected (Taha, 1996). Results for Sacramento in the early 90s pointed to a 35% and 40% air conditioning load reduction from feasible measures of tree planting and albedo increase, with several 0 kWh and hence zero emission days (Rosenfeld et al., 1993). On the other side, many conurbations suffer from a substantial lack of development space or excessively steep terrains which hinder the inclusion of green features or other mitigation interventions. This is reported, for instance, for the city of Hong Kong (Nichol et al., 2006) and for Singapore (Nichol, 1996). For these urbanscapes and for desert cities as well (Haddad et al., 2019), even small pockets of greenery within the congested inner city are of immense environmental importance, hence strategic planning in view of the natural topographic setting, climatic pattern and building layout is pivotal.

Overall, for most conventional mitigation strategies, different positive and negative effects have to be traded off against each other. Other than that, urban pollution control strategies based on emission reductions proved very and widely successful over the past decades, especially in terms of NO_x and nonmethane hydrocarbons. However, the application of exhaust control regulations in the industrial sector and of diesel emissions in the transport sector proved much less effective against photochemical oxidants (Khiem et al., 2010). The reason is that reaction-enhancing phenomena, whose magnitude was mild in the past are exacerbating, UHI at the forefront. Furthermore, transboundary air pollution from large city clusters (e.g. from East Asia) introduce complex long-range patterns which can seriously deteriorate the air quality over hundreds of kilometers. Overall, the current paradigms for pollutants formation, accumulation and transport need to be expanded to consider i) the vertical structure of the mixing layer and its dependence on atmospheric stability, ii) the preservation of the decoupling from the residual layer overnight, iii) the relative collocation of emission sources and the role of urban sprawl in different topographic contexts (Klein et al., 2014; Neu et al., 1994b). The conceptual framework in Fig. 7 attempts to recap most of the above considerations to guide researchers and practitioners in interpreting the UHI and UPI linkage, the arena of potential key factors and thereby the room for counteraction.

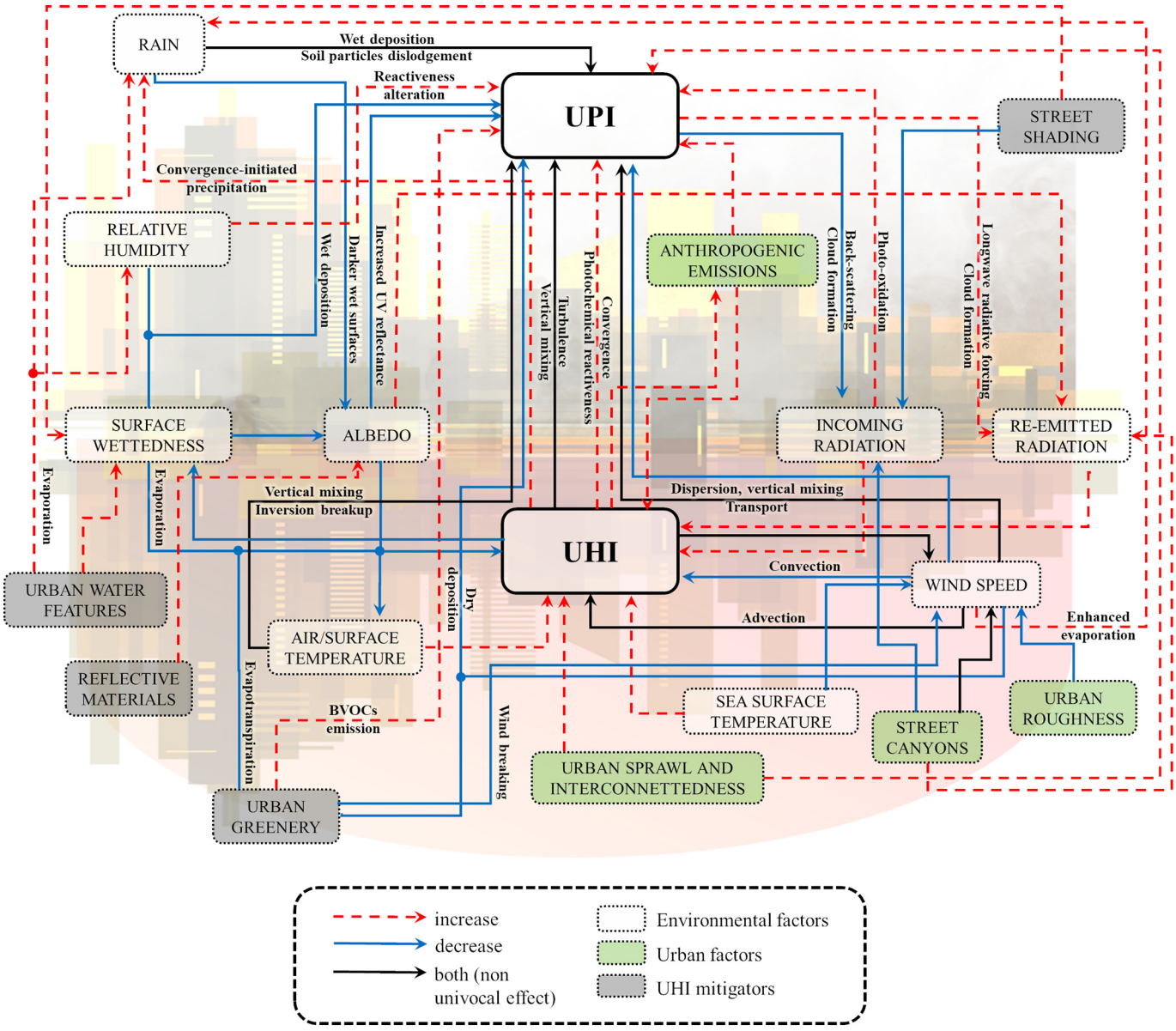

Fig. 7. Conceptual framework on the linkage between UHI and UPI. Phenomenological mechanisms are made explicit where appropriate for the sake of clarity.

6. Conclusions and outlook

Urban Heat Island and Urban Pollution Island are both manifestations of the urban metabolism and of the thermo-chemical perturbation that occurs when conventional built features replace natural features. The urban canopy meteorological forcing manifests into the generation of urban heat islands and convergent air circulations characterized by reduced wind speeds but enhanced vertical eddy mixing, which, in turn affect air chemistry, transport and inversion layer coupling/breaking mechanisms. As such, constructive and destructive interferences may establish depending on local topography, geography, climate and local-scale specificities.

According to the revised literature, synoptic conditions characterized by high temperature, low relative humidity, low wind speed and cloudlessness are conducive to UHI development and severe pollution episodes at the same time (Lai and Cheng, 2009). Urban breeze with low-level inversion and low-level convergence worsens both local overheating and air quality, especially in the nighttime. The effect of enhanced turbulence in the urban boundary layer is of paramount importance in determining the mutual relationship between UHI and UPI. Generally, both synergistic and antagonistic interactions are established depending on the considered class of pollutants (Huszar et al., 2020).

When designing mitigation scenarios, high site-specificity comes into play. If it is true that higher temperatures boost atmospheric chemistry cycles, it is likewise true that higher convective turbulence and vertical mixing is vital for pollutants dispersal. If it is true that higher albedo increases photochemical ozone production, it is likewise true that the temperature drop likely overcompensates. If it is true that greenery cleans and cools the air, it is likewise true that BVOC-emitting species might upend the balance.

Overall, a one-fits-all recipe is hard to ascertain (Crutzen, 2004), but by merging the results of the revised literature with those emerging from several affiliated sectors, a list of urban design criteria can be delineated:

- tree planting and greenery: i) vast parklands should be integrated in the urban texture to stimulate local breezes and provide higher volumetric heat capacity; ii) vertical greenscaping and rooftop gardens should be considered, especially in tall buildings long exposed to solar radiation to relieve the usage of AC systems; iii) plant cover in the form of overhanging creepers or suchlike should shade large

masses of asphalt and concrete; iv) low maintenance and low ozone-forming potential species should be preferred where possible;
- water: i) large water bodies should be surrounded by low-rise buildings to let greater rates of latent heat influx penetrate deeper inside the city; ii) artificial blue features, such as misting systems, should be arranged as multiple small-scale interventions, devised in view of dominant wind patterns and synergistic cooling (Ulpiani, 2019);
- buildings and built surfaces: i) aerodynamically rough urban profiles and radial streetscaping should be encouraged to trigger the turbulent heat diffusion between buildings and prevent pollutant stagnation; iii) appropriate shading provisions should be in place to avoid unnecessary indoor overheating and dilute the use of air conditioning systems; iv) centralized large buildings and hotels should move towards heat recovery systems to recycle the pumped out hot air into hot water supply or secondary circuits; v) high-albedo roofs and pavements should be preferred over conventional paradigms yet a dedicated legislation should advice on potential UV drawbacks (Epstein et al., 2017);
- traffic: i) private transport restrictions and dedicated regulations to manage number and type of vehicles in the hot spots of a city should be put in place, especially in tropical developing countries; ii) on-board air conditioning systems based on environmentally-friendly technologies (e.g. thermoelectric devices (Qian et al., 2016)) should be installed; iii) bus stations and other pollutants sources (e.g. landfills) should be relocated whenever the coupling with the HIC determines the onset of intense UPIs; technological advances in emission control strategies (e.g. hybrid vehicles, alternative fuels) should progress to better balance stack and tailpipe emissions with benefits in terms of air quality;
- awareness: a strong disabler to UHI and UPI prevention is the level of consideration citizen and urban planners tend to devote to climate-responsive design over aesthetics, economics and beautification of the city. To stimulate a participatory and fast-learning approach, citizen science projects are aiming at mobilizing and sensitizing citizens on the challenges and opportunities of living the built realm (Rajagopalan et al., 2017);
- abatement strategies: from a UHI perspective, NO_x abatement strategies appear to be more promising than VOC abatement strategies given the minor sensitivity to temperature increases (Sarrat et al., 2006; Cardelino and Chameides, 1990), yet the choice is strictly site-specific. On a general note, knowing the ozone chemical regime (ozone sensitivity to NOx and VOCs unit change) is crucial to plan effective abatement strategies (Martilli et al., 2003) not just in large conurbations but also in downwind smaller cities (Zhu et al., 2015). The regime could be estimated with the Sillman method which establishes at 0.28 the threshold over which the ratio of $HCHO/NO_y$ (sum of the total nitrogen species) produces NO_x-limited regime (Sillman, 1995).

The concomitant action on all of the above points is suggested for future counteraction and disentanglement of heat and pollution islands. Citizen-oriented technologies and information platforms should become a priority in shaping the cities of tomorrow (Arnesano et al., 2019). Against this backdrop, scientific breakthroughs in the field of materials sciences are expected to pave the way to new mitigation technologies. Among them, passive daytime radiative cooling (Santamouris and Feng, 2018) and elastocaloric cooling (Ulpiani et al., 2019) hold great promise.

All things considered, the various impacts of climate change, urbanization and changes in lifestyles (e.g. changes in occupancy and consumption patterns, emission control strategies, LULC conversions) should be harmoniously combined and holistically investigated to give plausible and consistent narratives of the intricate nexus between UHI and UPI (Santamouris, 2020). The topic is envisaged to receive much more attention in the future, as perceptions of unhealthy and stressful urban environments have been recently emphasized by the COVID-19 pandemic (Akbari et al., 1990; Setti et al., 2020; Wu et al., 2020; Qin et al., 2020) and bushfire season (Ulpiani et al., 2020), thus enforcing the paramount need for improved urban environmental quality, improved coping strategies and improved monitoring towards a more salutogenic approach to urban life (Nichol et al., 2006). This review attempts to be a first step in this direction.

Declaration of competing interest

The authors declare that they have no known competing financial interests or personal relationships that could have appeared to influence the work reported in this paper.

Appendix A

Table A1
List of referenced works in chronological order of publication and corresponding city/cities of investigation. Observation data and UHII, territorial and temporal frames. Bold and italic are used for mean and peak UHI to highlight when the analysis refers to SUHI and AUHI+SUHI, respectively. The abbreviation n.s. stands for non-specified.

Ref & Year	City	Mean UHII [°C]	Peak UHII [°C]	LULCs	Season & solar condition	Observation data
(Cardelino and Chameides, 1990)	Atlanta	2	n.s.	3 types: urban, suburban, rural	All seasons and any solar condition	O_3 from Georgia DNR Air temperature at airport from National Weather Service Mean summer temperature at four sites (1 urban, 2 suburban, 1 rural)
(Yoshikado and Tsuchida, 1996)	Tokyo	2	7.5	4 types: heavily urbanized, suburban, urban near-shore, rural residential	Winter, any solar condition	Hourly air temperature, wind speed and direction, pollutants (PMs, NO_2, O_3) at urban site (AQMS station) Hourly air temperature, wind speed and direction, sunshine duration at rural site (AMeDAS stations)
(Taha, 1996)	Los Angeles	n.s.	n.s.	9 types: from 0 to 16,000 metric tons of vegetation biomass (2000 step size)	Summer, clear days only	Meteorological and ozone air quality data from 28 stations in 1987 and 1991
(Khan and Simpson, 2001)	Brisbane	1	6	4 types: Urban or built-up land, Agricultural land, Forest land, Large water body	Summer, clear days only	Vertical profiles of temperature, specific humidity, wind direction and wind speed from early morning radiosonde from the Brisbane airport Hourly temperature data at one urban/industrial site (Ipswich air quality station) and at a suburban area (Eagle Farm air quality station)

Table A1 (*continued*)

Ref & Year	City	Mean UHII [°C]	Peak UHII [°C]	LULCs	Season & solar condition	Observation data
(Junk et al., 2003)	Trier	1.2	2.6	5 types: main terrace (120 m above valley bottom), southwest City Border, 2× inner city, suburban	All seasons and any solar condition	Climatological data from 2 DWD weather stations Meteorological and air quality data (NO_2, SO_2, CO, O_3, PM10) from 2 ZIMEN stations Ozone at suburban ZIMEN station Meteorological data from 4 automatic stations (Dept. of Climatology) Thermo-hygrographs from 5 DWD screen houses Mobile meteorological and air quality data from instrumented van
(Lo and Quattrochi, 2003)	Atlanta	n.s.	n.s.	6 types: high-density urban use, low-density urban use, cultivated/exposed land, cropland/-grassland, forest, water	Spring and summer, clear days only	Color-infrared aerial photographs (from NASA's Advanced Thermal and Land Applications Sensor, ATLAS) USGS digital orthophoto quads (from National Aerial Photography Program, NAPP) Land-cover map of Georgia (from ERDAS, Inc. Georgia Department of Natural Resources) USGS Levels I and II land-use digital maps
(Martilli et al., 2003)	Athens	5.25	10	2 types: downtown, suburban	Summer, clear days only	O_3, NO and NO_2 from the MEDiterranean CAmpaign of PHOto-chemicalTracers-TRAnsport and ChemicalEvolution (MEDCAPHOT-TRACE) experimental campaign
(Dousset and Gourmelon, 2003)	Paris	n.s.	7	6 types: water, urban densely built, suburban residential, light bare soils, densely vegetated (forest), lawns and fields	All seasons and any solar condition	Multispectral image from SPOT-2 satellite +22 images from satellites NOAA-12 and NOAA-14 Surface ozone concentration measurements (ESQUIF experiment)
(Jonsson et al., 2004)	Dar es Salaam	3 (wet season) 0.75 (dry season)	4 (wet season) 3.5 (dry season)	2 types: urban, rural	Wet and dry seasons, any solar condition	Particulate matter, air temperature, wind speed and direction at the rural (airport) station (10 m height) Particulate matter, air temperature, relative humidity, wind speed and direction at the urban site (2 m height)
(Sarrat et al., 2006)	Paris	1.25	3.5	3 types: urban (urbanization rate > 50%), suburban (urbanization rate between 10 and 50%), rural	Summer, clear days only	2 m air temperature and humidity at 24 Météo France stations (4 urban, 13 suburban, 7 rural) Pollutant concentrations (from ARAT aircraft measurements)
(Wilby, 2008)	London	2	10	2 types: urban, rural	All seasons and any solar condition	Daily minimum temperature differences between urban and rural stations
(Stone, 2008)	45 cities	n.s.	n.s.	2 types: urban, rural	All seasons and any solar condition	LULCs and sprawl index from (Ewing et al., 2002) Number of NAAQS ozone exceedances from EPA report Annual temperature trends and average ozone season temperature from National Oceanic and Aeronautical Administration's National Climatic Data Center Population from 2000 US Census
(Stathopoulou et al., 2008)	Athens	6	12	3 types: urban, suburban, rural	All seasons and any solar condition	Hourly air temperature and relative humidity (5 m height) from 23 met stations Hourly ozone, NO_2 and NO (5 m height) from 3 met stations
(Ward et al., 2016)	Paris	n.s.	n.s.	2 types: urban built, urban parklands	All seasons and any solar condition	Air temperature, relative humidity, precipitation and pollution in green and built-up areas (1.8 m height)
(Lai and Cheng, 2009)	Taichung	3	5.4	2 types: urban, rural	Autumn, any solar condition	Hourly meteorological and air quality (PM10, PM2.5, CO_2, CO, SO_2) data from different governmental stations 3 h-spaced vertical meteorological data from tethersonde (at 0, 50, 100, 300, 6,001,000 m)
(Papanastasiou et al., 2010)	Volos	n.s.	8.2	2 types: urban, suburban	Summer, any solar condition	Air temperature, relative humidity, wind speed and direction at two sites (urban/suburban) Solar radiation at the suburban site PM10 at the urban site
(Khiem et al., 2010)	Tokyo	n.s.	n.s.	n.s.	Summer, any solar condition	21 years (1985 to 2005) of summer-averaged daily maximum ozone concentrations at 34 monitoring sites in the central Kanto area of Japan from the National Institute for Environmental Studies (NIES) 21 years (1985 to 2005) of summer-averaged

(*continued on next page*)

Table A1 (*continued*)

Ref & Year	City	Mean UHII [°C]	Peak UHII [°C]	LULCs	Season & solar condition	Observation data
						daily maximum temperature and wind speed at 1 monitoring site from the JMA of Japan Hourly ozone, temperature and wind speed from monitoring sites throughout the Tokyo area from NIES (1 month)
(Jin et al., 2011)	Shanghai	2	8	17 types: Evergreen Needleleaf Forest, Evergreen Broadleaf Forest, Deciduous Needleleaf Forest, Deciduous Broadleaf Forest, Mixed Forest, Closed Shrubland, Open Shrubland, Woody Savannas, Savannas, Grassland, Permanent Wetland, Cropland, Urban and Built-up, Cropland/Natural Vegetation Mosaic, Snow and Ice, Barren or Sparsely Vegetated, Water	All seasons, clear days only	Monthly observations of skin temperature, albedo, and land cover data (MODIS Terra) Aerosol optical thickness (MODIS Collection 5) Aerosol optical thickness (AERONET) Regional wind circulation from the European Centre for Medium-Range Weather Forecasts
(Poupkou et al., 2011)	Thessaloniki	0.5 (day) 1.5 (night)	7 (day) > 7 (night)	4 types: (urban traffic, urban industrial, rural industrial, suburban)	All seasons and any solar condition	O_3 monitored at two sites (rural industrial, suburban) NO_2, PM10, temperature, relative humidity, wind speed and direction monitored at four sites (urban traffic, urban industrial, rural industrial, suburban)
(Krüger et al., 2011)	Curitiba	0	2.2	2 types: urban, rural	All seasons, clear days only	Weather data from INMET rural station Air temperature, relative humidity, wind speed and direction, solar radiation and globe temperature at 2 different urban points per day
(Chen et al., 2011)	Houston	1.5	n.s.	4 types: industrial/commercial, low-density residential, high-density residential, open space (mostly lawn grasses)	Summer, n.s.	Hourly 10 m wind speed and direction, 2 m air temperature, relative humidity from 29 Texas Commission on Environmental Quality TCEQ stations (20 urban stations out of 29) Hourly wind data from 6 wind profilers Hourly sea surface temperature from NCEP EDAS
(Pandey et al., 2012)	Delhi	−1.75 (day) 2.5 (night)	−6 (day) 7 (night)	7 types: agriculture (18.80%), fallow land (55.65%), road (1.22%), rural settlement (1.77%), urban settlement (12.30%), vegetation (9.29%), water body (0.97%)	Autumn and winter, any solar condition	Day and night thermal maps (MODIS satellite) Surface wind speed data (Safderjung Airport Site of Delhi) Atmospheric temperature at 850 and 975 hPa (radiosonde data from Wyoming University) Solar spectral irradiance (field measurements in 4 sites) Daily average PM2.5 concentrations at one site (from the Central Pollution Control Board)
(Merbitz et al., 2012)	Aachen	n.s.	1.63	19 types: continuous urban fabric, discontinuous urban fabric, industrial or commercial units, roads and railroads, mineral extraction sites, dump sites, green urban areas, sport facilities, non-irrigated arable land, fruit trees and berry plantations, pastures, complex cultivation patterns, broad-leaved forest, mixed forest, moors and heathland, inland marshes, water courses, water bodies	Summer, any solar condition	PM, air temperature and chemical data from 3 stations (suburban, regional background and urban traffic stations) Mobile PM, temperature and relative humidity measurements along 4 bus routes PM chemical characterization by gravimetric microbalance sensor
(Vailshery et al., 2013)	Bangalore	n.s.	n.s.	1 type: urban heavily trafficked	Summer, clear days only	Ambient air temperature, surface temperature, relative humidity and traffic count at 4 points per street, 10 streets PMs and SO_2 at 2 points per street, 10 streets
(Feizizadeh and Blaschke, 2013)	Tabriz	n.s.	n.s.	8 types: river & water bodies, green lands, bare lands, airport, under construction, market area, industry area, constructed area	Summer, n.s.	VNIR bands from ASTER satellite PMs at 8 ground-based air-pollution stations LULC from aerial photography and photogrammetric methods
(Klein et al., 2014) + (Hu et al., 2013a)	Oklahoma	2	4.5	3 types: urban, suburban, rural	Summer, any solar condition	Nocturnal boundary layer profile from two sonic anemometers + sodar and wind profiler measurements (Join Urban 2003 tracer experiment) O_3 data from six monitoring sites (1 urban, 4 suburban, 1 rural), NO_x from 2 sites (1 urban, 1 suburban) Data from 3 Oklahoma Mesonet stations
(Plocoste et al., 2014)	Grand-Camp, Lauricisque, Raizet	1.7	4.2	4 types: urban, mangrove, landfill, suburban	All seasons and any solar condition	VOCs by mass spectrometer (4 sites in the landfill, 9 in urban areas and 2 in rural sites) Tradewinds (buoys measurements) Temperature at 8 sites, 4 urban, 1 mangrove, 2 landfill, 1 suburban Hourly average temperature, wind speed and direction, rainfall intensity, nebulosity (from Météo France Guadeloupe station)

Table A1 (*continued*)

Ref & Year	City	Mean UHII [°C]	Peak UHII [°C]	LULCs	Season & solar condition	Observation data
(Rendón et al., 2014)	Metropolitan Area of the Aburrá Valley	n.s.	n.s.	2 types: urban, rural	n.s., clear days only	Annual carbon emissions
(Czarnecka and Nidzgorska-Lencewicz, 2014)	Gdańsk	1.5	4	4 types: urban center, inland, port, coast	Summer, any solar condition	Hourly air temperature, relative humidity and wind speed + pollution concentrations (NO_2, tropospheric ozone, CO, PM10,PM2.5 and SO_2) at four stations
(Papanastasiou et al., 2015)	Athens Thessaloniki Volos	3.5	5	2 types: urban, suburban	Summer, any solar condition	O_3 monitored at three sites (center of Athens, suburb of Athens, suburb of Thessaloniki) NO_2 monitored at five sites (2× center of Athens, center of Thessaloniki, suburb of Athens, suburb of Thessaloniki) PM10 monitored at six sites (2× center of Athens, center of Thessaloniki, center of Volos, suburb of Athens, suburb of Thessaloniki) Temperature and relative humidity monitored at three sites (center of Athens, center of Thessaloniki, center of Volos)
(Taha, 2015)	Sacramento San Francisco Fresno Los Angeles	2	4	7 types: residential, commercial/services, industrial, transportation/communication, industrial and commercial, mixed urban or built up, other urban or built up	Summer, any solar condition	none
(Zhu et al., 2015)	Shanghai	2	3	6 types: closed shrublands, croplands, water, mixed forests, savannas, urban and built-up	Summer, any solar condition	Air temperature, wind speed and wind direction from 3 monitoring sites (Kunshan, Shanghai west, Shanghai center) O_3 and NO_x from 5 monitoring sites (1 Kunshan, 3× Shanghai center)
(Cao et al., 2016)	39 cities	2.1 ± 0.3 (day) 3.4 ± 0.2 (night)	5.6	2 types: urban, rural	All seasons and any solar condition	Surface temperature and longwave radiation (satellite observations, MODIS) Aqua land surface temperature (MODIS MYD11A2) Aerosol (MODIS Level 2 MYD04_3K)
(Fallmann et al., 2016)	Stuttgart	n.s.	n.s.	3 types: low density residential (vegetation accounting for 20–70%, urban fraction = 0.6), high-density residential (vegetation <20%, urban fraction = 0.8) and industrial/commercial (urban fraction = 0.9)	Summer, clear days only	Data from 3 urban measurement stations (2 at street level, close to emission sources +1 at roof level in the urban center). Average height of 10.3 m
(Epstein et al., 2017)	Los Angeles	n.s.	n.s.	6 types: nonresidential low slope, nonresidential high slope, high-rise low slope residential hotel and motel, high-rise high slope residential hotel and motel, redisential low slope, residential high slope	All seasons and any solar condition	Solar reflectance from monthly MODIS measurements Aircraft-based remote sensing measurements of rooftops in Los Angeles and Long Beach
(Swamy et al., 2017)	Chennai	n.s.	4	3 types: background, commercial and residential	Summer, n.s.	Hourly 10 m weather data from 2 monitoring sites (background and residential) Temperature, wind speed and direction from 3 monitoring sites (background, commercial and residential) Temperature, relative humidity, ozone measured by an instrumented van at 2 sites (background and residential) Ozone data from the continuous ambient air quality monitoring station (CAAQMS) at residential and background sites Hourly 10 m wind velocity and hourly 2 m and 2500 m relative humidity from weather station and radio sounding data
(Li et al., 2018)	Berlin	n.s.	n.s.	24 types: continuous urban fabric, discountinuous urban fabric, industrial or commercial, road and rail networks, port areas, airports, mineral extraction sites, dump sites, construction sites, green urban areas, sport and leisure facilities, non-irrigated arable land, fruit trees, pastures, complex cultivation patterns, agriculture & natural vegetation, broad-leaved forest, coniferous forest, mixed forest, natural grasslands, moors and heatland, transitional woodland-shrub, inland marshes, water bodies	Summer, clear days only	AOD (from MODIS MYD04_3K, Aqua satellite, dark target algorithms) LST (from MODIS MYD11_A1, Aqua satellite) Surface albedo of urban and rural areas (MODIS Albedo 16-Day L3 Global product MCD43C3) Air density, surface temperature, air temperature, sensible heat flux, latent heat flux, precipitation, cloud, local climate sensitivity and energy redistribution factor from MERRA 2 reanalysis data PM10 at 12 sites (3 rural, 3 urban, 6 trafficked urban) Radiation at 7 sites (5 urban, 1 near-city rural, 1 far-city rural) Cloud at 4 sites (2 urban, 1 near-city rural, 1 far-city rural)

(continued on next page)

Table A1 (*continued*)

Ref & Year	City	Mean UHII [°C]	Peak UHII [°C]	LULCs	Season & solar condition	Observation data
(Wang et al., 2018)	25 cities (Shanghai)	1.24 °C	2.27 °C	5 types: farm land, forest, grassland, built-up area, water body	All seasons and any solar condition	Air temperature at 4 sites (2 urban, 1 near-city rural, 1 rural) Wind at 1 site (near-city rural) Hourly ground-level O_3 and NO_2 from 139 air quality monitoring stations - China Environment Monitoring Center (CEMC) Land cover data from the National Geomatics Center of China (NGCC; GlobelLand30–2010) MYD11A28-day land surface temperature (LST) from MODIS (1 km resolution) Monthly NDVI from MYD13A3 product (1 km resolution) Elevation data from Advanced Spaceborne Thermal Emission and Reflection Radiometer (ASTER) Global Digital Elevation Model (GDEM) (90 m resolution) Surface meteorological parameters and air temperature from the National Meteorological Information Center Population data from China City Statistical Yearbook
(Huszar et al., 2020)	Prague Berlin	n.s.	n.s.	n.s.	All seasons and any solar condition	Gridded E-OBS data from (den Besselaar et al., 2011) O_3 and PM2.5 surface concentrations from the European Environment Agency AirBase station data
(Ulpiani et al., 2020)	Sydney	0.5	7	2 types: urban, suburban	Summer, any solar condition	1 min, 1.1 m air temperature, relative humidity, barometric pressure, precipitation, wind (speed and direction), solar radiation, UV radiation, UV index, PM1, PM2.5 and PM10, at the urban site Hourly air temperature data from 7 BoM stations in Greater Sydney (2000–2017)

Table A2
Details of simulated scenarios: software, spatial and temporal domain, inputs and parameterizations. The abbreviation n.s. stands for non-specified.

Ref & year	Software	Computational domain	Time	Input data (beyond observation data)	Parametric analysis
(Cardelino and Chameides, 1990)	OZIPM4	n.s.	1974–1988	EPA's MOBILE4 model for effect of temperature and volatility on evaporative emissions Natural emissions inventory (Landsat)	10 scenarios of emission control and urbanization: 1/6) 50% VOCS reduction or 50% NO_x reduction (base cases); 2/7) scenario 1/6 + 20% natural emissions reduction; 3/8) scenario 2/7 + 2 °C UHI induced pzone photochemistry enhancement; 4/9) scenario 3/8 + 2 °C UHI induced natural emission increase; 5/10) scenario 4/9 + 2 °C UHI induced anthropogenic emissions increase
(Taha, 1996)	CSUMM (Colorado State University Mesoscale Model) + UAM-IV (Urban Airshed Model)	3865x595km^2, 5 × 5km^2 resolution, 10 km vertical height + 50 cm soil depth	Two days, starting at 4 am	Vegetation biomass distribution data from Horie et al. (1991)	2 scenarios of increased urban vegetation: from 16 to 17% and from 16 to 18%. 3 levels of BVOC-emitting species: low-emitters (<2 μg/gh of isoprene and <1 μg/gh of monoterpenes), medium-emitters (4 μg/gh of isoprene and 2 μg/gh of monoterpenes on average) and high-emitters (20 μg/gh of isoprene and 5 μg/gh of monoterpenes on average).
(Khan and Simpson, 2001)	Modified Colorado State University (CSU) mesoscale model	100x100km^2 2500 50 × 50 grids, interspace 2 km	4 h spin-up, 24 h simulation	Anthropogenic heat fluxes from 1996 Census of Population, fuel consumption data, waste heat from coal-fired power plants and small industries, energy consumption data and Bureau of Statistics	3 heat flux scenarios: 1) no UHI, no anthropogenic heat, 2) UHI, no anthropogenic heat, 3) UHI + anthropogenic heat
(Junk et al.,	ENVI-met	Cathedral square in the center of	June, 3 pm	n.s.	None

Table A2 (*continued*)

Ref & year	Software	Computational domain	Time	Input data (beyond observation data)	Parametric analysis
2003)		Trier (240x220m^2)			
(Martilli et al., 2003)	Non-hydrostatic, Boussinesq, anelastic mesoscale model (in-house) + Building Effect Parameterization (BEP) [An urban surface exchange parameterisation for mesoscale models] + Transport and photochemistry Eulerian model (TAPOM)	72x72km^2, 2x2km^2 resolution (36 grid points per side) + 8 additional grid cells at the lateral boundaries (spacing ranging from 2.4 to 8.7 km). Total domain of 151x151km^2. Vertical resolution of min 10 m (lowest 5 levels) up to 1 km (top of domain, at 8.5 km). Temporal resolution of the emission 1 h, spatial resolution 2x2km^2	28 h (4 h spin-up)	Emission inventories from previous studies	2 model approaches: dynamic and thermodynamic urban surface exchanges VS standard mesoscale models built on constant flux-layer and surface energy budget 2 scenarios of emission control: 25% NO_x emission reduction, 25% VOC emission reduction
(Dousset and Gourmelon, 2003)	GIS (version n.s.)	50x50km^2 20 m to 1 km resolution	March 91,998 August 6–10, 1998	NOAA-AVHRR statistical infrared images Classified multispectral SPOT-HRV images	none
(Sarrat et al., 2006)	Coupled Meso-NHC and TEB	Two nested domains: 810x810km^2 large-scale domain (15 km resolution), 150x150km^2 small-scale domain (3 km resolution)	16–18 Jul 1999	Anthropogenic emissions from GENEMIS inventory LULCs from CORINE Land Cover database	2 heat flux scenarios: URBAN (with TEB, urban surface), NO-URB (without TEB, natural surface)
(Wilby, 2008)	SDSM	n.s.	1961–2050	Predictand-predictors correlations	4 general circulation models: the Canadian Centre for Climate Modelling and Analysis model (CGCM2); the Commonwealth Scientific and Industrial Research Organisation model (CSIRO Mk2); the Max-Planck-Institut for Meteorology model (ECHAM4), the Hadley Centre's coupled ocean/-atm climate model (HadCM3).
(Lai and Cheng, 2009)	TAPM air pollution model (CSIRO)	Four domains: 80 × 80 grids at resolutions of 12 km, 3.6 km, 1.2 km and 0.4 km) 25 vertical layers (from 10 to 8000 m)	n.s.	n.s.	none
(Khiem et al., 2010)	MM5 + CMAQ	3 nested domains: 51 × 61, 73 × 88 and 100 × 121 grid points with 9, 3 and 1 km horizontal resolution 23 vertical levels up to 100 hPa level (14 m thick lowest level)	1 month (from 9 am July 31 to midnight August 31, 2005) 15 h spin-up	Boundary and initial conditions from NCEP FNL Terrain, land use, and land-water mask datasets from USGS 25-category land use/land cover classification system hourly NMHC and NOx emissions data by (Hayami and Kobayashi, 2004)	none
(Krüger et al., 2011)	ENVI-met (Version 3.1 beta 4)	1440x600m^2	March, 6 h run (3 pm–9 pm)	SVF and H/W ratio from city plans, aerial photographs and visual surveys NO_x rate of emission, type of substance, size of particle from indirect derivation into SOURCES. DAT file	4 simulation scenarios: 1) 0.3 m/s northerly winds, 2) 0.3 m/s easterly winds, 3) 1.4 m/s northerly winds, 4) 1.4 m/s easterly winds
(Chen et al., 2011)	WRF + Noah + single-layer-UCM	4 nested domains: 70 × 70, 121 × 121, 172 × 172, 190 × 190 grid points with 27, 9, 3 and 1 km resolution. 38 vertical layers up to near 50 hPa level (100 m near-surface resolution, 1 km top-domain resolution)	36 h, starting at midnight (30 Aug)	Initial conditions from National Centers for Environmental Protection NCEP LULCs from USGS 2001 National Land Cover Data set	Daily versus hourly surface sea temperature input Urban land VS cropland 3 soil moisture levels: realistic-intermediate, completely dry, completely wet
(Merbitz et al., 2012)	ArcGIS 9.2 (ESRI) + Matlab R2010b	8x6km^2, 10x10m^2 cell size Circular buffers of 200-to-800 m size	May–July 2010	LULCs from CORINE land cover 2000 Elevation from airborne radar scanning Population census Traffic data from municipal administration	None
(Klein et al., 2014) + (Hu et al., 2013a)	WRF-Chem	2 nested domains: 22.5 and 4.5 km horizontal grid spacing 48 vertical layers up to 100 hPa level (12 m near-surface resolution, 1.64 km top-domain resolution)	54 h, starting at midnight of each episode (three 2-day episodes)	Initial and boundary conditions from NCEP FNL GFS (meteorological data) and MOZART4 (chemicals)	None
(Rendón	EULAG	25.6 × 6.4km^2, 6.4 km height	Daytime,	n.s.	6 scenarios of urbanization: 0%

(*continued on next page*)

Table A2 (*continued*)

Ref & year	Software	Computational domain	Time	Input data (beyond observation data)	Parametric analysis
et al., 2014)		(25 m grid size at the surface, 121 m at the top of the domain)	6 am-6 pm		(rural), 20%, 40%, 60%, 80%, 100% (fully urbanized)
(Taha, 2015)	uMM5	Four city-scale domains (1 km horizontal resolution)	CART selected episodes	Meteorological initial and boundary conditions, upper-air and surface data from NCEP/-NCAR reanalysis Surface characteristics from USGS Level-II land-use classification system and the National Land Cover Data (NLCD) Photochemical model CAMx	Change in albedo: +0.02–0.05 Past (1999–2005) and future (2018) emission policies
(Zhu et al., 2015)	WRF + Noah + BEP + CMAQ	3 nested domains: 181 × 151, 181 × 151, 100 × 95 grid points with 13.5, 4.5, and 1.5 km resolution. 30 vertical layers up to 50 hPa level (lowest 22 levels below 2 km)	For WFR + Noah +BEP: 48 h, starting at midnight (11 Aug, 24 h spin-up) For CMAQ: 72 h, starting at midnight (10 Aug, 40 h spin-up)	Boundary and initial conditions for WRF + Noah+BEP from NCEP GFS-FNL LULCs from MODIS 20 category land use data Boundary and initial conditions for CMAQ from MOZART-4 Anthropogenic emissions from Intercontinental Chemical Transport Experiment-Phase B Emission inventory from Transport and Chemical Evolution over the Pacific (TRACE-P) BVOCs inventory from Global Emission Inventory Activity 1990	Urban land VS cropland
(Cao et al., 2016)	n.s.	n.s.	n.s.	Surface emissivity data (MODIS) Land cover (MODIS MCD12Q1, resolution 500 m) Meteorological initial and boundary conditions from NCAR Offline attribution of UHI according to dominant biophysical drivers, aerodynamic resistance and energy redistribution factor	None
(Fallmann et al., 2016)	Coupled WRF-Chem and BEP	600x450km^2 200 × 150 grid cells 36 vertical levels (6 in the lowest 100 m, further refined by BEP)	Aug 09 - Aug 182,003 (first day used as spin up)	Meteorological boundary conditions (0.5 Deg ERA-Interim) Anthropogenic emissions (MACC 7 km emission inventory) Biogenic emissions (MEGAN emission database) Lateral chemical boundary conditions (MOZART output) Gas-phase chemistry (RADM2 - Regional Acid Deposition Model) Aerosol dynamics and chemistry (MADE/SORGAM module) Longwave and shortwave radiation (RRTMG scheme) Cumulus (Grell Devenyi ensemble) Land surface model (Noah LSM) Photolysis scheme (FastJ)	3 UHI mitigation scenarios: greenery (0.12 to 0.8 fraction), albedo increase (0.2 to 0.7 roof and facades albedo), building density decrease (main road width from min 15 to max 22 m)
(Epstein et al., 2017)	WRF + CMAQ	624 × 408km^2, three nested grids: 4 km resolution covering the modelling domain 18 vertical layers	A calendar year (2012 for baseline)	Rooftop SR standards from Title24 for the SoCAB Temperature-dependent 2012 SoCAB emissions inventory Land-use data for 2012 from the Southern California Association of Governments (SCAG) Building footprint data from the US Army Corps of Engineers	4 scenarios of increased reflectance and emissions: enhanced visible/infrared reflectance; enhanced visible/infrared reflectance + Title24 emissions, enhanced visible/infrared reflectance + Title24 emissions + Title24 meteorology, enhanced visible/infrared and UV reflectance + Title24 emissions + Title24 meteorology
(Swamy et al., 2017)	ENVI-Met	3 locations: 0.9 × 0.9 × 0.55km^3, 10x10x2m^2 grid dimensions each	15 May - 15 June 2016	Building materials and surface land use materials from ASTM	4 air velocity profiles: 0.2, 1, 2 and 5 m/s
(Huszar et al., 2020)	RegCM4 + CMAx	3 telescopic domains: 189 × 141, 189 × 165 and 93 × 69 grid points with 27, 9 and 3 km horizontal resolution 23–41 vertical layers (60-70 m thick lowest level) for RegCM4, 18 vertical layers for CAMx	2007–2011	Boundary and initial conditions for RegCM4 from NCEP Boundary and initial conditions for CMAx from MOZART-4 LULCs from CORINE CLC and United States Geological Survey (USGS) database	6 different methods to calculate the vertical eddy diffusion coefficient (Kv) Urban land VS cropland 3 horizontal resolutions: 27, 9, and 3 km

Table A2 (*continued*)

Ref & year	Software	Computational domain	Time	Input data (beyond observation data)	Parametric analysis
				Average building heights, urban canyon height-to-width ratios, fraction of pervious surface, roof area and impervious surfaces from LandScan dataset Emission datasets from TNO Monitoring Atmospheric Composition and Climate (MACC)-III and Register of Emissions and Air Pollution Sources (REZZO) Traffic emissions dataset from ATEM	

References

Abadie, L.M., Chiabai, A., Neumann, M.B., 2019. Stochastic diffusion models to describe the evolution of annual heatwave statistics: a three-factor model with risk calculations. Sci. Total Environ. 646, 670–684. https://doi.org/10.1016/j.scitotenv.2018.07.158.

Ado, H., 1992. Numerical study of the daytime urban effect and its interaction with the sea breeze. J. Appl. Meteorol. 31, 1146–1164.

Akbari, H., Levinson, R., 2008. Evolution of cool-roof standards in the US. Adv. Build. Energy Res. 2, 1–32.

Akbari, H., Rosenfeld, A.H., Taha, H., 1990. Summer Heat Islands, Urban Trees, and White Surfaces.

Anquetin, S., Guilbaud, C., Chollet, J.-P., 1999. Thermal valley inversion impact on the dispersion of a passive pollutant in a complex mountainous area. Atmos. Environ. 33, 3953–3959.

Arnesano, M., Casaccia, S., di Perna, C., Passerini, G., Principi, P., Revel, G.M., Scalise, L., Tomasini, E.P., Ulpiani, G., 2019. Citizen-oriented technologies in the cities of tomorrow. In: Longhi, S., Monteriù, A., Freddi, A., Frontoni, E., Germani, M., Revel, G.M. (Eds.), First Outst. 50 Years "Università Politec. Delle Marche". Springer International Publishing, Cham, pp. 143–160 https://doi.org/10.1007/978-3-030-32762-0_8.

Bader, D.C., McKee, T.B., 1985. Effects of shear, stability and valley characteristics on the destruction of temperature inversions. J. Clim. Appl. Meteorol. 24, 822–832.

Baklanov, A., Lawrence, M., Pandis, S., Mahura, A., Finardi, S., Moussiopoulos, N., Beekmann, M., Laj, P., Gomes, L., Jaffrezo, J.-L., Borbon, A., Coll, I., Gros, V., Sciare, J., Kukkonen, J., Galmarini, S., Giorgi, F., Grimmond, S., Esau, I., Stohl, A., Denby, B., Wagner, T., Butler, T., Baltensperger, U., Builtjes, P., van den Hout, D., van der Gon, H.D., Collins, B., Schluenzen, H., Kulmala, M., Zilitinkevich, S., Sokhi, R., Friedrich, R., Theloke, J., Kummer, U., Jalkinen, L., Halenka, T., Wiedensholer, A., Pyle, J., Rossow, W.B., 2010. MEGAPOLI: concept of multi-scale modelling of megacity impact on air quality and climate. Adv. Sci. Res. 4, 115–120. https://doi.org/10.5194/asr-4-115-2010.

Baklanov, A., Molina, L.T., Gauss, M., 2016. Megacities, air quality and climate. Atmos. Environ. 126, 235–249. https://doi.org/10.1016/j.atmosenv.2015.11.059.

Block, A.H., Livesley, S.J., Williams, N.S.G., 2012. Responding to the urban Heat Island: a review of the potential of green infrastructure. Vic. Cent. Clim. Chang. Adapt., 1–62. http://staging.202020vision.com.au/media/1026/responding-to-the-urban-heat-island-a-review-of-the-potential-of-green-infrastructure.pdf.

Bornstein, R., Lin, Q., 2000. Urban heat islands and summertime convective thunderstorms in Atlanta: three case studies. Atmos. Environ. 34, 507–516. https://doi.org/10.1016/S1352-2310(99)00374-X.

Boy, M., Kulmala, M., 2002. Influence of Spectral Solar Irradiance on the Formation of New Particles in the Continental Boundary Layer.

Braham, R.R., Semonin, R.G., Auer, A.H., Changnon, S.A., Hales, J.M., 1981. Summary of urban effects on clouds and rain. Metromex a Rev. Summ. Springer, pp. 141–152.

Bretz, S., Akbari, H., Rosenfeld, A., 1998. Practical issues for using solar-reflective materials to mitigate urban heat islands. Atmos. Environ. 32, 95–101. https://doi.org/10.1016/S1352-2310(97)00182-9.

Burchell, R.W., Lowenstein, G., Dolphin, W.R., Galley, C.C., Downs, A., Seskin, S., Still, K.G., Moore, T., 2002. Costs of Sprawl–2000.

Burkart, K., Canário, P., Breitner, S., Schneider, A., Scherber, K., Andrade, H., Alcoforado, M.J., Endlicher, W., 2013. Interactive short-term effects of equivalent temperature and air pollution on human mortality in Berlin and Lisbon. Environ. Pollut. 183, 54–63. https://doi.org/10.1016/j.envpol.2013.06.002.

Cao, C., Lee, X., Liu, S., Schultz, N., Xiao, W., Zhang, M., Zhao, L., 2016. Urban heat islands in China enhanced by haze pollution. Nat. Commun. 7, 1–7. https://doi.org/10.1038/ncomms12509.

Cardelino, C.A., Chameides, W.L., 1990. Natural hydrocarbons, urbanization, and urban ozone. J. Geophys. Res. 95, 971–979. https://doi.org/10.1029/jd095id09p13971.

Carter, W.P.L., Winer, A.M., Darnall, K.R., Pitts Jr., J.N., 1979. Smog chamber studies of temperature effects in photochemical smog. Environ. Sci. Technol. 13, 1094–1100.

Hayhoe, K., Cayan, D., Field, C.B., Frumhoff, P.C., Maurer, E.P., Miller, N.L., Moser, S.C., Schneider, S.H., Cahill, K.N., Cleland, E.E., et al., 2004. Emissions pathways, climate change, and impacts on California. Proc. Natl. Acad. Sci. 101, 12422–12427.

Chandler, T.J., 1968. Discussion of the paper by marsh and foster. The bearing of the urban temperature field upon urban pollution patterns. Atmos. Env. 2, 619–620.

Chen, Y., Jiang, W.M., Zhang, N., He, X.F., Zhou, R.W., 2009. Numerical simulation of the anthropogenic heat effect on urban boundary layer structure. Theor. Appl. Climatol. 97, 123–134.

Chen, F., Miao, S., Tewari, M., Bao, J.W., Kusaka, H., 2011. A numerical study of interactions between surface forcing and sea breeze circulations and their effects on stagnation in the greater Houston area. J. Geophys. Res. Atmos. 116, 1–19. https://doi.org/10.1029/2010JD015533.

Chen, B., Yang, S., De Xu, X., Zhang, W., 2014. The impacts of urbanization on air quality over the Pearl River Delta in winter: roles of urban land use and emission distribution. Theor. Appl. Climatol. 117, 29–39. https://doi.org/10.1007/s00704-013-0982-1.

Chubarova, N., Nezval, Y., Sviridenkov, I., Smirnov, A., Slutsker, I., 2012. Smoke Aerosol and its Radiative Effects during Extreme Fire Event over Central Russia in Summer. vol. 2010, pp. 557–568. https://doi.org/10.5194/amt-5-557-2012.

Ciais, P., Reichstein, M., Viovy, N., Granier, A., Ogée, J., Allard, V., Aubinet, M., Buchmann, N., Bernhofer, C., Carrara, A., Chevallier, F., De Noblet, N., Friend, A.D., Friedlingstein, P., Grünwald, T., Heinesch, B., Keronen, P., Knohl, A., Krinner, G., Loustau, D., Manca, G., Matteucci, G., Miglietta, F., Ourcival, J.M., Papale, D., Pilegaard, K., Rambal, S., Seufert, G., Soussana, J.F., Sanz, M.J., Schulze, E.D., Vesala, T., Valentini, R., 2005. Europe-wide reduction in primary productivity caused by the heat and drought in 2003. Nature 437, 529–533. https://doi.org/10.1038/nature03972.

Colbeck, I., Chung, M.-C., Eleftheriadis, K., 2002. Formation and transport of atmospheric aerosol over Athens, Greece, water. Air Soil Pollut. Focus. 2, 223–235.

Colette, A., Chow, F.K., Street, R.L., 2003. A numerical study of inversion-layer breakup and the effects of topographic shading in idealized valleys. J. Appl. Meteorol. 42, 1255–1272.

Cotrufo, M.F., Soong, J.L., Horton, A.J., Campbell, E.E., Haddix, M.L., Wall, D.H., Parton, W.J., 2015. Formation of soil organic matter via biochemical and physical pathways of litter mass loss. Nat. Geosci. 8, 776–779.

Crutzen, P.J., 2004. New directions: the growing urban heat and pollution "'island'" effect—impact on chemistry and climate. Atmos. Environ. 38 (38), 3539–3540. https://doi.org/10.1029/2001.

Csavina, J., Field, J., Félix, O., Corral-Avitia, A.Y., Sáez, A.E., Betterton, E.A., 2014. Effect of wind speed and relative humidity on atmospheric dust concentrations in semi-arid climates. Sci. Total Environ. 487, 82–90. https://doi.org/10.1016/j.scitotenv.2014.03.138.

Czarnecka, M., Nidzgorska-Lencewicz, J., 2014. Intensity of urban heat island and air quality in Gdańsk during 2010 heat wave. Polish J. Environ. Stud. 23, 329–340.

den Besselaar, E.J.M., Haylock, M.R., der Schrier, G., Klein Tank, A.M.G., 2011. A European daily high-resolution observational gridded data set of sea level pressure. J. Geophys. Res. Atmos. 116.

Dickinson, R.E., 1986. Biosphere/atmosphere transfer scheme (BATS) for the NCAR community climate model. Tech. Report, NCAR.

Diem, J.E., Mote, T.L., 2005. Interepochal changes in summer precipitation in the southeastern United States: evidence of possible urban effects near Atlanta, Georgia. J. Appl. Meteorol. 44, 717–730.

Donovan, R.G., Stewart, H.E., Owen, S.M., MacKenzie, A.R., Hewitt, C.N., 2005. Development and application of an urban tree air quality score for photochemical pollution episodes using the Birmingham, United Kingdom, area as a case study. Environ. Sci. Technol. 39, 6730–6738. https://doi.org/10.1021/es050581y.

Dousset, B., Gourmelon, F., 2003. Satellite multi-sensor data analysis of urban surface temperatures and landcover. ISPRS J. Photogramm. Remote Sens. 58, 43–54. https://doi.org/10.1016/S0924-2716(03)00016-9.

Edwards, P.M., Brown, S.S., Roberts, J.M., Ahmadov, R., Banta, R.M., Degouw, J.A., Dube, W.P., Field, R.A., Flynn, J.H., Gilman, J.B., 2014. Others, high winter ozone pollution from carbonyl photolysis in an oil and gas basin. Nature 514, 351–354.

Eliasson, I., Thorsson, S., Andersson-Sköld, Y., 2003. Summer nocturnal ozone maxima in Göteborg, Sweden. Atmos. Environ. 37, 2615–2627. https://doi.org/10.1016/S1352-2310(03)00205-X.

Elsayed, I.S.M., 2012. Mitigation of the urban heat island of the city of Kuala Lumpur, Malaysia. Middle East J. Sci. Res. 11, 1602–1613. https://doi.org/10.5829/idosi.mejsr.2012.11.11.1590.

Emmanuel, R., 2005. Thermal comfort implications of urbanization in a warm-humid city: the Colombo Metropolitan Region (CMR), Sri Lanka. Build. Environ. 40, 1591–1601.

Epstein, S.A., Lee, S.M., Katzenstein, A.S., Carreras-Sospedra, M., Zhang, X., Farina, S.C., Vahmani, P., Fine, P.M., Ban-Weiss, G., 2017. Air-quality implications of widespread

adoption of cool roofs on ozone and particulate matter in southern California. Proc. Natl. Acad. Sci. U. S. A. 114, 8991–8996. https://doi.org/10.1073/pnas.1703560114.
Escobedo, F.J., Kroeger, T., Wagner, J.E., 2011. Urban forests and pollution mitigation: analyzing ecosystem services and disservices. Environ. Pollut. 159, 2078–2087.
Estournel, C., Vehil, R., Guedalia, D., Fontan, J., Druilhet, A., 1983. Observations and modeling of downward radiative fluxes (solar and infrared) in urban/rural areas. J. Clim. Appl. Meteorol. 22, 134–142. https://doi.org/10.1175/1520-0450(1983)022<0134:OAMODR>2.0.CO;2.
Ewing, R.H., Pendall, R., Chen, D.D.T., 2002. Measuring Sprawl and its Impact. Smart Growth America Washington, DC.
Fallmann, J., Forkel, R., Emeis, S., 2016. Secondary effects of urban heat island mitigation measures on air quality. Atmos. Environ. 125, 199–211. https://doi.org/10.1016/j.atmosenv.2015.10.094.
Fan, H., Sailor, D.J., 2005. Modeling the impacts of anthropogenic heating on the urban climate of Philadelphia: a comparison of implementations in two PBL schemes. Atmos. Environ. 39, 73–84.
Feizizadeh, B., Blaschke, T., 2013. Examining urban heat island relations to land use and air pollution: multiple endmember spectral mixture analysis for thermal remote sensing. IEEE J. Sel. Top. Appl. Earth Obs. Remote Sens. 6, 1749–1756. https://doi.org/10.1109/JSTARS.2013.2263425.
Feyisa, G.L., Dons, K., Meilby, H., 2014. Efficiency of parks in mitigating urban heat island effect: an example from Addis Ababa. Landsc. Urban Plan. 123, 87–95. https://doi.org/10.1016/j.landurbplan.2013.12.008.
Fochesatto, G.J., Drobinski, P., Flamant, C., Guedalia, D., Sarrat, C., Flamant, P.H., Pelon, J., 2001. Evidence of dynamical coupling between the residual layer and the developing convective boundary layer. Boundary-Layer Meteorol 99, 451–464.
Folberth, G.A., Rumbold, S.T., Collins, W.J., Butler, T.M., 2012. Global radiative forcing and megacities. Urban Clim. 1, 4–19.
Frumkin, H., Frank, L., Jackson, R.J., 2004. Urban Sprawl and Public Health: Designing, Planning, and Building for Healthy Communities. Island Press.
García de Jalón, S., Burgess, P.J., Curiel Yuste, J., Moreno, G., Graves, A., Palma, J.H.N., Crous-Duran, J., Kay, S., Chiabai, A., 2019. Dry deposition of air pollutants on trees at regional scale: a case study in the Basque Country. Agric. For. Meteorol. 278. https://doi.org/10.1016/j.agrformet.2019.107648.
Garcia-Herrera, R., Díaz, J., Trigo, R.M., Luterbacher, J., Fischer, E.M., 2010. A review of the european summer heat wave of 2003. Crit. Rev. Environ. Sci. Technol. 40, 267–306. https://doi.org/10.1080/10643380802238137.
Givati, A., Rosenfeld, D., 2004. Quantifying precipitation suppression due to air pollution. J. Appl. Meteorol. 43, 1038–1056.
Gorsevski, V., Taha, H., Quattrochi, D., Luvall, J., 1998. Air pollution prevention through urban Heat Island mitigation: an update on the urban Heat Island pilot project. Proc. ACEEE Summer Study., 23–32 https://doi.org/10.1017/S0963926807004373.
Habeeb, D., Vargo, J., Stone, B., 2015. Rising heat wave trends in large US cities. Nat. Hazards 76, 1651–1665.
Haddad, S., Ulpiani, G., Paolini, R., Synnefa, A., Santamouris, M., 2019. Experimental and theoretical analysis of the urban overheating and its mitigation potential in a hot arid city – Alice Springs. Archit. Sci. Rev., 1–16 https://doi.org/10.1080/00038628.2019.1674128.
Haeger-Eugensson, M., Holmer, B., 1999. Advection caused by the urban heat island circulation as a regulating factor on the nocturnal urban heat island. Int. J. Climatol. A J. R. Meteorol. Soc. 19, 975–988.
Halberstadt, M.L., 1989. Effective control of highway vehicle hydrocarbon emissions, JAPCA. Int. J. Air Pollut. Control Waste Manag 39.
Hayami, H., Kobayashi, S., 2004. Modeling of concentration of atmospheric secondary aerosol. CRIEPI Rep. 3037, 17.
Haywood, J., Boucher, O., 2000. Estimates of the direct and indirect radiative forcing due to tropospheric aerosols: a review. Rev. Geophys. 38, 513–543. https://doi.org/10.1029/1999RG000078.
He, B.J., 2018. Potentials of meteorological characteristics and synoptic conditions to mitigate urban heat island effects. Urban Clim. 24, 26–33. https://doi.org/10.1016/j.uclim.2018.01.004.
He, B.J., Ding, L., Prasad, D., 2019. Enhancing urban ventilation performance through the development of precinct ventilation zones: a case study based on the greater Sydney, Australia. Sustain. Cities Soc. 47, 101472. https://doi.org/10.1016/j.scs.2019.101472.
Hoek, G., Beelen, R., De Hoogh, K., Vienneau, D., Gulliver, J., Fischer, P., Briggs, D., 2008. A review of land-use regression models to assess spatial variation of outdoor air pollution. Atmos. Environ. 42, 7561–7578.
Horie, Y., Sidawi, S., Ellefsen, R., 1991. Inventory of Leaf Biomass and Emission Factors for Vegetation in California's South Coast Air Basin, Final Rep.. Contract No. 90. p. 63.
Hu, X.M., Klein, P.M., Xue, M., Lundquist, J.K., Zhang, F., Qi, Y., 2013a. Impact of low-level jets on the nocturnal urban heat island intensity in Oklahoma city. J. Appl. Meteorol. Climatol. 52, 1779–1802. https://doi.org/10.1175/JAMC-D-12-0256.1.
Hu, X.M., Klein, P.M., Xue, M., Zhang, F., Doughty, D.C., Forkel, R., Joseph, E., Fuentes, J.D., 2013b. Impact of the vertical mixing induced by low-level jets on boundary layer ozone concentration. Atmos. Environ. 70, 123–130. https://doi.org/10.1016/j.atmosenv.2012.12.046.
Huszar, P., Juda-Rezler, K., Halenka, T., Chervenkov, H., Syrakov, D., Krüger, B.C., Zanis, P., Melas, D., Katragkou, E., Reizer, M., 2011. Others, effects of climate change on ozone and particulate matter over central and Eastern Europe. Clim. Res. 50, 51–68.
Huszár, P., Karlický, J., Belda, M., Halenka, T., Pišoft, P., 2018. The impact of urban canopy meteorological forcing on summer photochemistry. Atmos. Environ. 176, 209–228.
Huszar, P., Karlický, J., Ďoubalová, J., Šindelářová, K., Nováková, T., Belda, M., Halenka, T., Žák, M., Pišoft, P., 2020. Urban canopy meteorological forcing and its impact on ozone and PM2.5: role of vertical turbulent transport. Atmos. Chem. Phys. 20, 1977–2016. https://doi.org/10.5194/acp-20-1977-2020.
Ichinose, T., Shimodozono, K., Hanaki, K., 1999. Impact of anthropogenic heat on urban climate in Tokyo. Atmos. Environ. 33, 3897–3909.
Imhoff, M.L., Zhang, P., Wolfe, R.E., Bounoua, L., 2010. Remote sensing of the urban heat island effect across biomes in the continental USA. Remote Sens. Environ. 114, 504–513.
Izrael, Y., Hashimoto, M., Tegart, W., 1990. Potential impacts of climate change. Rep. IPCC Work. Gr. II.
Jacobson, M.Z., 1998. Studying the effects of aerosols on vertical photolysis rate coefficient and temperature profiles over an urban airshed. J. Geophys. Res. Atmos. 103, 10593–10604.
Jacobson, M.Z., 2001. GATOR-GCMM: 2. A study of daytime and nighttime ozone layers aloft, ozone in national parks, and weather during the SARMAP field campaign. J. Geophys. Res. Atmos. 106, 5403–5420.
Jacobson, M.Z., Ten Hoeve, J.E., 2012. Effects of urban surfaces and white roofs on global and regional climate. J. Clim. 25, 1028–1044. https://doi.org/10.1175/JCLI-D-11-00032.1.
Janssen, R.H.H., Tsimpidi, A.P., Karydis, V.A., Pozzer, A., Lelieveld, J., Crippa, M., Prévôt, A.S.H., Ait-Helal, W., Borbon, A., Sauvage, S., Locoge, N., 2017. Influence of local production and vertical transport on the organic aerosol budget over Paris. J. Geophys. Res. 122, 8276–8296. https://doi.org/10.1002/2016JD026402.
Jauregui, E., Luyando, E., 1999. Global radiation attenuation by air pollution and its effects on the thermal climate in Mexico City. Int. J. Climatol. A J. R. Meteorol. Soc. 19, 683–694.
Jin, M., Shepherd, J.M., 2008. Aerosol relationships to warm season clouds and rainfall at monthly scales over east China: urban land versus ocean. J. Geophys. Res. Atmos. 113.
Jin, M., Shepherd, J.M., Zheng, W., 2010. Urban surface temperature reduction via the urban aerosol direct effect: a remote sensing and WRF model sensitivity study. Adv. Meteorol. 2010, 1–14. https://doi.org/10.1155/2010/681587.
Jin, M.S., Kessomkiat, W., Pereira, G., 2011. Satellite-observed urbanization characters in Shanghai, China: aerosols, urban heat island effect, and land-atmosphere interactions. Remote Sens. 3, 83–99. https://doi.org/10.3390/rs3010083.
Joabsson, A., Christensen, T.R., Wallén, B., 1999. Vascular plant controls on methane emissions from northern peatforming wetlands. Trends Ecol. Evol. 14, 385–388.
Johnson, M., Isakov, V., Touma, J.S., Mukerjee, S., Özkaynak, H., 2010. Evaluation of land-use regression models used to predict air quality concentrations in an urban area. Atmos. Environ. 44, 3660–3668. https://doi.org/10.1016/j.atmosenv.2010.06.041.
Jonsson, P., Bennet, C., Eliasson, I., Selin Lindgren, E., 2004. Suspended particulate matter and its relations to the urban climate in Dar es Salaam, Tanzania. Atmos. Environ. 38, 4175–4181. https://doi.org/10.1016/j.atmosenv.2004.04.021.
jun Li, L., Wang, Y., Zhang, Q., Yu, T., Zhao, Y., Jin, J., 2007. Spatial distribution of aerosol pollution based on MODIS data over Beijing, China. J. Environ. Sci. 19, 955–960. https://doi.org/10.1016/S1001-0742(07)60157-0.
Junk, J., Helbig, A., Lüers, J., 2003. Urban climate and air quality in Trier Germany. Int. J. Biometeorol. 47, 230–238. https://doi.org/10.1007/s00484-003-0162-6.
Kalashnikova, O.V., Mills, F.P., Eldering, A., Anderson, D., 2007. Application of satellite and ground-based data to investigate the UV radiative effects of Australian aerosols. Remote Sens. Environ. 107, 65–80. https://doi.org/10.1016/j.rse.2006.07.025.
Kang, H.-Q., Zhu, B., Zhu, T., Sun, J.-L., Ou, J.-J., 2014. Impact of megacity Shanghai on the urban heat-island effects over the downstream city Kunshan. Boundary-Layer Meteorol 152, 411–426.
Keller, M., Bustamante, M., Gash, J., Dias, P.S., 2013. Amazonia and Global Change. John Wiley & Sons.
Khan, S.M., Simpson, R.W., 2001. Effect of heat island on the meteorology of a complex urban airshed. Boundary-Layer Meteorol 100, 487–506. https://doi.org/10.1023/A:1019284332306.
Khiem, M., Ooka, R., Huang, H., Hayami, H., Yoshikado, H., Kawamoto, Y., 2010. Analysis of the relationship between changes in meteorological conditions and the variation in summer ozone levels over the Central Kanto area. Adv. Meteorol. 2010, 1–13. https://doi.org/10.1155/2010/349248.
Kim, Y., Sartelet, K., Raut, J.C., Chazette, P., 2015. Influence of an urban canopy model and PBL schemes on vertical mixing for air quality modeling over greater Paris. Atmos. Environ. 107, 289–306. https://doi.org/10.1016/j.atmosenv.2015.02.011.
Kjelgren, R., Montague, T., 1998. Urban tree transpiration over turf and asphalt surfaces. Atmos. Environ. 32, 35–41.
Klein, P.M., Hu, X.M., Xue, M., 2014. Impacts of mixing processes in nocturnal atmospheric boundary layer on urban ozone concentrations. Boundary-Layer Meteorol 150, 107–130. https://doi.org/10.1007/s10546-013-9864-4.
Kley, D., 1997. Tropospheric chemistry and transport. Science (80-.) 276, 1043–1044.
Knowlton, K., Rosenthal, J.E., Hogrefe, C., Lynn, B., Gaffin, S., Goldberg, R., Rosenzweig, C., Civerolo, K., Ku, J.-Y., Kinney, P.L., 2004. Assessing ozone-related health impacts under a changing climate. Environ. Health Perspect. 112, 1557–1563.
Kostmayer, P.H., 1989. The American landscape in the 21st century. Congr. Rec. 135, 9963.
Krüger, E.L., Minella, F.O., Rasia, F., 2011. Impact of urban geometry on outdoor thermal comfort and air quality from field measurements in Curitiba, Brazil. Build. Environ. 46, 621–634. https://doi.org/10.1016/j.buildenv.2010.09.006.
Lai, L.W., Cheng, W.L., 2009. Air quality influenced by urban heat island coupled with synoptic weather patterns. Sci. Total Environ. 407, 2724–2733. https://doi.org/10.1016/j.scitotenv.2008.12.002.
Lai, L.W., Cheng, W.L., 2010. Urban heat island and air pollution-an emerging role for hospital respiratory admissions in an urban area. J. Environ. Health 72, 32–35.
Langner, J., Bergström, R., Foltescu, V., 2005. Impact of climate change on surface ozone and deposition of sulphur and nitrogen in Europe. Atmos. Environ. 39, 1129–1141. https://doi.org/10.1016/j.atmosenv.2004.09.082.
Lee, D., 1993. Climate change and air quality in London. Geography. 78, 77–79.
Lee, C.S., Yu, C.C., Wang, T.Y., 2000. A meteorological analysis and forecast of air pollution episodes in Taiwan. EPA Taiwan ROC Rep. No. EPA-89-U1L1-03-186.

Leighton, P., 2012. Photochemistry of air pollution. Elsevier.
Leung, L.R., Gustafson, W.I., 2005. Potential regional climate change and implications to U.S. air quality. Geophys. Res. Lett. 32, 1–4. https://doi.org/10.1029/2005GL022911.
Levinson, R., Akbari, H., 2010. Potential benefits of cool roofs on commercial buildings: conserving energy, saving money, and reducing emission of greenhouse gases and air pollutants. Energy Effic 3, 53–109. https://doi.org/10.1007/s12053-008-9038-2.
Li, M., Song, Y., Mao, Z., Liu, M., Huang, X., 2016. Impacts of thermal circulations induced by urbanization on ozone formation in the Pearl River Delta region, China. Atmos. Environ. 127, 382–392. https://doi.org/10.1016/j.atmosenv.2015.10.075.
Li, H., Meier, F., Lee, X., Chakraborty, T., Liu, J., Schaap, M., Sodoudi, S., 2018. Interaction between urban heat island and urban pollution island during summer in Berlin. Sci. Total Environ. 636, 818–828. https://doi.org/10.1016/j.scitotenv.2018.04.254.
Li, Y., Zhang, J., Sailor, D.J., Ban-Weiss, G.A., 2019a. Effects of urbanization on regional meteorology and air quality in Southern California. Atmos. Chem. Phys. 19, 4439–4457. https://doi.org/10.5194/acp-19-4439-2019.
Li, Y., Barth, M.C., Steiner, A.L., 2019b. Comparing turbulent mixing of atmospheric oxidants across model scales. Atmos. Environ. 199, 88–101. https://doi.org/10.1016/j.atmosenv.2018.11.004.
Liao, J., Wang, T., Wang, X., Xie, M., Jiang, Z., Huang, X., Zhu, J., 2014. Impacts of different urban canopy schemes in WRF/Chem on regional climate and air quality in Yangtze River Delta, China. Atmos. Res. 145–146, 226–243. https://doi.org/10.1016/j.atmosres.2014.04.005.
Livada, I., Synnefa, A., Haddad, S., Paolini, R., Garshasbi, S., Ulpiani, G., Fiorito, F., Vassilakopoulou, K., Osmond, P., Santamouris, M., 2019. Time series analysis of ambient air-temperature during the period 1970–2016 over Sydney, Australia. Sci. Total Environ. 648, 1627–1638. https://doi.org/10.1016/j.scitotenv.2018.08.144.
Lo, C.P., Quattrochi, D.A., 2003. Land-use and land-cover change, urban heat island phenomenon, and health implications: a remote sensing approach. Photogramm. Eng. Remote. Sens. 69, 1053–1063.
Makhelouf, A., 2009. The effect of green spaces on urban climate. Iranian J. Environ. Health Sci. Eng. 6, 35–40.
Malek, E., Davis, T., Martin, R.S., Silva, P.J., 2006. Meteorological and environmental aspects of one of the worst national air pollution episodes (January, 2004) in Logan, Cache Valley, Utah, USA. Atmos. Res. 79, 108–122.
Mangold, A., De Backer, H., De Paepe, B., Dewitte, S., Chiapello, I., Derimian, Y., Kacenelenbogen, M., Léon, J.F., Huneeus, N., Schulz, M., Ceburnis, D., O'Dowd, C., Flentje, H., Kinne, S., Benedetti, A., Morcrette, J.J., Boucher, O., 2011. Aerosol analysis and forecast in the European Centre for Medium-Range Weather Forecasts Integrated Forecast System: 3. Evaluation by means of case studies. J. Geophys. Res. Atmos. 116, 1–23. https://doi.org/10.1029/2010JD014864.
Martilli, A., 2002. Numerical study of urban impact on boundary layer structure: sensitivity to wind speed, urban morphology, and rural soil moisture. J. Appl. Meteorol. 41, 1247–1266. https://doi.org/10.1175/1520-0450(2002)041<1247:NSOUIO>2.0.CO;2.
Martilli, A., Clappier, A., Rotach, M.W., 2002. An urban surface exchange parameterisation for mesoscale models. Boundary-Layer Meteorol 104, 261–304. https://doi.org/10.1023/A:1016099921195.
Martilli, A., Roulet, Y.A., Junier, M., Kirchner, F., Rotach, M.W., Clappier, A., 2003. On the impact of urban surface exchange parameterisations on air quality simulations: the Athens case. Atmos. Environ. 37, 4217–4231. https://doi.org/10.1016/S1352-2310(03)00564-8.
Meehl, G.A., Tebaldi, C., 2004. More intense, more frequent, and longer lasting heat waves in the 21st century. Science (80-.). 305, 994–997.
Meng, X., Zhang, Y., Zhao, Z., Duan, X., Xu, X., Kan, H., 2012. Temperature modifies the acute effect of particulate air pollution on mortality in eight Chinese cities. Sci. Total Environ. 435–436, 215–221. https://doi.org/10.1016/j.scitotenv.2012.07.008.
Merbitz, H., Buttstädt, M., Michael, S., Dott, W., Schneider, C., 2012. GIS-based identification of spatial variables enhancing heat and poor air quality in urban areas. Appl. Geogr. 33, 94–106. https://doi.org/10.1016/j.apgeog.2011.06.008.
Millstein, D., Menon, S., 2011. Regional climate consequences of large-scale cool roof and photovoltaic array deployment. Environ. Res. Lett. 6. https://doi.org/10.1088/1748-9326/6/3/034001.
Monn, C., Braendli, O., Schaeppi, G., Schindler, C., Ackermann-Liebrich, U., Leuenberger, P., 1995. Particulate matter < 10 μm (PM10) and total suspended particulates (TSP) in urban, rural and alpine air in Switzerland. Atmos. Environ. 29, 2565–2573. https://doi.org/10.1016/1352-2310(95)94999-U.
Mues, A., Manders, A., Schaap, M., Kerschbaumer, A., Stern, R., Builtjes, P., 2012. Impact of the extreme meteorological conditions during the summer 2003 in Europe on particulate matter concentrations. Atmos. Environ. 55, 377–391. https://doi.org/10.1016/j.atmosenv.2012.03.002.
Neu, U., Künzle, T., Wanner, H., 1994a. On the relation between ozone storage in the residual layer and daily variation in near-surface ozone concentration—a case study. Boundary-Layer Meteorol 69, 221–247.
Neu, U., Künzle, T., Wanner, H., 1994b. On the relation between ozone storage in the residual layer and daily variation in near-surface ozone concentration - a case study. Boundary-Layer Meteorol 69, 221–247. https://doi.org/10.1007/BF00708857.
Nichol, J.E., 1996. Analysis of the urban thermal environment with LANDSAT data. Environ. Plan. B Plan. Des. 23, 733–747.
Nichol, J., Wong, M.S., Fung, C., Leung, K.K.M., 2006. Assessment of urban environmental quality in a subtropical city using multispectral satellite images. Environ. Plan. B Plan. Des. 33, 39–58. https://doi.org/10.1068/b31195.
Nowak, D.J., 2002. The Effects of Urban Trees on Air Quality. USDA For. Serv.
Ohashi, Y., Genchi, Y., Kondo, H., Kikegawa, Y., Yoshikado, H., Hirano, Y., 2007. Influence of air-conditioning waste heat on air temperature in Tokyo during summer: numerical experiments using an urban canopy model coupled with a building energy model. J. Appl. Meteorol. Climatol. 46, 66–81.
Oke, T.R., 1982. The energetic basis of the urban heat island (Symons Memorial Lecture, 20 May 1980). Q. Journal, R. Meteorol. Soc 108, 1–24.
Oke, T.R., 2006. Towards better scientific communication in urban climate. Theor. Appl. Climatol. 84, 179–190. https://doi.org/10.1007/s00704-005-0153-0.
Oke, T.R., Mills, G., Christen, A., Voogt, J.A., 2017. Urban Climates. Cambridge University Press.
Padmanabhamurty, B., Hirt, M.S., 1974. The Toronto heat island and pollution distribution. Water Air Soil Pollut. 3, 81–89.
Pandey, P., Kumar, D., Prakash, A., Masih, J., Singh, M., Kumar, S., Jain, V.K., Kumar, K., 2012. A study of urban heat island and its association with particulate matter during winter months over Delhi. Sci. Total Environ. 414, 494–507. https://doi.org/10.1016/j.scitotenv.2011.10.043.
Papanastasiou, D.K., Melas, D., Bartzanas, T., Kittas, C., 2010. Temperature, comfort and pollution levels during heat waves and the role of sea breeze. Int. J. Biometeorol. 54, 307–317. https://doi.org/10.1007/s00484-009-0281-9.
Papanastasiou, D.K., Melas, D., Kambezidis, H.D., 2015. Air quality and thermal comfort levels under extreme hot weather. Atmos. Res. 152, 4–13. https://doi.org/10.1016/j.atmosres.2014.06.002.
Parrish, D.D., Zhu, T., 2009. Clean air for megacities. Science (80-.) 326, 674–675. https://doi.org/10.1126/science.1176064.
Peel, M.C., Finlayson, B.L., McMahon, T.A., 2007. Updated world map of the Köppen-Geiger climate classification. Hydrol. Earth Syst. Sci. Discuss. 4, 439–473.
Pickering, C., Byrne, J., 2014. The Benefits of Publishing Systematic Quantitative Literature Reviews for PhD Candidates and Other Early-Career Researchers. , p. 4360 https://doi.org/10.1080/07294360.2013.841651.
Pielke, R.A., Mahrer, Y., 1978. Verification analysis of the University of Virginia three-dimensional mesoscale model prediction over South Florida for 1 July 1973. Mon. Weather Rev. 106, 1568–1589.
Plocoste, T., Jacoby-Koaly, S., Molinié, J., Petit, R.H., 2014. Evidence of the effect of an urban heat island on air quality near a landfill. Urban Clim. 10, 745–757. https://doi.org/10.1016/j.uclim.2014.03.007.
Poupkou, A., Nastos, P., Melas, D., Zerefos, C., 2011. Climatology of discomfort index and air quality index in a large urban mediterranean agglomeration. Water Air Soil Pollut. 222, 163–183. https://doi.org/10.1007/s11270-011-0814-9.
Pulikesi, M., Baskaralingam, P., Rayudu, V.N., Elango, D., Ramamurthi, V., Sivanesan, S., 2006. Surface ozone measurements at urban coastal site Chennai, in India. J. Hazard. Mater. 137, 1554–1559.
Pyrgou, A., Hadjinicolaou, P., Santamouris, M., 2018. Enhanced near-surface ozone under heatwave conditions in a Mediterranean island. Sci. Rep. 8, 1–10. https://doi.org/10.1038/s41598-018-27590-z.
Qian, S., Nasuta, D., Rhoads, A., Wang, Y., Geng, Y., Hwang, Y., Radermacher, R., Takeuchi, I., 2016. Not-in-kind cooling technologies: a quantitative comparison of refrigerants and system performance. Int. J. Refrig. 62, 177–192. https://doi.org/10.1016/j.ijrefrig.2015.10.019.
Qin, N., Liang, P., Wu, C., Wang, G., Xu, Q., Xiong, X., Wang, T., Zolfo, M., Segata, N., Qin, H., Knight, R., Gilbert, J.A., Zhu, T.F., 2020. Longitudinal survey of microbiome associated with particulate matter in a megacity. Genome Biol. 21, 1–11. https://doi.org/10.1186/s13059-020-01964-x.
Rajagopalan, P., Santamouris, M., Andamon, M., 2017. Public engagement in urban microclimate research. Back to Futur. Next 50 Years. 51st Int. Conf. Archit. Sci. Assoc.
Ramanathan, V., Chung, C., Kim, D., Bettge, T., Buja, L., Kiehl, J.T., Washington, W.M., Fu, Q., Sikka, D.R., Wild, M., 2005. Atmospheric brown clouds: impacts on south Asian climate and hydrological cycle. Proc. Natl. Acad. Sci. U. S. A. 102, 5326–5333. https://doi.org/10.1073/pnas.0500656102.
Ramanathan, V., Ramana, M.V., Roberts, G., Kim, D., Corrigan, C., Chung, C., Winker, D., 2007. Warming trends in Asia amplified by brown cloud solar absorption. Nature 448, 575–578.
Reitebuch, O., Strassburger, A., Emeis, S., Kuttler, W., 2000. Nocturnal secondary ozone concentration maxima analysed by sodar observations and surface measurements. Atmos. Environ. 34, 4315–4329. https://doi.org/10.1016/S1352-2310(00)00185-0.
Rendón, A.M., Salazar, J.F., Palacio, C.A., Wirth, V., Brötz, B., 2014. Effects of urbanization on the temperature inversion breakup in a mountain valley with implications for air quality. J. Appl. Meteorol. Climatol. 53, 840–858. https://doi.org/10.1175/JAMC-D-13-0165.1.
Rendón, A.M., Salazar, J.F., Palacio, C.A., Wirth, V., 2015. Temperature inversion breakup with impacts on air quality in urban valleys influenced by topographic shading. J. Appl. Meteorol. Climatol. 54, 302–321. https://doi.org/10.1175/JAMC-D-14-0111.1.
Rinnan, R., Steinke, M., Mcgenity, T., Loreto, F., 2014. Plant volatiles in extreme terrestrial and marine environments. Plant Cell Environ. 37, 1776–1789. https://doi.org/10.1111/pce.12320.
Robaa, S.M., 2009. Urban-rural solar radiation loss in the atmosphere of greater Cairo region, Egypt. Energy Convers. Manag. 50, 194–202. https://doi.org/10.1016/j.enconman.2008.06.024.
Roberts, S., 2004. Interactions between particulate air pollution and temperature in air pollution mortality time series studies. Environ. Res. 96, 328–337. https://doi.org/10.1016/j.envres.2004.01.015.
Romero, H., Ihl, M., Rivera, A., Zalazar, P., Azocar, P., 1999. Rapid urban growth, land-use changes and air pollution in Santiago, Chile. Atmos. Environ. 33, 4039–4047. https://doi.org/10.1016/S1352-2310(99)00145-4.
Rosenfeld, A.H., Akbari, H., Bretz, S., SAilor, D., Taha, H., 1993. Mitigation of urban heat islands: materials, utility programs, updates. J. Energy Effic 1.
Rosenfeld, A.H., Akbari, H., Romm, J.J., Pomerantz, M., et al., 1998. Cool communities: strategies for heat island mitigation and smog reduction. Energ. Build 51 (28), 62 1998.

Rosenzweig, C., Solecki, W.D., Parshall, L., Chopping, M., Pope, G., Goldberg, R., 2005. Characterizing the urban heat island in current and future climates in New Jersey. Environ. Hazards. 6, 51–62. https://doi.org/10.1016/j.hazards.2004.12.001.

Ryu, Y.H., Baik, J.J., Kwak, K.H., Kim, S., Moon, N., 2013. Impacts of urban land-surface forcing on ozone air quality in the Seoul metropolitan area. Atmos. Chem. Phys. 13, 2177–2194. https://doi.org/10.5194/acp-13-2177-2013.

Santamouris, M., 2015. Analyzing the heat island magnitude and characteristics in one hundred Asian and Australian cities and regions. Sci. Total Environ. 512–513, 582–598. https://doi.org/10.1016/j.scitotenv.2015.01.060.

Santamouris, M., 2016. Cooling the buildings – past, present and future. Energy Build 128, 617–638. https://doi.org/10.1016/j.enbuild.2016.07.034.

Santamouris, M., 2020. Recent progress on urban overheating and heat island research. Integrated assessment of the energy, environmental, vulnerability and health impact. Synergies with the global climate change. Energy Build 207. https://doi.org/10.1016/j.enbuild.2019.109482.

Santamouris, M., Feng, J., 2018. Recent progress in daytime radiative cooling: is it the air conditioner of the future? Buildings 8. https://doi.org/10.3390/buildings8120168.

Santamouris, M., Kolokotsa, D., 2016. Urban Climate Mitigation Techniques.

Santamouris, M., Xirafi, F., Gaitani, N., Spanou, A., Saliari, M., Vassilakopoulou, K., 2012. Improving the microclimate in a dense urban area using experimental and theoretical techniques - the case of Marousi, Athens. Int. J. Vent. 11, 1–16. https://doi.org/10.1080/14733315.2012.11683966.

Santamouris, M., Cartalis, C., Synnefa, A., Kolokotsa, D., 2015. On the impact of urban heat island and global warming on the power demand and electricity consumption of buildings—a review. Energy Build 98, 119–124. https://doi.org/10.1016/j.enbuild.2014.09.052.

Santamouris, M., Haddad, S., Saliari, M., Vasilakopoulou, K., Synnefa, A., Paolini, R., Ulpiani, G., Garshasbi, S., Fiorito, F., 2018. On the energy impact of urban heat island in Sydney: climate and energy potential of mitigation technologies. Energy Build 166. https://doi.org/10.1016/j.enbuild.2018.02.007.

Sarrat, C., Lemonsu, A., Masson, V., Guedalia, D., 2006. Impact of urban heat island on regional atmospheric pollution. Atmos. Environ. 40, 1743–1758. https://doi.org/10.1016/j.atmosenv.2005.11.037.

Savijärvi, H., Liya, J., 2001. Local winds in a valley city. Boundary-Layer Meteorol 100, 301–319.

Seinfeld, J.H., Pandis, S.N., 2016. Atmospheric Chemistry and Physics: From Air Pollution to Climate Change. John Wiley & Sons.

Setti, L., Passarini, F., De Gennaro, G., Baribieri, P., Perrone, M.G., Borelli, M., Palmisani, J., Di Gilio, A., Torboli, V., Pallavicini, A., et al., 2020. SARS-Cov-2 RNA Found on Particulate Matter of Bergamo in Northern Italy: First Preliminary Evidence, MedRxiv.

Sharkey, T.D., Yeh, S., 2001. Isoprene emission from plants. Annu. Rev. Plant Biol. 52, 407–436.

Sillman, S., 1995. The use of NOy, H2O2, and HNO3 as indicators for ozone-NO x-hydrocarbon sensitivity in urban locations. J. Geophys. Res. Atmos. 100, 14175–14188.

Sillman, S., Samson, P.J., 1995. Impact of temperature on oxidant photochemistry in urban polluted rural and remote environments. J. Geophys. Res. 100. https://doi.org/10.1029/94jd02146.

Singh, S., Nath, S., Kohli, R., Singh, R., 2005. Aerosols over Delhi during pre-monsoon months: characteristics and effects on surface radiation forcing. Geophys. Res. Lett. 32, 1–4. https://doi.org/10.1029/2005GL023062.

Smith, W.H., 1984. Pollutant uptake by plants. Air Pollut. Plant Life. 417–450.

Sokhi, R.S., Baklanov, A., Piringer, M., 2017. Special issue of journal of urban climate: modelling of urban air pollution and climate interactions. Urban Clim. 22, 1. https://doi.org/10.1016/j.uclim.2017.11.002.

Solberg, S., Hov, A. Søvde, Isaksen, I.S.A., Coddeville, P., De Backer, H., Forster, C., Orsolini, Y., Uhse, K., 2008. European surface ozone in the extreme summer 2003. J. Geophys. Res. Atmos. 113, 1–16. https://doi.org/10.1029/2007JD009098.

Solecki, W.D., Rosenzweig, C., Pope, G.C., Chopping, M.J., Goldberg, R.A., Polissar, A.V., 2004. Urban Heat Island and Climate Change. An Assessment of Interacting and Possible Adaptations in the Camden, New Jersey Region, in.

Stathopoulou, E., Mihalakakou, G., Santamouris, M., Bagiorgas, H.S., 2008. On the impact of temperature on tropospheric ozone concentration levels in urban environments. J. Earth Syst. Sci. 117, 227–236. https://doi.org/10.1007/s12040-008-0027-9.

Stedman, J.R., 2004. The predicted number of air pollution related deaths in the UK during the August 2003 heatwave. Atmos. Environ. 38, 1087–1090. https://doi.org/10.1016/j.atmosenv.2003.11.011.

Stewart, H.E., Hewitt, C.N., Bunce, R.G.H., Steinbrecher, R., Smiatek, G., Schoenemeyer, T., 2003. A highly spatially and temporally resolved inventory for biogenic isoprene and monoterpene emissions: model description and application to Great Britain. J. Geophys. Res. Atmos. 108. https://doi.org/10.1029/2002JD002694.

Stone, B., 2008. Urban sprawl and air quality in large US cities. J. Environ. Manag. 86, 688–698. https://doi.org/10.1016/j.jenvman.2006.12.034.

Struzewska, J., Kaminski, J.W., 2008. Formation and transport of photooxidants over Europe during the July 2006 heat wave - observations and GEM-AQ model simulations. Atmos. Chem. Phys. 8, 721–736. https://doi.org/10.5194/acp-8-721-2008.

Swamy, G., Nagendra, S.M. Shiva, Schlink, U., 2017. Urban Heat Island (UHI) influence on secondary pollutant formation in a tropical humid environment. J. Air Waste Manag. Assoc. 67, 1080–1091. https://doi.org/10.1080/10962247.2017.1325417.

Taha, H., 1996. Modeling impacts of increased urban vegetation on ozone air quality in the south coast Air Basin. Atmos. Environ. 30, 3423–3430. https://doi.org/10.1016/1352-2310(96)00035-0.

Taha, H., 2008a. Meso-urban meteorological and photochemical modeling of heat island mitigation. Atmos. Environ. 42, 8795–8809. https://doi.org/10.1016/j.atmosenv.2008.06.036.

Taha, H., 2008b. Episodic performance and sensitivity of the urbanized MM5 (uMM5) to perturbations in surface properties in Houston Texas. Boundary-Layer Meteorol 127, 193–218.

Taha, H., 2015. Meteorological, air-quality, and emission-equivalence impacts of urban heat island control in California. Sustain. Cities Soc. 19, 207–221. https://doi.org/10.1016/j.scs.2015.03.009.

Theoharatos, G., Pantavou, K., Mavrakis, A., Spanou, A., Katavoutas, G., Efstathiou, P., Mpekas, P., Asimakopoulos, D., 2010. Heat waves observed in 2007 in Athens, Greece: synoptic conditions, bioclimatological assessment, air quality levels and health effects. Environ. Res. 110, 152–161. https://doi.org/10.1016/j.envres.2009.12.002.

Tingey, D.T., 1981. The Effect of Environmental Factors on the Emission of Biogenic Hydrocarbons from Live Oak and Slash Pine [*Pinus elliottii*, *Quercus virginiana*, USA].

Tong, N.Y.O., Leung, D.Y.C., Liu, C.H., 2011. A review on ozone evolution and its relationship with boundary layer characteristics in urban environments. Water Air Soil Pollut. 214, 13–36. https://doi.org/10.1007/s11270-010-0438-5.

Ulpiani, G., 2019. Water mist spray for outdoor cooling: a systematic review of technologies, methods and impacts. Appl. Energy 254, 113647. https://doi.org/10.1016/j.apenergy.2019.113647.

Ulpiani, G., Ranzi, G., Bruederlin, F., Paolini, R., Fiorito, F., Haddad, S., Kohl, M., Santamouris, M., 2019. Elastocaloric cooling: roadmap towards successful implementation in the built environment. AIMS Mater. Sci. 6, 1135–1152. https://doi.org/10.3934/matersci.2019.6.1135.

Ulpiani, G., Ranzi, G., Santamouris, M., 2020. Experimental evidence of the multiple microclimatic impacts of bushfires in affected urban areas: the case of Sydney during the 2019/2020 Australian season. Environ. Res. Commun. 2, 65005. https://doi.org/10.1088/2515-7620/ab9e1a.

Urmy, S.S., Williamson, C.E., Leach, T.H., Schladow, S.G., Overholt, E.P., Warren, J.D., 2016. Vertical Redistribution of Zooplankton in an Oligotrophic Lake Associated with Reduction in Ultraviolet Radiation by Wildfire Smoke. , pp. 3746–3753 https://doi.org/10.1002/2016GL068533 (Received).

Vailshery, L.S., Jaganmohan, M., Nagendra, H., 2013. Effect of street trees on microclimate and air pollution in a tropical city. Urban For. Urban Green. 12, 408–415. https://doi.org/10.1016/j.ufug.2013.03.002.

Wagner, P., Schäfer, K., 2017. Influence of mixing layer height on air pollutant concentrations in an urban street canyon. Urban Clim. 22, 64–79. https://doi.org/10.1016/j.uclim.2015.11.001.

Wang, Y., Hayashi, Y., Chen, J., Li, Q., 2014. Changing urban form and transport CO2 emissions: an empirical analysis of Beijing, China. Sustain 6, 4558–4579. https://doi.org/10.3390/su6074558.

Wang, L., Gao, Z., Miao, S., Guo, X., Sun, T., Liu, M., Li, D., 2015. Contrasting characteristics of the surface energy balance between the urban and rural areas of Beijing. Adv. Atmos. Sci. 32, 505–514. https://doi.org/10.1007/s00376-014-3222-4.

Wang, B., Harder, T.H., Kelly, S.T., Piens, D.S., China, S., Kovarik, L., Keiluweit, M., Arey, B.W., Gilles, M.K., Laskin, A., 2016. Airborne soil organic particles generated by precipitation. Nat. Geosci. 9, 433–437. https://doi.org/10.1038/ngeo2705.

Wang, Y., Du, H., Xu, Y., Lu, D., Wang, X., Guo, Z., 2018. Temporal and spatial variation relationship and influence factors on surface urban heat island and ozone pollution in the Yangtze River Delta, China. Sci. Total Environ. 631–632, 921–933. https://doi.org/10.1016/j.scitotenv.2018.03.050.

Ward, K., Lauf, S., Kleinschmit, B., Endlicher, W., 2016. Heat waves and urban heat islands in Europe: a review of relevant drivers. Sci. Total Environ. 569–570, 527–539. https://doi.org/10.1016/j.scitotenv.2016.06.119.

Whitlow, T.H., Bassuk, N.L., Reichert, D.L., 1992. A 3-year study of water relations of urban street trees. J. Appl. Ecol. 436–450.

Wilby, R.L., 2003. Past and projected trends in London's urban heat island. Weather 58, 251–260. https://doi.org/10.1256/wea.183.02.

Wilby, R.L., 2008. Constructing climate change scenarios of urban heat island intensity and air quality. Environ. Plan. B Plan. Des. 35, 902–919. https://doi.org/10.1068/b33066t.

Wu, X., Nethery, R.C., Sabath, B.M., Braun, D., Dominici, F., 2020. Exposure to Air Pollution and COVID-19 Mortality in the United States, MedRxiv.

Xie, M., Zhu, K., Wang, T., Feng, W., Gao, D., Li, M., Li, S., Zhuang, B., Han, Y., Chen, P., Liao, J., 2016. Changes in regional meteorology induced by anthropogenic heat and their impacts on air quality in South China. Atmos. Chem. Phys. 16, 15011–15031. https://doi.org/10.5194/acp-16-15011-2016.

Yoshikado, H., Tsuchida, M., 1996. High levels of winter air pollution under the influence of the urban heat island along the shore of Tokyo Bay. J. Appl. Meteorol. 35, 1804–1813. https://doi.org/10.1175/1520-0450(1996)035<1804:HLOWAP>2.0.CO;2.

Yun, G.Y., Ngarambe, J., Duhirwe, P.N., Ulpiani, G., Paolini, R., Haddad, S., Vasilakopoulou, K., Santamouris, M., 2020. Predicting the magnitude and the characteristics of the urban heat island in coastal cities in the proximity of desert landforms. The case of Sydney. Sci. Total Environ. 709, 136068. https://doi.org/10.1016/j.scitotenv.2019.136068.

Zannetti, P., 1990. Air Pollution Modeling. Theories, Computational Methods and Available Software. https://doi.org/10.1017/CBO9781107415324.004.

Zhang, J., Rao, S.T., 1999. The role of vertical mixing in the temporal evolution of ground-level ozone concentrations. J. Appl. Meteorol. 38, 1674–1691. https://doi.org/10.1175/1520-0450(1999)038<1674:TROVMI>2.0.CO;2.

Zhang, D.L., Shou, Y.X., Dickerson, R.R., 2009. Upstream urbanization exacerbates urban heat island effects. Geophys. Res. Lett. 36, 1–5. https://doi.org/10.1029/2009GL041082.

Zhang, D.L., Shou, Y.X., Dickerson, R.R., Chen, F., 2011. Impact of upstream urbanization on the urban heat island effects along the Washington-Baltimore corridor. J. Appl. Meteorol. Climatol. 50, 2012–2029. https://doi.org/10.1175/JAMC-D-10-05008.1.

Zhong, S., Qian, Y., Zhao, C., Leung, R., Wang, H., Yang, B., Fan, J., Yan, H., Yang, X.Q., Liu, D., 2017. Urbanization-induced urban heat island and aerosol effects on climate extremes in the Yangtze River Delta region of China. Atmos. Chem. Phys. 17, 5439–5457. https://doi.org/10.5194/acp-17-5439-2017.

Zhong, S., Qian, Y., Sarangi, C., Zhao, C., Leung, R., Wang, H., Yan, H., Yang, T., Yang, B., 2018. Urbanization effect on winter haze in the Yangtze River Delta region of China. Geophys. Res. Lett. 45, 6710–6718. https://doi.org/10.1029/2018GL077239.

Zhou, D., Zhao, S., Liu, S., Zhang, L., Zhu, C., 2014. Surface urban heat island in China's 32 major cities: spatial patterns and drivers. Remote Sens. Environ. 152, 51–61.

Zhu, B., Kang, H., Zhu, T., Su, J., Hou, X., Gao, J., 2015. Impact of Shanghai urban land surface forcing on downstream city ozone chemistry. J. Geophys. Res. Atmos. 120, 4340–4351. https://doi.org/10.1002/2014JD022859.

Zhu, K., Xie, M., Wang, T., Cai, J., Li, S., Feng, W., 2017. A modeling study on the effect of urban land surface forcing to regional meteorology and air quality over South China. Atmos. Environ. 152, 389–404. https://doi.org/10.1016/j.atmosenv.2016.12.053.